DEVELOPMENT OF EPOXY COMPOSITES REINFORCED WITH CARBON NANOTUBE AND NATURAL FIBER FOR COMMERCIAL APPLICATIONS

DEBANAN BHADRA

M.Sc. Engineering Thesis

DEPARTMENT OF AERONAUTICAL ENGINEERING
MILITARY INSTITUTE OF SCIENCE AND TECHNOLOGY
DHAKA, BANGLADESH

SEPTEMBER 2023

DEVELOPMENT OF EPOXY COMPOSITES REINFORCED WITH CARBON NANOTUBE AND NATURAL FIBER FOR COMMERCIAL APPLICATIONS

DEBANAN BHADRA (SN.0419220002)

A Thesis Submitted in Partial Fulfilment of the Requirements for the Degree of Master of Science in Aeronautical Engineering.

DEPARTMENT OF AERONAUTICAL ENGINEERING
MILITARY INSTITUTE OF SCIENCE AND TECHNOLOGY
DHAKA, BANGLADESH

SEPTEMBER 2023

DEVELOPMENT OF EPOXY COMPOSITES REINFORCED WITH CARBON NANOTUBE AND NATURAL FIBER FOR COMMERCIAL APPLICATIONS

M.Sc. Engineering Thesis

By

DEBNAN BHADRA (SN. 0419220002)

Approved as to style and content by the Board of Examination in September, 2023:

Dr Muammer Din Arif, Assistant Professor Department of Mechanical Engineering, MIST.	Chairman (Supervisor)
Air Cdre Md Aminul Haque Senior Instructor & Head Department of Aeronautical Engineering, MIST.	Member (Ex-officio)
Dr Shahida Begum Professor Department of Mechanical Engineering, MIST.	Member (Internal)
Dr. Md. Sayem Hossain Bhuiyan Assistant Professor Department of Mechanical Engineering, MIST.	Member (Internal)
Dr Md Afsar Ali Professor Department of Mechanical Engineering, BUET.	Member (External)

DEVELOPMENT OF EPOXY COMPOSITES REINFORCED WITH CARBON NANOTUBE AND NATURAL FIBER FOR COMMERCIAL APPLICATIONS

DECLERATION

I hereby declare that the study reported in this thesis entitled above is my own original work and has not been submitted before anywhere for any degree or other purposes. Further certify that the intellectual content of this thesis is the product of my own work and that all the assistance received in preparing this thesis and sources have been acknowledged and cited in the reference Section.

_____

Debanan Bhadra

Department of Aeronautical Engineering MIST, Dhaka

ABSTRACT

Development of Epoxy Composites Reinforced with Carbon Nanotube and Natural Fiber for Commercial Applications

The global economy has gone through significant alterations in recent years, particularly after Covid-19 epidemic, with an increasing importance on biodegradability, resource efficacy, as well as environmental responsibility. Keeping that in mind, this study focuses on developing composite materials with Epoxy resin as matrix material, natural fibers as reinforcements and Multi-Walled Carbon Nanotubes (MWCNT) as nanofiller. This present study is intended to develop natural fiber and MWCNT reinforced epoxy composites with a view to investigate their physical and mechanical properties, as well as to model the mechanical properties using Finite Element Method (FEM). However, as there are lot of different natural fibers with varying mechanical properties, this study has employed a fuzzy Multi Criteria Decision Making method to select the best natural fibers among twelve alternatives and found that the pineapple fiber and coir fiber are the top two candidates among different fibers. Therefore, this study used pineapple, coir, and sisal fiber as natural fiber reinforcements. Alkali treatment using sodium hydroxide (NaOH) was employed for surface modification of natural fibers, enhancing their compatibility with the epoxy matrix. Moreover, ultrasonication technique was used for achieving uniform dispersion of CNTs within the epoxy matrix. Different physical properties such as, density, void contents, and water absorption, as well as some mechanical properties such as tensile strength, Young's modulus, elongation at break, flexural strength, flexural modulus, Rockwell hardness number and impact energy were measured. Fourier Transform InfraRed (FTIR) spectroscopy was carried out to observe the change of molecular structure of the composites because of the interaction among epoxy, natural fibers and MWCNT. Scanning Electron Microscopic (SEM) images were analyzed to understand the microstructure of the composites. Furthermore, Microstructure-Free Finite Element Model (MF-FEM) was applied to simulate the mechanical behavior of the composites. Findings from the study showed satisfactory improvement in most of the physical and mechanical properties with addition of MWCNT up to a certain extent. However, addition of CNT resulted in increased density and brittleness of the composites.

সারসংক্ষেপ

Development of Epoxy Composites Reinforced with Carbon Nanotube and Natural Fiber for Commercial Applications

গত কয়েক বছরে বিশ্বজনীন অর্থনীতিতে গুরুত্বপূর্ণ পরিবর্তন ঘটেছে, বিশেষ করে কোভিড-১৯ মহামারীর পরে, যেখানে জীবাণুবিয়োজ্যতা, সম্পদ কার্যক্ষমতা, এবং পরিবেশগত দায়বদ্ধতার উপর বাড়তি গুরুত্ব দেয়া হচ্ছে। এটি মাথায় রেখে, এই গবেষণায় ম্যাট্রিক্স উপাদান হিসাবে ইপক্সি রজন, শক্তিবৃদ্ধি হিসাবে প্রাকৃতিক ফাইবার এবং ন্যানোপূরক হিসেবে বহু-দেয়াল কার্বন ন্যানোটিউব (MWCNT) সমৃদ্ধ যৌগিক উপকরণগুলি বিকাশের উপর দৃষ্টি নিবদ্ধ করা হয়েছে। এই বর্তমান অধ্যয়নটির উদ্দেশ্য হল প্রাকৃতিক ফাইবার এবং বহু-দেয়াল কার্বন ন্যানোটিউব (MWCNT) সমৃদ্ধ ইপোক্সি কম্পোজিটগুলিকে তাদের ভৌত এবং যান্ত্রিক বৈশিষ্ট্যগুলি তদন্ত করা, সেইসাথে সসীম উপাদান পদ্ধতি (FEM) ব্যবহার করে যান্ত্রিক বৈশিষ্ট্যগুলির মডেল করা। কিন্তু, যেহেতু বিভিন্ন যান্ত্রিক বৈশিষ্ট্য সহ প্রচুর বিভিন্ন প্রাকৃতিক তন্তু রয়েছে, তাই এই গবেষণাটি বারোটি বিকল্পের মধ্যে সেরা প্রাকৃতিক তন্তু নির্বাচন করতে একটি ফাজি বহু নির্ণায়ক সিদ্ধান্ত গ্রহণ পদ্ধতি নিযুক্ত করেছে এবং দেখা গেছে যে আনার এবং নারিকেল তন্তু হল বিভিন্ন তন্তুগুলির মধ্যে শীর্ষ দুই প্রার্থী। অতএব, এই গবেষণায় প্রাকৃতিক তন্তু শক্তিবৃদ্ধি হিসাবে আনারস, নারিকেল এবং সিসাল তন্তুসমূহ ব্যবহার করা হয়েছে। সোডিয়াম হাইড্রোক্সাইড (NaOH) ব্যবহার করে ক্ষার চিকিৎসা প্রাকৃতিক তন্তুগুলির পৃষ্ঠের পরিবর্তনের জন্য নিযুক্ত করা হয়েছিল যা ইপোক্সি ম্যাট্রিক্সের সাথে তাদের সামঞ্জস্য বৃদ্ধি করে। অধিকন্তু, কৌশল ইপোক্সি ম্যাট্রিক্সের মধ্যে কার্বন ন্যানোটিউব এর অভিন্ন বিচ্ছুরণ অর্জনের জন্য ব্যবহৃত হয়েছিল। বিভিন্ন ভৌত বৈশিষ্ট্য যেমন, ঘনত্ব, অকার্যকর বিষয়বস্তু এবং জল শোষণ, সেইসাথে কিছু যান্ত্রিক বৈশিষ্ট্য যেমন প্রসার্য শক্তি, ইয়ং'স মডুলাস, বিরতিতে প্রসারিত হওয়া, নমনীয় শক্তি, নমনীয় মডুলাস, রকওয়েল কঠোরতা সংখ্যা এবং প্রভাব শক্তি পরিমাপ করা হয়েছিল। ফুরিয়ার ট্রান্সফর্ম ইনফ্রারেড স্পেকট্রোস্কোপি ইপোক্সি, প্রাকৃতিক তন্তু এবং কার্বন ন্যানোটিউবর মধ্যে মিথস্ক্রিয়ার কারণে কম্পোজিটগুলির আণবিক কাঠামোর পরিবর্তন পর্যবেক্ষণ করার জন্য করা হয়েছিল। কম্পোজিটগুলির মাইক্রোস্ট্রাকচার বোঝার জন্য স্ক্যানিং ইলেক্ট্রন মাইক্রোস্কোপিক (SEM) চিত্রগুলি বিশ্লেষণ করা হয়েছিল। তদ্ব্যতীত, কম্পোজিটগুলির যান্ত্রিক আচরণ অনুকরণ করতে মাইক্রোস্ট্রাকচার মুক্ত সসীম উপাদান পদ্ধতি প্রয়োগ করা হয়েছিল। গবেষণার ফলাফলগুলি একটি নির্দিষ্ট পরিমাণ পর্যন্ত কার্বন ন্যানোটিউব যোগ করার সাথে বেশিরভাগ শারীরিক এবং যান্ত্রিক বৈশিষ্ট্যের সন্তোষজনক উন্নতি দেখায়। কিন্তু, কার্বন ন্যানোটিউব যোগ করার ফলে কম্পোজিটগুলির ঘনত্ব এবং ভঙ্গুরতা বৃদ্ধি পায়।

ACKNOWLEDGEMENTS

I'm moved to express my profound gratitude first and foremost to Dr. Muammer Din Arif. His tireless guidance, seasoned wisdom, and steadfast support have proven crucial to the successful completion of this thesis. His insightful feedback and thoughtful input have had an enormous impact on the direction of this research.

I must extend my acknowledgment to the Civil Engineering Department, the Mechanical Engineering Department, and the Environmental Water Resources and Coastal Engineering Department of MIST. Without the facilities of their state-of-the-art laboratories, the progress of this research would have been significantly hampered. The continuous support and diligent instruction from the lab technicians and faculty members of these departments turned this research into a genuinely collective endeavor.

Equally important is the role played by the Bangladesh Council of Scientific and Industrial Research (BCSIR) who carried out the Fourier Transform Infrared (FTIR) spectroscopy tests. Their specialized knowledge and prompt services were instrumental to the efficient and precise completion of the composite characterization process.

Each of the individuals and institutions I've mentioned here played a key role in bringing this thesis dissertation to fruition. The magnitude of their influence cannot be overstated, and their invaluable contributions will be appreciated and remembered for a long time to come.

TABLE OF CONTENTS

Page

LIST OF TABLES

Table Page

LIST OF FIGURES

Figure Page

LIST OF MAIN NOTATIONS

CNT	Carbon Nanotubes
MWCNT	Multi-Walled Carbon Nanotubes
NFRP	Natural Fiber Reinforced Polymer
PE	Polyester
PP	Polypropylene
PLA	Poly Lactic Acid
PVC	Polyvinyl Chloride
PVE	Polyvinyl ester
PF	Phenolic Formaldehyde
AHP	Analytic Hierarchy Process
TOPSIS	Technique for Order of Preference by Similarity to Ideal Solution
MCDM	Multi Criteria Decision Making

CHAPTER 1
INTRODUCTION

1.1 Introduction

In recent years, especially post-Covid-19, the global economy has witnessed a significant shift towards biodegradability, resource efficiency, and environmental accountability. In response to these challenges, there is a pressing need for materials that can deliver high performance while also being biodegradable and environmentally friendly. Traditional materials, such as metals and plastics, falter in fulfilling these dual objectives due to environmental repercussions and recyclability concerns. However, CNT and natural fiber-reinforced epoxy composites emerge as promising alternatives, encapsulating both high performance and environment friendliness. These composites not only align with the push for a green economy but also empower industries to adopt eco-friendly innovations, propelling research, investments, and job creation in nascent sectors. This study delves into these novel composites, aiming to foster their integration across industries for a greener, efficient global economy.

1.2 Carbon Nanotubes and Natural Fibers as Reinforcing Agents in Epoxy Composites

The use of carbon nanotubes (CNTs) and natural fibers as reinforcements in epoxy composites has garnered significant interest in recent years (Bellairu et al., 2022; Chen et al., 2017; Dilfi KF, Che, and Xian, 2019; P. K. Kushwaha, Pandey, and Kumar, 2014; Longkullabutra, Thamjaree, and Nhuapeng, 2010). These reinforcements offer unique properties that can synergistically augment the overall performance of epoxy composites while addressing some of the limitations discussed in the previous section. This section will provide an in-depth overview of carbon nanotubes and natural fibers, their properties, and their prospective for utilization as reinforcements in epoxy composites for commercial applications.

1.2.1 Natural Fibers as Reinforcements

Natural fibers, derived from plant, animal, or mineral sources, have gained significant interest as sustainable and environmentally friendly alternatives to synthetic fibers for reinforcement in composites. Some of the most common natural fibers used in composites include flax, hemp, jute, sisal, and kenaf. Natural fibers offer several advantages as reinforcements in epoxy composites, such as:

- Renewable and Biodegradable: Natural fibers are derived from renewable resources and are biodegradable, making them an environmentally friendly choice for reinforcement in composites (Chand and Fahim, 2021a).

- Low Density: Natural fibers typically have a minimal density compared to synthetic fibers, like glass or carbon, which can result in lightweight composites with desirable mechanical properties (Nurazzi et al., 2021).

- High Specific Strength and Stiffness: Natural fibers demonstrate high specific strength and stiffness (strength and stiffness per unit weight), making them effective reinforcements for lightweight composites (M. K. Singh and Singh, 2022b).

- Improved Toughness and Impact Resistance: Natural fibers can increase the toughness and impact resistance of epoxy composites, addressing the inherent brittleness of epoxy resins (M. K. Singh and Singh, 2022a).

1.2.2 Carbon Nanotubes as Reinforcements

Carbon nanotubes (CNTs) are a model of carbon with a nanostructure that consists of cylindrical carbon atoms organized in a hexagonal lattice. CNTs exhibit outstanding mechanical, electrical, as well as thermal properties that make them highly attractive for use as reinforcements in composites. Some of the key properties of CNTs include:

- High Strength and Stiffness: CNTs possess exceptional tensile strength and stiffness, with values several times higher than those of steel and carbon fibers. When incorporated into epoxy composites, CNTs can significantly improve the mechanical properties of the resulting material, making it suitable for demanding functions that require high strength and stiffness (Maruyama, 2021).

- High Aspect Ratio: CNTs have an elevated aspect ratio (length-to-diameter ratio), which allows for efficient stress transfer between the matrix and reinforcement. This property contributes to the augmentation of mechanical properties in CNT-reinforced epoxy composites (Othman and Wilkinson, 2019).

- Lightweight: CNTs have a low density, making them an attractive reinforcement for lightweight composite materials. The incorporation of CNTs in epoxy composites can result in a reduction in overall weight while maintaining or improving mechanical properties (V. Harik, 2018).

1.2.3 Synergistic Effects of Carbon Nanotubes and Natural Fibers in Epoxy Composites

The combination of carbon nanotubes and natural fibers as reinforcements in epoxy composites can lead to synergistic effects that increase the overall performance of the resulting material. Some of the key benefits of using both CNTs and natural fibers in epoxy composites include:

- Balanced Mechanical Properties: The incorporation of CNTs can improve the strength and stiffness of epoxy composites, while natural fibers can contribute to enhanced toughness and impact resistance. This combination can result in a balanced set of mechanical properties that are tailored to meet the specific demands of various commercial applications (Avilés et al., 2018).

- Multifunctionality: The amalgamation of CNTs and natural fibers in epoxy composites can result in materials with multifunctional properties, such as enhanced mechanical performance, electrical conductivity, and thermal properties. This multifunctionality can enable the development of composites that meet the diverse requirements of different industries and applications (Pantano, 2018).

- Improved Interfacial Bonding: The presence of both CNTs and natural fibers can lead to improved interfacial bonding between the matrix and reinforcements, resulting in enhanced load transfer and overall composite performance. The high aspect ratio of CNTs allows for efficient stress transfer, while the surface chemistry of natural fibers can promote strong adhesion with the epoxy matrix (Jafari, 2018).

- Enhanced Durability: The combination of CNTs and natural fibers can result in epoxy composites with enhanced durability, particularly in terms of resistance to moisture, UV radiation, and other environmental factors. The hydrophobic nature of CNTs can help mitigate the moisture sensitivity of natural fibers, while the presence of natural fibers can provide UV resistance and improved thermal stability (Parameswaranpillai et al., 2023).

- Sustainability and Environmental Benefits: Incorporating natural fibers in epoxy composites can contribute to the overall sustainability and environmental performance of the material. The use of renewable and biodegradable natural fibers can help reduce the environmental impact associated with the extraction and processing of synthetic reinforcements, while the incorporation of CNTs can enhance the performance of natural fiber-reinforced composites, making them more competitive with traditional materials (Thakur et al., 2018).

1.3 Challenges and Considerations for the Development of CNT and Natural Fiber-Reinforced Epoxy Composites

While the combination of CNTs and natural fibers in epoxy composites offers significant potential for the development of high-performance, sustainable materials, there are quite a few challenges that must be considered. The challenges are as follows:

- Dispersion of CNTs: Achieving consistent dispersion of CNTs within the epoxy matrix is critical for optimizing their reinforcing effects. However, the agglomeration of CNTs because of van der Waals forces can make dispersion difficult. Various techniques, such as sonication, surfactants, and chemical functionalization, can be employed to enhance CNT dispersion within the epoxy matrix (Malekimoghadam and Rafiee, 2018).

- Compatibility and Interfacial Bonding: Ensuring compatibility and effective interfacial bonding among the epoxy matrix, CNTs, and natural fibers is crucial for maximizing composite performance. Surface treatments and chemical functionalization of CNTs and natural fibers can be employed to improve their compatibility and adhesion with the epoxy matrix (Jain, 2023).

- Processing Techniques: The development of effective processing techniques that can accommodate the combination of CNTs and natural fibers in epoxy composites is essential for the successful commercialization of these materials (Mavinkere Rangappa et al., 2022; Reshwanth et al., 2022; Shahzad, Teacă, and Tanasă, 2022; Tanasă et al., 2022).

- Cost and Availability: The cost and availability of CNTs and natural fibers can be a limiting factor for their widespread adoption in epoxy composites. Research into more cost-effective production methods for CNTs and the development of high-performance natural fibers with consistent quality and supply are critical for the commercial viability of CNT and natural fiber-reinforced epoxy composites.

In conclusion, the combination of Carbon Nanotubes and natural fibers as reinforcements in epoxy composites offers a promising avenue for the development of high-performance, sustainable materials for commercial applications. The synergistic effects of these reinforcements can lead to improved mechanical properties, multifunctionality, and enhanced durability, making them suitable for a wide range of industries and applications. However, addressing the challenges and considerations related to dispersion, compatibility, processing techniques, and cost will be crucial.

1.4 Applications of CNT and Natural Fiber-Reinforced Epoxy Composites

To fully harness the potential of CNT and natural fiber-reinforced epoxy composites, it is essential to identify suitable commercial applications that can benefit from their unique properties and performance characteristics. By understanding the requirements and challenges of different industries, researchers can tailor the development of these materials to address specific needs and unlock new market opportunities. This section will explore some of the potential commercial applications for CNT and natural fiber-reinforced epoxy composites across various sectors (Mohan and Rajmohan, 2017; Nourbakhsh, Ashori, and Kargarfard, 2016; Saiteja, Jayakumar, and Bharathiraja, 2020; Sapiai, Jumahat, and Mahmud, 2018; Shen et al., 2014; Thakur et al., 2018; Venkatachalam et al., 2023; H. Wang et al., 2019; Wu et al., 2019; Yang et al., 2015).

1.4.1 Aerospace Applications

The innovative, sustainable aircraft cabin interior panels made from natural fiber-reinforced epoxy composites offer significant advantages in the aviation industry, primarily due to their lightweight nature and reduced environmental impact. Remarkably, these pioneering panels can reduce carbon dioxide emissions by 6,000 kilograms per square meter, half the ecological, human health, and resource availability risks compared to traditional panels (Rahman et al., 2023). Companies are leveraging this potential, with Airbus collaborating with German biotech firm AMSilk to develop biocomposites based on spider silk that are both lighter and stronger (Mayank et al., 2022). Similarly, Boeing Research and Technology is actively investigating the use of biomaterials for aircraft interiors. The company has employed biodegradable polymers or recyclable plastics combined with plant fibers, such as flax, for interior panels and is also working on developing flax sandwich panels for aircraft cabins (Arockiam, Jawaid, and Saba, 2018).

1.4.2 Automotive applications

In the last few years, the automotive and aerospace industries have been constantly seeking lightweight, high-strength component to improve fuel efficiency and reduce greenhouse gas emissions in various components of vehicles, initially in Europe, followed by North America. These components include entry panels, compartment trays, hat holders, dashboard panels, internal engine covers, sunshades, and boot interiors, among others. Even seat rear sections and external undercarriage frameworks have also been replaced with natural fiber reinforced composites (Souza et al., 2020). Composite board, developed in India, has replaced railcar-evaluated medium-density fiberboard (Jagaba et al., 2022). CNT and natural fiber-reinforced epoxy composites can offer significant weight reduction compared to conventional materials, while maintaining or even improving mechanical performance.

1.4.3 Construction and Building Materials

The construction industry can greatly benefit from the utilization of CNT and natural fiber-reinforced epoxy composites because of their high strength, durability, and resistance to environmental degradation. In the United States, decking often utilizes fiber/PE or wood fiber/PP. Natural Fiber reinforced composites also find applications in wall insulation, floor

laminates, window frames, and doors. Comparative studies involving wood-plastic composites (WPCs) with 50% wood floor content, designed to evaluate the potential use of natural fiber composite sheet piles, revealed that NFCs deliver superior performance than timber laminates in insulating structural panels (Aliyu Yaro et al., 2022; Asyraf et al., 2020).

1.4.4 Sporting Goods and Consumer Products

CNT and natural fiber-reinforced epoxy composites have the potential to revolutionize the sporting goods such as bicycles, tennis rackets, golf clubs, and skis, by providing lightweight, high-performance materials with improved sustainability. Surfing appears to be leading the way in the sports realm in terms of incorporating environmentally friendly materials. There are now multiple companies promoting surfboards constructed with natural fiber composites. Among the early pioneers in this field was Laminations Ltd. Their "Ecoboard" stood out due to its use of a bio-based adhesive and hemp fiber (Jagaba et al., 2022). Also, fishing poles can be fabricated from the natural fiber reinforced polymer composites (Yusup, Mahzan, and Kamaruddin, 2019).

1.4.5 Renewable Energy

The renewable energy industry can leverage the unique properties of CNT and natural fiber-reinforced epoxy composites for numerous purposes. These composites can be used to fabricate wind turbine blades, where their lightweight, high-strength, and fatigue-resistant properties can contribute to improved efficiency and reduced maintenance costs. Furthermore, their ability to dampen vibrations can help enhance the operational lifespan of wind turbines (Batu, Lemu, and Sirhabizuh, 2020; Miliket et al., 2022).

1.4.6 Consumer Goods

CNT and natural fiber reinforced composites have been explored as viable replacements for synthetic fibers across an array of products. In the realm of consumer goods, they have been incorporated into toy manufacturing and packaging materials. In the maritime sector, these composites have found application in the construction of ship railings. The electronics industry is not left behind, with these composites being used in the fabrication of protective casings for electronic devices, spanning from laptops to mobile phones. This breadth of

application indicates a versatile potential for these sustainable materials (B. Kumar et al., 2021).

By identifying these potential commercial applications and assessing the requirements, challenges, and opportunities associated with each, this research aims to provide valuable insights into the potential market for CNT and natural fiber-reinforced epoxy composites. This information can be used to guide further research and development efforts, optimize material design and manufacturing processes, and ultimately contribute to the successful commercialization and adoption of these innovative materials in various industries.

1.5 Objectives of this Study

The objectives of the study are as follows:

(i) To prepare natural fiber-reinforced epoxy polymer composites with carbon nanotube as filler material.

(ii) To test the mechanical properties such as tensile strength, impact strength, flexural strength, and hardness of the fabricated composite.

(iii) To model the fabricated composite using Finite Element Method (FEM) and validate with experimental results.

1.6 Structure of the Thesis

Chapter 1: The introduction chapter provides the background and context of the research, discusses the motivation for the study, introduces CNTs and natural fibers as nanofillers, and outlines the research objectives. It also presents the structure of the thesis.

Chapter 2: The literature review chapter synthesizes previous research on natural fiber reinforced epoxy composites, CNT-reinforced epoxy composites, and natural fiber/CNT-epoxy composites. This chapter will highlight the advancements, challenges, and gaps in the existing literature, providing a foundation for the current research.

Chapter 3: The materials and methods chapter will detail the selection and preparation of natural fibers, synthesis of CNT-reinforced epoxy composites, and characterization of

composite properties. This chapter will also describe the experimental and computational design, data collection, and data analysis procedures.

Chapter 4: The results and discussions chapter will present the findings of the study, including the effects of CNT incorporation on the mechanical properties of natural fiber reinforced epoxy composites. The results will be analyzed in the context of the research objectives and hypotheses, as well as the existing literature.

Chapter 5: The conclusions chapter will summarize the main findings of the research, discuss the implications of the results, and suggest recommendations for future research.

CHAPTER 2
LITERATURE REVIEW

2.1 Introduction

This research delves into epoxy composites reinforced with carbon nanotubes and natural fibers. A comprehensive literature review is conducted to grasp the broader scientific context, focusing on the preparation methods of these composites, a detailed analysis of their mechanical properties, and the application of the Finite Element Method (FEM) for modeling and validation. By amalgamating insights from various studies, this chapter bridges past research with the present investigation, enhancing the existing knowledge base while identifying potential research avenues. This exploration reaffirms the study's significance in the evolving discourse on epoxy composites.

2.2 Natural Fiber Reinforcements

Natural fibers are obtained from plants, animals, or mineral sources, and their utility in numerous applications has been recognized for centuries. Known for their biodegradability, low density, and availability, these fibers have been broadly explored for various uses. In the plant kingdom, a diverse range of fibers is found. Some examples include jute, flax, hemp, and sisal, among others. Derived primarily from the bast (or skin) of plants, these fibers exhibit a unique set of properties that make them particularly useful in many applications. In recent years, their potential in reinforcing polymer composites has been the subject of considerable interest. It has been found that their addition can enhance the mechanical properties of the developed composites, even though they might not possess the same strength or stiffness as synthetic counterparts (Chandramohan and Marimuthu, 2011).

Animal-derived fibers, such as wool, silk, and hair, have also been utilized for centuries, predominantly in the textile industry. Their warmth, resilience, and natural aesthetics make them preferred choices in many applications. They are typically protein-based, and although their use in composite materials is less prevalent than plant fibers, research into their potential for such applications is ongoing (Veit, 2023b).

Mineral fibers, such as asbestos, were once widely used due to their heat and fire resistance. However, their use has dramatically declined because of health concerns. Other mineral fibers, like basalt and glass, while not 'natural' in the traditional sense, are derived from abundant natural resources and thus often grouped with natural fibers(Dhaliwal, 2019).

In the quest for sustainable and green technologies, the utilization of natural fibers is becoming increasingly attractive. Their eco-friendly nature, along with their natural abundance and renewability, positions them as potential alternatives to synthetic materials. However, challenges remain, including their natural variability, moisture absorption, and compatibility with different matrix materials (Kicińska-Jakubowska, Bogacz, and Zimniewska, 2012). Despite these challenges, the prospective application of natural fibers involving polymer matrix composites in a variation of uses, remains a subject of intense research and development.

Some important information from literature regarding chemical treatment of natural fibers, mechanical properties of natural fiber reinforced as well as natural fiber and CNT reinforced composites along with mechanical properties of each variant of different natural fibers are presented in tabular forms. Table 2.1 represents the internal construction of some natural fibers in the existing literature. Table 2.2 represents the treatment parameters and observed effects of different natural fibers. Table 2.3 represents the mechanical properties of different natural fiber reinforced composites. Table 2.4 illustrates some key observations for natural fiber and CNT reinforced polymer composites. Table 2.5 illustrates some mechanical properties of each variant of different natural fibers.

2.2.1 Structure of Natural Fibers

Natural fibers, fundamental building blocks in the plant world, are constituted primarily of cellulose, lignin, and hemicellulose. These biopolymers, inherently complex in structure, significantly influence the mechanical properties and functional utility of the fibers. The internal structure of natural fibers is illustrated in Fig 2.1.

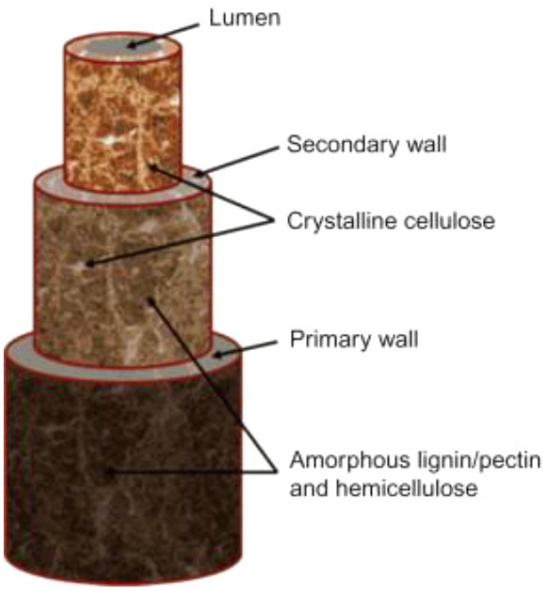

Fig 2.1: Internal structure of natural fibers (Bhattacharyya, Subasinghe, and Kim, 2015).

Cellulose is the utmost plentiful biopolymer on the planet, serving as the fundamental structural element of the plant cell walls. Its structure is characterized by elongated, straight chains of D-glucose units linked through β-1,4-glycosidic bonds (Bhattacharyya, Subasinghe, and Kim, 2015). These chains form a highly ordered crystalline structure because of the existence of numerous intra and intermolecular hydrogen bonds. This strong hydrogen bonding imparts high tensile strength and stiffness to the cellulose fibers, making the fibers an appealing reinforcement material in composite uses.

Lignin, the second most abundant natural polymer, provides rigidity and resistance against microbial attacks to the plant cell wall. Unlike cellulose, lignin is a complex, amorphous polymer composed of phenylpropane units, making its structure highly irregular and diverse. This non-uniform structure contributes to its role as a binder, packing spaces within the cell wall between cellulose and hemicellulose and thus adding rigidity and resistance to compression (Veit, 2023a).

Hemicellulose, on the other hand, is a shorter-chain polysaccharide compared to cellulose, composed of different sugar units including glucose, xylose, mannose, and others. Unlike the crystalline structure of cellulose, hemicellulose has a random, branched structure, making it amorphous. It works as a bridge between cellulose as well as lignin in the plant cell wall, contributing to the overall strength and flexibility of the fibers (Fuqua, Huo, and Ulven, 2012).

Table 2.1: Internal formation of several natural fibers

Fiber	Cellulose (%)	Hemicellulose (%)	Lignin (%)	Reference
Banana	64	19	5	(Adeniyi, Ighalo, and Onifade, 2019)
Coir	42.1	15.2	35.3	(Siakeng et al., 2018)
Flax	62-72	16-18	2-2.5	(Siakeng et al., 2018)
Hemp	67-75	16-18	3.8-3.3	(Cheung et al., 2009)
Jute	59-71	12-13	12-13	(Cheung et al., 2009)
Luffa	57-66	17-30	15-20	(Anbukarasi and Kalaiselvam, 2015)
Kenaf	31-57	18-24	8-13	(Siakeng et al., 2018)
Oil palm	43.7	29.02	13.13	(Cheung et al., 2009)
Pineapple	70-82	18-18	5-12	(Siakeng et al., 2018)
Sugarcane	32-55	27-32	19-25	(Karp et al., 2013)

The interplay of cellulose, hemicellulose along with lignin in the fiber formation contributes to the final properties of the natural fibers. These properties, including tensile strength, stiffness, and thermal stability, are further influenced by the comparative quantities and arrangement of these elements in the fiber. However, variability in these structures, due to species differences and growth conditions, often results in variability in fiber properties. This natural variability presents a challenge in the usage of natural fibers in composites. Despite these challenges, the significant potential of natural fibers in sustainable material applications continues to drive extensive research and development efforts (S. Kumar, Manna, and Dang, 2022).

2.2.2 Treatments for Natural Fibers

Natural fibers, acquired from plant or animal origins, have been increasingly explored as reinforcing agents in polymer matrix composites because of their obtainability, renewability, and environmental affability. However, their hydrophilic nature, variability in properties, and impoverished adhesion to hydrophobic polymer matrix can often limit their potential applications. To mitigate these issues, various treatment methods are incorporated to amend the surface characteristics of natural fibers. Among different treatment approaches, such as physical, biological and chemical treatment methods, chemical treatments are commonly utilized to enhance the quality of natural fibers (Akhil et al., 2023).

It was observed from literature that Alkali treatment is among the utmost common techniques for chemical treatment of natural fibers (CHICHANE, BOUJMAL, and El BARKANY, 2023). In this process, the fibers are submerged in an alkali solution, typically NaOH. It results in the elimination of lignin, hemicellulose, and additional non-cellulosic counterparts from the exterior of the fiber. Particularly, hemicellulose is more vulnerable to alkaline hydrolysis compared to cellulose because of its amorphous construction and lower degree of polymerization. As non-cellulosic components are largely accountable for the hydrophilic behavior of various natural fibers, their removal decreases fibers' water absorption capacity and enhances their affinity with hydrophobic polymer (Jagadeesh et al., 2022). Furthermore, it increases the fiber's surface roughness resulting from the consequence of partial removal of surface layers, leading to a fibrillated structure. The increased roughness enhances the mechanical interlocking involving the fibers and the polymer matrix, which can significantly enhance the mechanical properties of the fabricated composites (Alarifi, 2023).

Table 2.2: Chemical treatment parameters of various fibers

Fiber	Matrix	Chemical	Conc (wt.%)	Time (mins)	Temp (°C)	Observation	Reference
Banana	PP	NaOH	5	300	25	Increased tensile, flexural and impact properties	(Komal et al., 2018)
Banana	PE	NaOH	4	240	25	Decreased water absorption properties	(Kumari, Rai, and Kumar, 2018)
Coir	Epoxy	NaOH	5	30	20	Increased mechanical properties	(Yan et al., 2016)
Coir	Epoxy	NaOH	10	900	25	Enhanced mechanical properties	(Oliveira et al., 2018)
Jute	Epoxy	NaOH	5	60	25	Increased mechanical properties	(Jothibasu et al., 2020)
Jute	PLA	NaOH + Silane	5	120	25	Reduced fiber crystallinity, intensified mechanical properties	(Zafar, Maiti, and Ghosh, 2016)
Jute	PVE	NaOH	5	240	30	Enhanced mechanical and electrical properties	(Sudha and Thilagavathi, 2018)
Kenaf	PE	NaOH	6	720	25	Increased mechanical properties	(Yong et al., 2015)
Kenaf	PF	Silane	2	180	25	Increased mechanical properties	(Asim et al., 2018)
Kenaf	Epoxy	NaOH	6	180	25	Intensified mechanical properties	(Asim et al., 2016)
Pineapple	Epoxy	NaOH	6	180	25	Increased mechanical properties	(Asim et al., 2016)
Pineapple	PF	Silane	2	180	25	Improved mechanical properties	(Asim et al., 2017)
Pineapple	PP	NaOH	5	150	70	Increased mechanical properties	(Das, Rahman, and Hasan, 2018)
Sisal	PE	NaOH	5	30	30	Decreased water absorption properties	(Gupta and Singh, 2019)
Sisal	Epoxy	NaOH	6	1440	25	Enhanced insulation properties	(Jabbar and Jabbar, 2017)
Sisal	PLA	Silane	2	180	25	Increased mechanical properties	(Orue et al., 2016)
Sisal	PE	NaOH	10	1440	25	Reduced water absorption and increased mechanical properties	(Prasanna Venkatesh, Ramanathan, and Srinivasa Raman, 2016)

PP - Polypropylene; PE - Polyester; PLA- Poly Lactic Acid; PVE-Polyvinyl ester; PF-Phenolic Formaldehyde

Table 2.3: Mechanical properties of natural fiber reinforced polymer composites

Matrix	Fiber	Fabrication Method	Flexural strength (MPa)	Impact Strength (kJ/m^2)	Tensile strength (MPa)	Reference
Epoxy	Bagasse	Hand lay-up	56.70	110.66	42.40	(D. Verma et al., 2012)
Epoxy	Jute	Hand lay-up	55.8	65	43	(S. S. Kumar, 2020; Mishra and Biswas, 2013)
Epoxy	Hemp	Hand lay-up	39.24	-	40.66	(Hasan and Rayyaan, 2014)
Epoxy	Abaca	Hand lay-up	-	-	21.67	(Sinha, Narang, and Bhattacharya, 2018)
Epoxy	Sisal	Hand lay-up	52.80	56.70	37.4	(Joseph et al., 1999)
Epoxy	Pineapple	Hand lay-up	-	94.6	66.40	(Mittal and Chaudhary, 2018)
Epoxy	Banana	Hand lay-up	76.73	149.66	59	(Mittal and Chaudhary, 2018)
Epoxy	Coir	Hand lay-up	46.63	26.43	23.68	(Sapuan et al., 2006)
Epoxy	Oil Palm	Vacuum assisted RTM	-	-	6.95	(Sarikaya, Çallioğlu, and Demirel, 2019)
Epoxy	Ramie	Vacuum assisted RTM	90	84	72	(Athijayamani et al., 2009)
Polyester	Coir	Compression molding	3.60	-	-	(Monteiro, Terrones, and D'almeida, 2008)
Polyester	Hemp	Compression molding	49.09	-	31.46	(Neves et al., 2020)
PP	Bamboo	Hand lay-up	30	26.80	22.70	(Gu et al., 2018)
PP	Pineapple	Hand lay-up	13.67	-	15.67	(Alzebdeh, Nassar, and Arunachalam, 2019)
PP	Coir	Hand lay-up	21.5	47 J/m	-	(Mir et al., 2013)
PP	Glass	Compression molding	46.58	32.56	21.57	(Ray et al., 2020)
PP	Sisal	Compression molding	44.84	40.45	20.81	(Ray et al., 2020)
PP	Jute	Compression molding	50.64	30.05	21.44	(Ray et al., 2020)

Table 2.4: Key observations for natural fiber and CNT reinforced polymer composites

Matrix	Fiber	Observations	Reference
Epoxy	Bamboo	The authors experimented with varying MWCNT from 0 wt.% to 3 wt.% and observed that maximum tensile strength was 33 MPa and maximum flexural strength was 80 MPa for 3 wt.% CNT. The maximum tensile strength was increased by 22.22% and maximum flexural strength was increased 33.33% when CNT was added. However, no dispersion study for CNT was carried out. Moreover, other mechanical and physical properties were absent in the study.	(Thakur et al., 2018)
Epoxy	Flax	The authors carried out an experiment with varying MWCNT from 0 wt.% to 3 wt.% and stated that maximum tensile strength of 43 MPa and maximum tensile modulus of 3.75 GPa was obtained when 1 wt.% CNTs was used. The increase in tensile strength was 12.5 % and Young's modulus was 19% relative to composites without CNT. CNTs were dispersed with sonication and dispersion effect was visible.	(H. Wang et al., 2019)
Epoxy	Kenaf	The authors tested tensile and flexural properties with varying CNT from 0 wt.% to 1 wt.%. They observed that the inclusion of CNT effected with decreased tensile strength, Young's modulus, flexural strength and flexural modulus whereas impact strength increased with addition of CNT. The dispersion effect was not carried out, however they predicted that the tensile and flexural properties decreased because of poor dispersion of CNT.	(Sapiai, Jumahat, and Mahmud, 2018)
Epoxy	Bamboo	The authors experimented with tensile, flexural and impact properties along with water absorption of the composites with 0.15 wt.% of plasma treated MWCNT. It was observed that, tensile strength, Young's modulus, flexural strength, flexural modulus and impact strength increased 6.67%, 2.7%, 5.8%, 31% and 84.5% respectively. Also, the addition of CNT resulted in reduced water absorption of 23.18%. However, they did not analyze with varying CNT, therefore, their study did not have dispersion effect. Also, regression equations were not discussed.	(P. K. Kushwaha, Pandey, and Kumar, 2014)

Table 2.4 (Continued)

Matrix	Fiber	Observations	Reference
Epoxy	Ramie	The authors carried out tensile and flexural testing with CNT grafted Ramie fiber with varying MWCNT from 0 wt.% to 1 wt.%. It was observed that the tensile and flexural properties increased with incorporation of CNT up to 0.7 wt.% of CNT. After that strengthening CNT brought about a slight reduction in those properties. However, other mechanical and physical properties were absent in the study. Also, regression equations were not discussed.	(Dilfi KF, Che, and Xian, 2019)
Epoxy	Hemp	The authors tested tensile properties with varying CNT from 0 vol.% to 4 vol.% and documented an increase in tensile strength of maximum 30.02 MPa for increasing CNT vol.%. However, other mechanical and physical properties were absent in the study. Also, regression equations were not discussed.	(Longkullabutra, Thamjaree, and Nhuapeng, 2010)
Epoxy	Coir and fly ash	The authors carried out tensile testing with varying CNT wt.% from 0 to 1 and reported that the maximum tensile strength of 19.574 MPa resulted from addition of 1 wt.% of CNT and maximum Young's modulus was obtained with 0.25 wt.% CNT. Other mechanical and physical properties were absent in their study. Moreover, the effect of agglomeration was not discussed.	(Venkatachalam et al., 2023)
Epoxy	Agave Cantala	The authors conducted tensile strength, flexural strength, and impact energy testing with varying CNT from 0 wt.% to 1 wt.%. They documented that the maximum tensile strength of 51 MPa and flexural strength of 53 MPa was due to the addition of 1 wt.% CNT. But maximum impact energy was measured to 56.3 KJ/m^2 at 0.17 wt.% CNT. However, other mechanical and physical properties were absent in the study. Also, regression equations were not discussed. Effect of agglomeration was also absent in their study.	(Bellairu et al., 2022)
Epoxy	Ramie	The authors investigated flexural strength and flexural modulus with varying CNT from 0 wt.% to 0.6 wt.% and reported 34 and 37% increase respectively at 0.6 wt.% CNT. However, other mechanical and physical properties were absent in the study. Also, regression equations were not discussed. Effect of agglomeration was also absent in their study.	(Shen et al., 2014)

Table 2.4 (Continued)

Matrix	Fiber	Observations	Reference
PP	Poplar	The authors experimented tensile, flexural and impact properties varying MWCNT from 0 to 3.5 wt.% and reported maximum tensile strength of 63.2 MPa, maximum Young's modulus of 3.89 GPa, maximum flexural strength of 45 MPa, and maximum flexural modulus of 3.5 GPa for 2.5 wt.% MWCNT. Maximum impact energy of 35 J/m was reported for addition of 1.5 wt.% of MWCNT. However, other mechanical and physical properties were absent in the study. Also, regression equations were not discussed.	(Nourbakhsh, Ashori, and Kargarfard, 2016)
PP	Bagasse	The authors experimented tensile, flexural and impact properties varying MWCNT from 0 to 3.5 wt.% and reported maximum tensile strength of 44.3 MPa, maximum Young's modulus of 2.77 GPa, maximum flexural strength of 37 MPa, and maximum flexural modulus of 3.5 GPa for 2.5 wt.% MWCNT. Maximum impact energy of 26 J/m was reported for addition of 2.5 wt.% of MWCNT. However, other mechanical and physical properties were absent in the study. Also, regression equations were not discussed.	(Nourbakhsh, Ashori, and Kargarfard, 2016)
Epoxy	Jute	The authors tested tensile, flexural and impact strength by varying MWCNT from 2 to 10 vol.% and documented maximum tensile strength of 36 MPa at 6 vol.% CNT, maximum flexural strength of 22 MPa at 8 vol.% CNT and maximum impact strength 1200 J/m^2 at 6 vol.% CNT. However, other mechanical and physical properties were absent in the study. Also, regression equations were not discussed.	(Saiteja, Jayakumar, and Bharathiraja, 2020)
Epoxy	Flax, Jute, and Banana	The authors investigated tensile strength, tensile modulus along with Brinell hardness number with varying CNT from 0 wt.% to 1 wt.% and reported maximum tensile strength of 222 MPa, tensile modulus of 1.3 GPa and maximum hardness number of 64 at 1wt.% CNT. However, other mechanical and physical properties were absent in the study. Also, regression equations were not discussed. Agglomeration effect was not visible in this study.	(Mohan and Rajmohan, 2017)

Table 2.4 (Continued)

Matrix	Fiber	Observations	Reference
Polyurethane	Cotton	The authors conducted tensile strength testing with varying CNT from 5 wt.% to 8 wt.%. They documented that the maximum tensile strength of 30 MPa was due to the addition of 6 wt.% CNT. However, other mechanical and physical properties were absent in the study. Also, regression equations were not discussed.	(Wu et al., 2019)
PLA	Bassalt	The authors investigated tensile strength, tensile modulus along with elongation at break with 0 and 1 wt.% CNT and reported maximum tensile strength of 75 MPa, tensile modulus of 2.7 GPa at 1 wt.% CNT and minimum elongation at break of 2.1% at 1wt.% CNT. However, other mechanical and physical properties were absent in the study. Also, regression equations were not discussed. Agglomeration effect was not visible in this study.	(Yang et al., 2015)
PLA	Kenaf	The authors tested tensile and impact strength by varying MWCNT from 0 to 1 wt.% and documented maximum tensile strength of 91.5 MPa and maximum impact strength 44.9 J/m at 1 wt.% CNT. However, other mechanical and physical properties were absent in the study. Also, regression equations were not discussed. Agglomeration effect was not visible.	(Chen et al., 2017)

Table 2.5: Mechanical properties of each variant of different natural fibers

Alternatives	Code	Attributes				Alternatives	Code	Attributes			
		Tensile strength (MPa)	Density (g/cm3)	Young's modulus (GPa)	Elongation at break (%)			Tensile strength (MPa)	Density (g/cm3)	Young's modulus (GPa)	Elongation at break (%)
Banana	A1	721.5	1.4	29.5	7	Pineapple	H1	1020	1.74	71	14.5
	A2	500	1.35	12	5.25		H2	513.5	1.2	1.44	2
	A3	355	1.35	33.8	5.3		H3	898.5	1.5	82	14.5
Bagasse	B1	256	1.25	22.05	1.1		H4	513.5	1.2	1.44	10.3
	B2	256	1.25	22.05	1.1	Flax	I1	922.5	1.5	25.75	2.4
	B3	290	1.2	17	1.1		I2	1087.5	1.5	18	2.25
	B4	155	1.2	23.4	1.01		I3	1171.5	1.45	53.5	2.25
Cotton	C1	543.5	1.55	9.05	6.5		I4	672	1.5	65.3	2.2
	C2	543.5	1.55	9.25	6.5		I5	690	1.5	27	2.95
	C3	543.5	1.55	9.05	7.5		I6	1172.5	1.45	27.6	2.25
	C4	442	1.5	9.05	6.5		I7	690	1.5	65.3	2.95
	C5	543.5	1.55	9.05	6.5		I8	1150	1.4	27.6	1.4
	C6	400	1.51	12	7.5		I9	690	1.5	70	2.95
	C7	442	1.55	16.75	6.83		I10	922.5	1.45	27.6	2.6
Ramie	D1	669	1.28	86	4.6		I11	916.85	1.48	63.8	2.42
	D2	469	1.5	86	2.6	Hemp	J1	690	1.45	65	2.8
	D3	669	1.5	57	2.6		J2	830	1.5	46	3
Ramie	D4	445	1.28	76.25	2.5	Hemp	J3	585	1.45	64	2.25
	D5	700	1.28	76.25	2		J4	644.5	1.48	56.75	1.6
	D6	700	1.5	24.5	2.5		J5	585	1.45	35	1.6
	D7	560	1.5	44	2.8		J6	690	1.48	56.75	1.6
	D8	500	1.5	94.7	2.8		J7	725	1.48	70	1.6
	D9	669	1.42	68.09	2.8		J8	690	1.48	70	2.06
Coir	E1	212	1.2	5	27.5		J9	805.5	1.49	70	2.06
	E2	175.5	1.2	5	33.2		J10	693.9	1.47	70	2.06
	E3	162.5	1.31	5	33.2						

Table 2.5 (continued)

Alternatives	Code	Attributes				Alternatives	Code	Attributes			
		Tensile strength (MPa)	Density (g/cm3)	Young's modulus (GPa)	Elongation at break (%)			Tensile strength (MPa)	Density (g/cm3)	Young's modulus (GPa)	Elongation at break (%)
Coir	E4	162.5	1.31	4.4	30	Sisal	K1	495	1.43	17.4	5
	E5	175	1.2	4.4	20		K2	681	1.4	18.7	4.5
	E6	220	1.25	5	30		K3	531.5	1.42	23.5	2.25
	E7	175	1.2	6	27.5		K4	573	1.5	15.7	4.5
	E8	153	1.17	5	28.8		K5	531.5	1.42	23.5	2.25
	E9	179.4	1.23	6.5	28.8		K6	573	1.5	15.7	2.5
Jute	F1	586.5	1.38	21.5	1.9		K7	650	1.33	38	2.25
	F2	277	1.4	32.5	1.4		K8	573	1.5	15.7	4.5
	F3	596.5	1.4	43	1.65		K9	575.5	1.48	15.7	3.47
Jute	F4	560	1.4	55	1.65	Kenaf	L1	737.5	1.5	40.5	2.55
	F5	596.5	1.46	26.5	1.65		L2	361	1.19	57	2.1
	F6	583	1.3	43	1.65		L3	576.5	1.4	33.75	1.6
	F7	560	1.4	26.5	1.8		L4	930	1.45	53	2.1
	F8	583	1.3	20	1.65		L5	576.5	1.4	33.75	1.6
	F9	600	1.46	26.5	1.48		L6	930	1.3	53	4.25
	F10	583	1.3	36.5	1.65		L7	612.5	1.3	53	1.6
	F11	550	1.4	33.1	1.65		L8	930	1.2	53	2.25
Bamboo	G1	216.5	0.75	29	1.3		L9	585	1.34	33.5	2.26
	G2	470	0.85	21.5	3.1						
	G3	470	0.85	21.5	3.1						
	G4	185	0.85	14	2.5						

The alkali treatment also induces changes at the molecular level. It results in a rise in the number of cellulose crystallites owing to the elimination of amorphous hemicellulose. This contributes to an intensification of the crystallinity index of the fiber, which may enhance the mechanical characteristics of the fiber itself (Zwawi, 2021).

However, the effectiveness of the alkali treatment relies on several factors, including the intensity of the alkali solution, treatment duration, and temperature. High concentrations and longer treatment durations can lead to excessive removal of hemicellulose and even damage the cellulose structure. Therefore, optimization of these parameters is crucial to achieve the desired fiber properties without confronting the consistency of the cellulose structure (Birniwa et al., 2023).

The introduction of NaOH into natural fibers has positive effects on overall composite structure. It was observed that NaOH encouraged the ionization of the hydroxyl group into an alkoxide and brought about better mechanical properties (Valadez-Gonzalez et al., 1999). Silveira et. al. analyzed a combination of alkaline treatment and graphene oxide coating in hemp fibers for engineering applications (da Silveira et al., 2022).

Acetylation is another chemical treatment wherein the hydroxyl groups in the cellulose get replaced with acetyl groups, thereby reducing fiber's hydrophilicity. Silane treatment, in contrast, affects the foundation of a coupling agent on fiber surface, enabling reaction both with the hydrophilic fiber as well as the hydrophobic polymer matrix, and improve their interfacial adhesion (Murugan et al., 2020).

An innovative methodology for silane treatment for flax fiber to enhance interfacial adhesion in developed epoxy composites was investigated by Fathi et. al. A unique silane treatment technique was introduced, eliminating the need for pre-hydrolysis as well as curing/dehydration of silanol groups (Fathi et al., 2019). The main goal of Aphichartsuphapkhajorn et. al. was to enhance the mechanical characteristics of the composites, specifically concentrating on treatment approaches (Aphichartsuphapkhajorn, Arao, and Kubouchi, 2019).

In addition to chemical treatments, physical methods like corona treatment or plasma treatment can also be used. These treatments modify the fiber surface by creating functional groups that can improve adhesion with the polymer matrix. Moreover, they do not rely on

the use of chemicals, making them more environmentally friendly. Sari et. al., focused on the impact of plasma alteration of polyethylene on natural fiber composites manufactured through rotational molding. The production of composite employed a rotational molding technique (Sari et al., 2019). The exploration carried out on Ramie fiber aimed at quantifying the effects of plasma-surface adjustment on ramie plant fibers, positioning it as a potentially effective means for straightforward as well as effective surface adjustment (Hamad et al., 2019).

Biological treatments using enzymes or fungi have also been explored. These treatments can selectively degrade the non-cellulosic components of the fiber, leading to an enrichment of cellulose and potentially improving the fiber's mechanical properties (Koohestani et al., 2019).

Overall, the treatment of natural fibers has a vital contribution in optimizing their performance as reinforcements in polymer composites. Also, it assists to conquer some of the inherent limitations of natural fibers, including their hydrophilicity and poor affinity with polymer matrices. These methods, whether they are chemical, physical, or biological, enable the enhancement of natural fiber-reinforced polymer composites with improved properties along with broader application possibilities.

2.2.3 Specific Mechanical Properties of Natural Fibers

The mechanical properties of natural fibers have drawn considerable attention due to their potential as ecological, renewable substitutes to synthetic fibers in various purposes. These mechanical characteristics include tensile strength, modulus of elasticity (stiffness), elongation at break (ductility), and impact strength, among others.

Tensile strength, the capacity of a material to resist breaking under tension, varies among different varieties of natural fibers. For instance, it was observed that flax fibers possessed high tensile strength, even rivaling that of certain synthetic fibers. This property is largely attributed to their high cellulose content and crystallinity (Samant et al., 2023).

The modulus of elasticity, the degree of a material's stiffness or resistance to elastic deformation, is another critical mechanical property of natural fibers. The specific values depend on the type of fiber, with fibers like hemp and flax exhibiting relatively high moduli due to their high cellulose content and orientation. This property makes these fibers

attractive for applications where rigidity is desired (Palanikumar, Thiagarajan, and Latha, 2022).

The elongation at break, or ductility, represents the capability of the fiber to deform without breaking. While this varies among natural fibers, in general, they exhibit lower elongation at break relative to synthetic fibers. This is due to the highly ordered, crystalline structure of cellulose, which restricts deformation (D. Verma and Senal, 2019).

Impact strength, the competence of a material to resist impact without shattering, is also a significant consideration in the use of natural fibers. It was observed that while generally lower compared to their synthetic complements, certain bio fibers like sisal and jute demonstrated decent impact strength (Gholampour and Ozbakkaloglu, 2020).

It's worth noting that these mechanical properties can be affected by a variety of factors. These include the fiber's source (species, part of the plant, etc.), extraction process, and any post-processing or treatment methods applied. For instance, treatments such as alkalization can affect the mechanical properties by altering the fiber surface and improving compatibility with a matrix material.

Despite their advantageous mechanical properties, natural fibers also present challenges such as moisture absorption, which can lead to swelling and affect mechanical properties, and variability in properties due to natural sources. As a result, ongoing research is focused on overcoming these challenges to further broaden the applicability of natural fibers in countless industrial applications.

2.2.4 Factors Controlling Mechanical Properties of Natural Fibers

A myriad of factors influences the mechanical properties of plant fibers, including their biological source, extraction process, and post-harvest treatments.

- **Biological Source**: The biological source of plant fibers, including the species of the plant, age, and segment of the plant from where the fiber is obtained, significantly affects the fiber's mechanical properties. For instance, flax fibers demonstrate high tensile strength and stiffness (Goudenhooft, Bourmaud, and Baley, 2019).

- **Extraction Process**: The method employed for extracting the fibers from the plant can also affect their mechanical properties. Retting, a common extraction method, involves the use of bacteria and moisture to break down the pectin holding the fibers together. Different retting methods, such as water, chemical, or enzymatic retting, can influence the quality and, consequently, the mechanical properties of the fibers (Derrouiche et al., 2015).

- **Maturity of Plant**: The age or maturity of the plant at the time of fiber extraction can affect the mechanical properties of the resultant fibers. Generally, mature plants yield fibers with higher mechanical properties because of the higher cellulose amount and intensity of polymerization (Hameed, 2016).

- **Fiber Morphology**: The physical structure of the fiber, such as its diameter, length, and surface characteristics, can affect its mechanical properties. Longer fibers with fewer defects often display higher tensile strength because of the increased continuity of the cellulose chains (Mazzanti et al., 2019).

- **Post-Harvest Treatments**: Post-harvest treatments, such as drying, mercerization, or bleaching, can alter the mechanical properties of plant fibers. These treatments can remove impurities, modify the surface, or change the chemical structure of the fibers, thereby affecting their interaction with other materials (in the case of composites) and their overall mechanical performance (J. Li et al., 2019).

- **Environmental Conditions**: Environmental factors, like humidity and temperature, can impact the mechanical properties of plant fibers. High humidity can lead to moisture absorption, causing swelling and a reduction in mechanical properties (Karimah et al., 2021).

- **Chemical Composition**: The relative composition of cellulose, hemicellulose, and lignin in the fibers influences their mechanical properties. Higher cellulose content often results in improved tensile strength and stiffness, while lignin content can affect the fiber's hardness and resistance to microbial degradation (Alotaibi et al., 2019).

Understanding these controlling factors is critical in the development of plant fiber-based materials, allowing for the customization of fiber properties for specific applications.

However, the inherent variability in natural fibers presents a challenge, necessitating ongoing research to fully exploit their potential in various industrial applications.

Table 2.2 represents some of the mechanical properties of the natural fiber reinforced polymer composites in the existing literature.

2.3 Selection of Natural Fibers

Choosing constituent materials for a composite entails various factor, with the primary challenge being the ranking of the utmost efficient solution from available alternatives. The use of Multi-Criteria Decision-Making (MCDM) techniques can also be suggested for the selection of composite material constituents, as they provide pragmatic advice to decision-makers from a set number of substitutes. Numerous fuzzy MCDM models estimate the performance of substitutes, thereby offering the most advantageous solution amongst various choices.

2.3.1 The Evaluation of Criteria Weight Using the Fuzzy AHP Method

The AHP method, originated by Thomas L. Saaty, is recognized as one of the most renowned MCDM techniques for assessing substitutes via a criteria order (Saaty Thomas, 1980). Rather than making an exact decision, this tactic was designed to offer the optimal answer to an MCDM issue. Not only did it depict and quantify elements of a problem, but it also linked them to broader objectives and evaluated varying solutions (Mitra et al., 2015).

The Fuzzy AHP, using a hierarchy order in which the decision substitutes are placed at the bottom, followed by sub-criteria, criteria, and objectives sequentially one after another into the top, delivered the most agreeable solution to an MCDM issue without the need for precise input. This method was utilized in the resolution of numerous MCDM problems related to material selection. The AHP model was utilized by Salwa et al. to choose the optimal natural fiber out of nine regarding food packing objectives. Furthermore, sensitivity testing of the scheme was conducted and a stable preference for orderliness was obtained (Salwa et al., 2019). The AHP scheme was employed to determine the priority of criteria to choose a composite regarding structural utilization (Patnaik et al., 2020). The fuzzy AHP scheme was applied to assign priority to criteria for a MCDM issue of merchant

selection (Chatterjee and Stević, 2019). Again, fuzzy AHP scheme was used to discern the highest critical attribute for competent web application safety (R. Kumar, Agrawal, and Khan, 2020). The fuzzy AHP scheme was integrated for evaluation of data reliability for healthcare data (Zarour et al., 2021).

2.3.2 The Evaluation of Natural Fibers' Order of Preferences Using the Fuzzy TOPSIS Method

Introduced by Hwang and Yoon in 1981, the TOPSIS scheme was employed because of the following causes (Zeleny, 2012): a. The theory of TOPSIS was simple, comprehensible, and computations were effortlessly performable, b. The approach of TOPSIS facilitated the pursuit of the best preferences for every single criterion in simple algebraic expressions, c. The importance could be integrated using different schemes like Entropy or AHP, and the relative order of priority can be effortlessly executed. The TOPSIS method addressed numerous material selection related MCDM problems and other engineering aspects.

Numerous MCDM issues related to material selection were solvable using the TOPSIS method. Further, TOPSIS and combined AHP-TOPSIS approaches were effective in tackling MCDM problems across different facets of engineering. A TOPSIS analysis was carried out by Mansor et al. to find out the preference order among three different thermosetting matrices regarding motorized bumper beam application (Mansor et al., 2014). The TOPSIS approach was implemented by Amarnath et al. to discern the optimal solution for flax fiber components in composites (Amarnath, Babu, and Kumar, 2021). The fuzzy TOPSIS approach was utilized by Kushwaha et al. to rank system failures for a sugar mill company's cutting system (D. K. Kushwaha, Panchal, and Sachdeva, 2020). The fuzzy TOPSIS approach was employed to prioritize merchants regarding dairy product delivery (Cakar and Çavuş, 2021). The unified fuzzy AHP-TOPSIS approach was adopted to pinpoint most effective procedure regarding software consistency estimation (Sahu et al., 2021). An unified fuzzy AHP-TOPSIS approach was utilized for rating the instruments and strategies regarding safety measures in consultation facilities (Alosaimi et al., 2021). The same approach was applied for assessing several confidentiality conditions in healthcare administration (Ansari et al., 2021). An unified fuzzy AHP-TOPSIS approach was used to prioritize security risks in healthcare management web applications (Alharbi et al., 2021).

2.3.3 Sensitivity to the Stimulated Disruption to Attribute Weightages

Sensitivity assessment, progressively frequent in engineering as well as other applications, is a necessary measure to check feasibility for a developed technique or model (Ionescu-Bujor and Cacuci, 2004). It is crucial to conduct a sensitivity assessment of the MCDM approaches to ascertain constancy of the achieved order of priority. Sensitivity was characterized as "to ascertain how a given model (numerical or otherwise) depends on its input factors" (Saltelli et al., 2005). A sensitivity assessment of the criteria importance for TOPSIS approach, as utilized in the evaluation of water condition, was conducted by Li et al. who documented the applicability of the TOPSIS approach given its sensitivity to criteria weights (P. Li et al., 2013). A similar approach was undertaken for assessing the stability of the derived preference order in the study conducted to assess policies against floods, where they used Monte Carlo simulation and obtained an understanding of the stable conditions (da Silva, Alencar, and de Almeida, 2022).

2.4 Polymer Matrix Material

The polymer matrix serves as the backbone of a composite material, enveloping and binding the reinforcing fibers together and translating the applied stress across the composite. This continuous phase, when chosen and processed correctly, not only dictates the composite's overall performance but also provides protection to the embedded fibers (Sharma et al., 2020).

The nature of the polymer matrix is mainly characterized by its chemical composition, molecular structure, and physical properties, all of which play a crucial role in defining the composite's attributes. For instance, thermosetting polymers, including epoxy resins, unsaturated polyester resins, and polyurethane, are often used as matrices due to their excellent thermal stability, chemical resistance, and mechanical properties. A comprehensive review was conducted on the progress of thermosetting polymers with concluding remarks of epoxy resin being a good option to develop PMCs (Liu et al., 2021a). On the other hand, thermoplastic polymers, such as polypropylene, polyethylene, and nylon, are appreciated for their recyclability and processability. For example, bamboo fiber reinforced Polypropylene composites were observed to be having better processability and mechanical properties (Yeh and Yang, 2020).

A critical aspect of the polymer matrix is its compatibility with the reinforcing fibers. It's essential that a robust interfacial adhesion exists concerning the fibers and polymer for effective stress transfer. This compatibility can be affected by factors like surface energy, roughness, and chemical functionalities of both the fiber and the matrix. Jute fiber reinforced polymer composites resulted in having robust interfacial adhesion which increased the mechanical properties (Chandekar, Chaudhari, and Waigaonkar, 2020a). In case of bio fiber-reinforced composites, the hydrophilic character of natural fibers can cause compatibility issues with hydrophobic polymer matrices. Various surface treatments and modifications, such as alkalization, silanization, or the utilization of coupling agents, have been explored to enhance this interfacial adhesion (Vigneshwaran et al., 2020).

Moreover, the processing conditions, like temperature, pressure, and curing time, can affect the matrix properties and thus the composite's performance. For instance, improper curing can lead to a network with incomplete cross-linking, reducing the mechanical and thermal performance of the composite (Naik, Singh, and Sharma, 2022).

Lastly, the polymer matrix's role in governing the composite's environmental impact should not be overlooked. With increasing concerns over environmental sustainability, biodegradable and bio-based polymer matrices have gained substantial attention in recent years. They offer the potential for reducing the environmental footprint of composites without significantly compromising their performance. It was documented in a recent study that Poly lactic acid (PLA) had been the best applied environment friendly polymer, without significantly compromising their performance (Ashothaman, Sudha, and Senthilkumar, 2023).

To summarize, the polymer matrix is a vital component of composite materials, with its choice and processing methods significantly influencing the composite's mechanical, thermal, and environmental performance. The ongoing research aims to optimize these matrices, particularly in conjunction with natural fibers, to develop high-performance, environmentally friendly composite materials.

2.4.1 Thermosetting and Thermoplastic Polymer

Polymers are widely categorized into two primary categories depending on their behavior under heat: thermosetting and thermoplastic polymers. Each of these polymer classes

exhibits distinct characteristics and properties, making them suitable for different applications.

Thermosetting polymers, often referred to as thermosets, are polymers that, once cured or hardened into a permanent shape, cannot be remelted or reshaped upon subsequent heating. This irreversible curing process involves the formation of three-dimensional cross-linked networks, which impart high thermal stability, chemical resistance, and structural rigidity to these polymers (Quirino et al., 2021). Common examples of thermosetting polymers include epoxy resins, polyester resins, and polyurethanes. These materials find extensive application in industries where material durability, resistance to harsh environments, and structural integrity are required. In the realm of composite materials, epoxy resins are extensively employed as matrices because of their excellent adhesion, mechanical properties, and dimensional stability (Capricho, Fox, and Hameed, 2020).

On the other hand, thermoplastic polymers, or thermoplastics, are polymers that soften upon heating and harden upon cooling—a process that can be repeated numerous times without significant degradation of the polymer. This reversibility is because of the lack of cross-linking in their structure, which allows the polymer chains to slide past each other upon heating (Devaraju and Alagar, 2021). Prominent examples of thermoplastic polymers include polyethylene (PE), polypropylene (PP), polystyrene (PS), and polyvinyl chloride (PVC). These materials exhibit higher elongation and impact resistance compared to thermosets and are easier to process and recycle, making them popular choices in industries like packaging, automotive, and consumer goods. In the context of composites, thermoplastic matrices offer advantages such as processability, recyclability, and the potential for yielding damage-tolerant structures (Alshammari et al., 2021).

In conclusion, thermosetting and thermoplastic polymers, each with their unique set of properties, serve as critical components in a broad scope of purposes. The choice between a thermoset and a thermoplastic polymer depends largely on the specific application requirements, including mechanical performance, thermal resistance, processability, and environmental impact. Understanding these polymers' distinct properties aids in selecting the appropriate material for specific applications and in designing new materials for future needs.

2.4.2 Epoxy Resin as a Thermosetting Polymer

Epoxy resin, a class of thermosetting polymer resins, are known for their high performance and versatility. They are characterized by the presence of an epoxide group, which contains an oxygen atom bonded to two carbon atoms forming a triangular ring. This chemical structure contributes to epoxy's unique and desirable attributes (Capricho, Fox, and Hameed, 2020).

Epoxy resin is a liquid that is converted into a solid polymer through a chemical reaction known as curing or cross-linking. This reaction is typically induced by the addition of a hardener or curing agent, which opens the epoxide rings and facilitates the creation of a dense, three-dimensional cross-linked network. The resulting epoxy polymer exhibits excellent mechanical properties, chemical resistance, and dimensional stability, as reported in existing literature (Saba et al., 2016).

One of the key strengths of epoxy resins is their excellent adhesion to a wide range of materials. This adhesive property is attributed to their ability to form covalent bonds with the substrate material and the inherent polar nature of the epoxy group. Consequently, they are extensively used in adhesive applications, from everyday household use to aerospace and automotive industries (Soares and Alves, 2018).

Many researchers reported that epoxy resins also demonstrated remarkable mechanical properties, with high tensile strength, rigidity, along with impact resistance. These characteristics made them an ideal choice as the matrix material in composite applications, providing structural integrity and distributing the applied loads across the reinforcing fibers (Dilfi KF, Che, and Xian, 2019; Fathi et al., 2019; Kiran et al., 2020; Mittal and Chaudhary, 2018; Sinha, Narang, and Bhattacharya, 2018; Zhao and Li, 2008).

Epoxy resins are also found to be superior for their excellent chemical and corrosion resistance in existing literature. This resistance is largely attributed to the densely cross-linked network that offers minimal opportunities for the intrusion of aggressive chemicals. Therefore, epoxy coatings are often applied to protect surfaces from chemical attack or environmental degradation (Radhamani, Lau, and Ramakrishna, 2020).

However, some challenges are associated with the use of epoxy resins, despite having significant advantages. These include relatively high cost compared to other thermosets,

potential shrinkage during curing, and sensitivity to moisture and ultraviolet radiation. However, ongoing research continues to address these issues, developing new epoxy formulations and processing techniques to expand their application scope (A. Verma, Jain, and Mishra, 2022).

2.5 Nanofillers in Natural Fiber Reinforced Polymer Composites

Natural fiber reinforced polymer composites have obtained substantial consideration in past years because of their wide range of desirable attributes including cost-effectiveness, biodegradability, low density, and the potential for high mechanical strength. However, one issue that can often impede the performance of these composites is the poor compatibility between the natural fibers and the polymer matrix. It is in this realm that nanofillers have proven to be an essential factor, providing a bridge that enhances the interaction and compatibility between the constituents.

Nanofillers, being at the nanometric scale, introduce a variety of beneficial properties to natural fiber reinforced polymer composites. Not only do they significantly increase the mechanical properties of the composites, but they also improve thermal stability, reduce water absorption, and increase resistance to ultraviolet radiation. Fu et al. reported that by manipulating the size, shape, and type of nanofiller, the physical, chemical, and mechanical properties of the polymer composites can be tailored to suit specific requirements (Fu et al., 2019).

Among the many types of nanofillers, nano clays, carbon nanotubes, graphene, and nano silica are frequently used. Chan along with other researchers observed that nano clays, due to their layered structure and large surface area, can enhance the thermal and mechanical properties of the composite. Carbon nanotubes and graphene, with their extraordinary mechanical strength and electrical conductivity, can dramatically improve the composite's performance. Nano silica, on the other hand, can enhance the composite's resistance to wear and thermal degradation (Chan et al., 2021).

The integration of nanofillers into natural fiber reinforced polymer composites, however, is not without challenges. In a recent literature, it was reported that the dispersion of nanofillers in the polymer matrix is a significant concern that must be carefully managed to avoid agglomeration, which can result in poor performance. Various techniques have

been developed to address this issue, including surface modification of the nanofillers, use of suitable solvents, and ultrasonic dispersion (Mohanavel et al., 2022).

2.5.1 Carbon Nanotubes (CNT) as a nanofiller

Carbon nanotubes (CNTs), discovered in 1991, have since revolutionized material science due to their outstanding properties. Possessing remarkable strength, electrical conductivity, and thermal properties, CNTs have found widespread applications across various fields. In the context of natural fiber reinforced polymer composites, CNTs have shown immense potential in improving their overall performance (Devnani and Sinha, 2019).

Primarily, CNTs are classified into two types: Single-walled carbon nanotubes (SWCNTs) and Multi-walled carbon nanotubes (MWCNTs). Qiu and Yang studied CNT structure in details and reported that SWCNTs consist of a single graphene sheet seamlessly wrapped into a cylindrical shape, while MWCNTs are composed of several concentrically arranged graphene sheets, akin to the structure of Russian nesting dolls. Each type has its unique properties and is utilized based on the specific demands of the composite material (Qiu and Yang, 2017).

The inclusion of CNTs into natural fiber reinforced polymer composites is marked by several beneficial effects. Xue documented that the extraordinary mechanical strength of CNTs, almost 100 times greater than that of steel at a fraction of the weight, contributes to a significant enhancement of the composite's strength and stiffness. Furthermore, due to their impressive thermal stability, CNTs can effectively improve the thermal properties of the composite, reducing the likelihood of degradation under high-temperature conditions (Xue, 2017).

Moreover, CNTs have shown potential in reducing the water absorption of natural fiber reinforced polymer composites, a common drawback of such materials. Many studies reported that by acting as a protective layer around the natural fibers, CNTs limit the water uptake, thereby preserving the composite's mechanical properties (Amjad et al., 2022; W. Li et al., 2023; Vinay et al., 2022).

However, despite their immense potential, the integration of CNTs into natural fiber reinforced polymer composites is not without challenges. Rubel and his team studied the agglomeration effect of CNTs and found that the uniform dispersion of CNTs within the

composite, crucial for optimal performance, is often hard to achieve. Agglomerations can lead to stress concentrations, negatively impacting the composite's mechanical properties. Techniques such as ultrasonic dispersion, chemical functionalization, and use of suitable solvents have been employed to improve dispersion and adhesion of CNTs within the polymer matrix (Rubel et al., 2019).

2.5.2 Multi Walled Carbon Nanotubes (MWCNT) in Natural Fiber Reinforced Polymer Composites

Multi-walled carbon nanotubes (MWCNTs) have emerged as a novel nanofiller in the development of high-performance polymer matrix composites. By introducing MWCNTs into a polymer matrix, new material systems can be developed that combine the inherent properties of the polymer with the exceptional characteristics of MWCNTs, such as their high mechanical strength, electrical and thermal conductivity, and large aspect ratio (Hao and Ma, 2017).

Soni and his research team discussed that the important attribute of MWCNTs that makes them effective as nanofillers is their high aspect ratio. This means that they have a long length relative to their diameter, which enhances their ability to interact with the polymer matrix and form a percolating network, even at low filler concentrations. Such networks can considerably improve the composite's load transfer capability, resulting in enhanced mechanical properties, including tensile strength, impact resistance, and modulus (Soni, Thomas, and Kar, 2020).

Dwivedi and his team studied electrical properties of NFRP composites with sisal fiber and observed that addition of MWCNT can endow the polymer matrix composites with conductive or even semi-conductive properties, which are typically absent in pure polymers. This enables the creation of electrostatic discharge (ESD) safe materials or thermally conductive composites, expanding their potential applications in industries such as electronics, automotive, aerospace, and energy (Dwivedi et al., 2017).

However, the effectiveness of MWCNTs as nanofillers greatly depends on their dispersion within the polymer matrix and their interfacial interaction with the polymer. Many researchers observed that the poor dispersion or weak interfacial adhesion can lead to the formation of agglomerates, which act as stress concentration sites and impair the composite's performance. Kim and his team reported that techniques such as surface

functionalization of MWCNTs or the use of suitable processing methods could be employed to ensure good dispersion and strong matrix-filler interactions (Kim et al., 2021; Lavagna et al., 2021; Norizan et al., 2020).

2.5.3 Agglomeration and Dispersion of CNTs

The degree of dispersion is critical, as it significantly influences the overall performance of the composite material. Clustering or agglomeration of CNTs can lead to heterogeneous distribution, thereby limiting the mechanical properties and electrical conductivity of the composites. Therefore, achieving uniform dispersion of CNTs within a polymer matrix is vital (N. P. Singh, Gupta, and Singh, 2019).

Agglomeration in carbon nanotubes (CNTs) is primarily attributed to the inherent attractive van der Waals forces that exist between them. These forces, a result of temporary fluctuations in electron distribution around the atoms of the CNTs, prompt them to stick together, forming bundles or clusters, a phenomenon referred to as agglomeration (Tanabi and Erdal, 2019).

The high aspect ratio (length to diameter) of CNTs, coupled with their large surface area, enhances the strength of these van der Waals interactions. The consequence is a strong tendency for the nanotubes to clump together, forming agglomerates that may be challenging to disperse evenly within a matrix. It's also worth noting that agglomeration is often a consequence of attempts to stabilize CNTs during production or storage, where they tend to naturally clump together to minimize their total surface energy (Cha et al., 2017).

Agglomeration poses a significant challenge in the utilization of CNTs in composite materials because it can lead to inconsistent properties throughout the material, thereby limiting the composite's overall performance. Hence, developing methods to overcome this agglomeration issue is an area of intense research in nanotechnology (Rubel et al., 2019).

One of the challenges lies in ensuring the even distribution and adequate bonding of CNTs within the epoxy matrix. Several techniques such as sonication, surface functionalization of CNTs, and use of suitable dispersants have been proposed to achieve this objective. A wide range of methods has been employed to address the dispersion challenge. Broadly, these methods are classified into two categories - mechanical dispersion methods and chemical dispersion methods (W. Jian and Lau, 2020).

Mechanical dispersion methods involve the use of external force or energy to disperse CNTs in the matrix. Sonication, a common mechanical method, uses ultrasonic energy to disperse the nanotubes (Andhare and Raju, 2016; Huang et al., 2016; Madhesh and Kalaiselvam, 2014; Sayuti et al., 2013). Another frequently used method is ball milling, which involves the grinding of CNTs to facilitate their dispersion. However, these mechanical methods can damage the CNTs, thus compromising their intrinsic properties (Stanciu et al., 2020).

Chemical dispersion methods, on the other hand, involve the modification of CNT surfaces to enhance their compatibility with the polymer matrix. These methods include covalent functionalization and non-covalent functionalization (Norizan et al., 2020). Covalent functionalization chemically modifies the CNT surface to improve dispersion but may also disrupt the inherent structure of the CNTs, thereby affecting their properties. Non-covalent functionalization employs surfactants or polymers to encapsulate the CNTs, improving their dispersion without altering their structure (Lavagna et al., 2021).

Sedimentation studies have often been employed in the field of nanoscience to understand the dispersion of Carbon Nanotubes (CNTs) within a solution. These studies leverage the natural process of sedimentation, where the nanotubes, under the influence of gravity, settle at the bottom of a suspension over time. A critical aspect of sedimentation studies lies in monitoring the rate at which the CNTs precipitate. This rate is determined by the degree of dispersion of the nanotubes in the solution. A faster rate of precipitation often implies poor dispersion, as the CNTs tend to cluster and agglomerate, making them heavier and causing them to settle more rapidly (Soni, Tody, and Thomas, 2021; F. Wang et al., 2021; Yadav, Gupta, and Sharma, 2021).

In contrast, a slow rate of precipitation suggests better dispersion of the CNTs, which is desired for effective performance of CNT-reinforced composites. When CNTs are adequately dispersed, they can distribute stresses more evenly across the composite material, thereby enhancing its overall mechanical properties. However, achieving this state of optimal dispersion requires meticulous control over the conditions of the suspension, including its pH, temperature, and the use of appropriate surfactants or dispersants. By carefully observing and analyzing sedimentation behavior, researchers can infer crucial information about the dispersion of CNTs and thus guide the production

process to create superior composite materials (H. Li and Qiu, 2019; Zaman, Kaya, and Kaya, 2020).

2.6 Fabrication Methods for Natural Fiber and CNT Reinforced Epoxy Composites

Fabrication of natural fiber and carbon nanotube (CNT) reinforced epoxy composites involves careful selection of procedures to ensure proper distribution and integration of the constituents. Among the variety of methods employed, hand lay-up, compression molding, vacuum bagging, and resin infusion are most common.

2.6.1 Hand Lay-up Method

Hand lay-up, often regarded as the most straightforward approach, has been extensively employed. The research led by Nayak, and his team described that the hand layup process involved manual placement of natural fibers and Epoxy/CNT mixture into a mold. Once layered, the setup was left to cure at room temperature or heated slightly to accelerate the curing process. Hand lay-up offered advantages such as simplicity and minimal equipment requirement. However, the quality of the composite heavily relied on the skill and precision of the operator (Nayak et al., 2021).

2.6.2 Compression Molding Method

Compression molding is another widely used technique in composite fabrication. Natural fibers, CNTs, and epoxy resin are combined, placed into a mold, and subjected to high pressure. The heat and pressure accelerate curing and enhance the bonding between the composite constituents. While compression molding offers improved uniformity and better control over composite thickness, it requires precise control over temperature and pressure, often necessitating specialized equipment (Yallew et al., 2020).

2.6.3 Vacuum Bagging Method

Vacuum bagging, on the other hand, is a variation of hand lay-up where a vacuum is applied to the lay-up inside a sealed bag. This process assists in compacting the fibers and resin, promoting better impregnation and removal of any entrapped air or excess resin. It leads to a composite with a better surface finish and increased dimensional stability (Reddy et al., 2022).

2.6.4 Resin Infusion Method

Resin infusion, also known as vacuum-assisted resin transfer molding (VARTM), is a technique particularly useful for large composite structures. The dry fiber and CNT arrangement is placed in a mold, sealed with a vacuum bag, and resin is infused under vacuum. Resin infusion ensures a high fiber volume fraction, uniform resin distribution, and excellent composite properties (Torres-Arellano, Renteria-Rodríguez, and Franco-Urquiza, 2020).

2.6.5 Injection Molding Method

Injection molding is a popular manufacturing process extensively employed in the production of complex and high-volume plastic parts. Owing to its ability to produce parts with intricate geometries and excellent dimensional accuracy, it is a cornerstone in sectors such as automotive, consumer goods, and medical devices.

In the injection molding process, plastic in the form of pellets is first fed into a hopper. The material then enters a heated barrel where it is melted into a molten state. This molten plastic is subsequently forced, or 'injected,' into a mold cavity by a reciprocating screw or a ram injector (M. Li et al., 2020).

2.7 Factors Controlling the Performance of Natural Fiber and CNT Reinforced Epoxy Composites

The performance of natural fiber and carbon nanotube (CNT) reinforced epoxy composites is determined by different factors ranging from the inherent properties of the components to the methods used in their fabrication.

- The type and properties of the natural fibers employed play a critical role. Factors such as the fiber type (e.g., flax, jute, kenaf), fiber morphology, and the treatment of these fibers to improve their compatibility with the epoxy matrix all impact the final composite performance. For instance, surface treatments like alkalization or silanization can significantly enhance the fiber-matrix bonding, leading to improved mechanical properties (Chandekar, Chaudhari, and Waigaonkar, 2020b; Faruk et al., 2014a; Fathi et al., 2019).

- The dispersion and orientation of CNTs within the matrix, alongside their interaction with natural fibers and epoxy, are crucial determinants of composite performance. Proper dispersion of CNTs can enhance the composite's strength and electrical conductivity, whereas agglomeration can lead to weaknesses in the composite structure. Functionalization of CNTs can also contribute to better dispersion and improved bonding with the matrix (M. Q. Jian et al., 2017).

- The epoxy resin's characteristics, such as its viscosity, curing behavior, and mechanical properties, significantly influence the composite's performance. A resin with a lower viscosity may improve fiber and CNT wetting and thus enhance the interfacial bonding (Liu et al., 2021b).

- The fabrication method used can directly impact the properties of the resulting composite. Methods that ensure homogenous distribution of fibers and CNTs and a void-free matrix tend to produce composites with superior mechanical and physical properties. Factors like pressure, temperature, and curing time during the fabrication process can also influence the performance of the composite (H. Wang et al., 2019).

- The interface between the natural fibers, CNTs, and epoxy matrix forms a critical factor governing composite performance. A strong interfacial bond can transfer stress efficiently, leading to improved mechanical properties. Conversely, a weak interface can cause debonding or matrix cracking, impairing the composite's performance (Sapiai, Jumahat, and Mahmud, 2018; Soni, Thomas, and Kar, 2020).

In summary, controlling the myriad factors is crucial for optimizing the performance of natural fiber and CNT reinforced epoxy composites. Understanding the interplay of these variables can lead to composite materials with tailored properties suitable for a broad range of applications.

2.8 Finite Element Method

The Finite Element Method (FEM) has been a vital numerical technique in the field of composite materials, particularly in the analysis and prediction of their mechanical behavior. One of the significant concepts incorporated within FEM is the Representative

Volume Element (RVE), which greatly contributes to the understanding and modeling of the complex nature of composite materials (David Müzel et al., 2020).

2.8.1 Representative Volume Element (RVE)

RVE is a theoretical concept adopted to simulate and predict the properties of heterogeneous materials, such as composite materials, using a microscopic representative unit. The objective is to establish a volume small enough to be computationally manageable, yet large enough to encapsulate the material's heterogeneity (Catalanotti, 2016).

RVE finds its application predominantly in the micro-mechanical modeling of composite materials. For instance, a typical RVE for fiber-reinforced composites would consist of a fiber embedded within a matrix. When this RVE is subjected to loads and boundary conditions representative of the actual composite's loading scenario, one can extract the averaged stress and strain responses, hence predicting the composite's macroscopic behavior (Palizvan, Tahaye Abadi, and Sadr, 2020).

In the context of FEM, RVE methods allow researchers to create detailed numerical models of composites. These models account for the intricate interaction between the composite's constituents – the matrix, the fibers, and possibly the interface region. The application of boundary conditions is a vital aspect of this approach, with periodic boundary conditions commonly employed to simulate an infinite array of RVEs (Naili et al., 2020).

The advantages of employing RVE methods with FEM in composite materials research are multifold. First, they provide a way to capture the microstructural effects on composite behavior, thus enhancing the accuracy of simulations. Second, RVE-based models can be used to study the effect of variations in microstructural parameters, such as fiber volume fraction, fiber orientation, or interfacial properties, on the overall material response (Palizvan, Tahaye Abadi, and Sadr, 2020).

However, the use of RVE methods within FEM is not without challenges. The size of the RVE, the imposition of suitable boundary conditions, and the computational cost associated with these high-fidelity models are all significant considerations that must be adequately addressed (Kou et al., 2023).

2.8.2 Microstructure Free Finite Element Model (MF-FEM)

The Microstructure-Free Finite Element Method (MF-FEM) represents an advanced and progressive approach towards the study of composite materials. As a computational technique, it is devised to counter some of the primary challenges associated with conventional finite element methods, such as the necessity for detailed microstructural information and the significant computational overhead involved (Luo, 2022a).

MF-FEM, as the name suggests, is a method that circumvents the need for explicit microstructural representation. Instead, it operates based on homogenized constitutive relationships that encompass the behavior of the material in an averaged sense. This ability to conduct numerical analysis without needing to model the microstructure is particularly advantageous for complex, heterogeneous materials like composites. In typical finite element analysis, the microstructure of a composite is meticulously represented. This includes individual fibers, the matrix, and the interface regions, which is both computationally intensive and challenging to model accurately. MF-FEM simplifies this process by replacing the microstructural detail with an equivalent continuum description, which is derived from the averaged behavior of the material (Luo, 2022b).

Luo carried out MF-FEM analysis and reported that the composite material's behavior is characterized in terms of macroscopic parameters. This abstraction level greatly reduces the computational cost associated with finite element analysis. Consequently, larger and more complex structures can be evaluated with fewer computational resources compared to conventional microstructural-based approaches (Luo, 2022b).

Luo conducted FEM analysis and validated with available experimental data for two constituent materials only. His study was not expanded into three constituent materials with large phase contrast. However, it was observed that the accuracy of the MF-FEM heavily relies on the homogenization process that generates the constitutive laws from the microstructural details. This process requires a comprehensive understanding of the composite material's behavior and its interaction mechanisms. Thus, the primary challenge for MF-FEM lies in developing reliable and accurate constitutive laws that can capture the complex interaction between the different constituents of a composite material.

2.9 Key Takeaways from the Existing Literature

The broad spectrum of scientific literature and investigations in the field of composite materials has yielded a plethora of insightful findings, each contributing to the depth of understanding surrounding the complex nature of these materials. This expansive body of knowledge lends itself to the formulation of key takeaways, serving as pillars of foundational comprehension and potential launching points for further research.

1. Epoxy as Polymer Matrix: An abundance of literature suggests that epoxy resins are a preferred choice for the polymer matrix in the formation of composites. Primarily, this preference is driven by the excellent adhesion, low shrinkage, high strength, and considerable resistance to chemicals and moisture that epoxy possesses. These characteristics enhance the overall performance and durability of the resulting composite materials.

2. Selection of Natural Fibers via Fuzzy MCDM: The process of selecting appropriate natural fibers for composite materials can be guided by the Fuzzy Multiple Criteria Decision Making (MCDM) approach. The versatility and applicability of this method have been highlighted in numerous studies, indicating its effectiveness in providing an optimal solution to complex decision-making problems.

3. Enhancement of Mechanical Properties with CNT: Inclusion of Carbon Nanotubes (CNTs) in the fabrication of natural fiber reinforced epoxy composites has been revealed as a significant factor in enhancing their mechanical properties. Evidence from existing literature establishes the correlation between CNT addition and improved tensile strength, flexural strength, and impact resistance.

4. Importance of CNT Dispersion and Agglomeration: The dispersion of CNTs and the study of their agglomeration behavior are vital to understanding and optimizing the performance of CNT-reinforced composites. Successful dispersion can mitigate the negative effects of agglomeration, such as the creation of weak points in the composite, thereby enhancing material properties.

5. Essential Tests for Comprehensive Understanding: Thorough characterization of a composite demands the execution of multiple tests including, but not limited to, tensile, flexural, and impact tests, as well as hardness assessments and physical and

morphological examinations. These testing regimes contribute to a well-rounded analysis of a composite's properties and performance.

6. Microstructure-Free FEM for Computational Analysis: For the computational analysis of natural fiber and CNT reinforced composites, the Microstructure Free Finite Element Method (MF-FEM) is a recommended tool. Acknowledged for its efficiency in model creation and accuracy in predictive analysis, MF-FEM holds substantial promise in the realm of composite materials study.

In conclusion, these takeaways form a multifaceted portrait of the vast and intricate world of natural fiber and CNT reinforced polymer composites. They highlight key considerations, validate prominent methodologies, and reveal valuable insights, all of which contribute to an evolving understanding of the composite materials field.

2.10 Research Gaps in the Existing Literature

While the research involving natural fiber and carbon nanotube (CNT) reinforced epoxy composites has grown significantly over the years, several gaps persist in the existing literature that need to be addressed.

- Despite the escalating progress in the field of natural fiber reinforced polymer composites, a distinct research gap can be observed with respect to the selection of appropriate natural fibers. Most of the existing studies have centered on the mechanical and physical properties of the composites, with less attention being given to the systematic evaluation and selection of the optimal fiber type. This oversight leaves a considerable void in the literature, particularly concerning the utilization of Multi-Criteria Decision Making (MCDM) methods to navigate the complex selection process. By employing fuzzy logic, which uses degrees of truth rather than traditional binary or Boolean logic, more nuanced and comprehensive conclusions can be drawn regarding fiber suitability.

- A comprehensive understanding of the interfacial interactions between the natural fibers, CNTs, and the epoxy matrix remains limited. Studies have often focused on either natural fiber-matrix or CNT-matrix interactions independently, but the three-way interaction in a composite structure containing both has been less explored,

especially for pineapple, sisal, and coir fiber reinforced composites. Thus, investigations into the synergetic effects of natural fibers and CNTs, as well as their collective influence on the properties of the epoxy matrix, are lacking.

- The impact of different types and proportions of natural fibers and CNTs on the composite properties has not been thoroughly examined. A broader range of fibers and CNTs need to be studied to better understand how their individual characteristics influence the overall composite properties.

- The optimal dispersion of CNTs within the epoxy matrix and its effects on the composite properties have yet to be fully elucidated. The agglomeration of CNTs can significantly impair the composite's properties, but methods to improve and control dispersion are not well-established.

- There is a notable research gap in the implementation of Microstructure Free Finite Element Method (MF-FEM) for natural fiber and CNT reinforced Epoxy composites. Its application for natural fiber and CNT reinforced composites has not been widely explored. This gap in the literature suggests a significant opportunity for advancing our understanding of these materials and their performance, specifically through the application of MF-FEM, thus facilitating more accurate and efficient design and implementation of these innovative composites.

Overall, while significant strides have been made in the study of natural fiber and CNT reinforced epoxy composites, much remains to be learned. Addressing these gaps will be essential to fully harness the potential of these materials in commercial applications.

CHAPTER 3
MATERIALS AND METHODOLOGY

3.1 Introduction

The methodology chapter of the present study primarily focused on the comprehensive and systematic exploration of the potential of natural fibers, specifically sisal, pineapple, and coir, as reinforcement in epoxy carbon nanotube (CNT) composites. Initially, a meticulous selection process was undertaken to determine the most suitable natural fiber for this purpose. A fuzzy multi-criteria decision-making (MCDM) approach was adopted, enabling a thorough and objective analysis of the options at hand.

Following the identification of the most suitable natural fibers, a sedimentation analysis was performed. This crucial step allowed for the determination of the optimal weight percentages of CNT to be incorporated into the composites, facilitating the creation of materials with desirable properties. After that, fabrication of composite materials was described.

Upon the establishment of the composite formulations, a wide range of characterization tests were conducted. These assessments focused on various key metrics, including tensile strength, Young's modulus, elongation at break, flexural strength, flexural modulus, Rockwell hardness number, impact energy, density, void content, and water absorption properties. The surface morphology and the chemical interactions within the composites were also scrutinized using Scanning Electron Microscopy (SEM) and Fourier Transform Infrared (FTIR) spectroscopy respectively.

In parallel with the experimental analyses, a computational approach was also adopted. Microstructure-free Finite Element Modeling (MF-FEM) was utilized to predict the Young's modulus of the developed composites. This predictive model provided valuable insights that complemented the experimental results, contributing to a deeper understanding of the behavior of these novel composites.

The culmination of the study was the implementation of Grey Relational Analysis (GRA). This technique was employed to rank the developed composites based on their properties as determined by the experimental tests. The ranking provided a clear and quantitative measure of the overall performance of each composite formulation, thereby assisting in the

identification of the most promising material combinations for future applications. The rigorous methodology adopted in this study ensured a comprehensive, scientifically sound, and insightful exploration of the potential of natural fibers in epoxy CNT composites.

3.2 Selection of Natural Fiber as Constituent Materials

Methodical procedures were used to select natural fibers for use in commercial applications. Mechanical property data for natural fibers was compiled and analyzed to gain context before the selection process began. In doing so, material's density, tensile strength, Young's modulus, and the elongation at break were taken into account. The relative significance of each criterion was then used in a fuzzy AHP analysis to determine how much weight each criterion would receive. After that, various fiber variants were scored and ranked based on their performance using fuzzy TOPSIS assessment. Following these procedures, the optimal variant for every fiber was chosen for further study. Depending on their performance metrics and rankings, these fibers were evaluated to find the most suitable alternative. A sensitivity analysis was carried out in conjunction with the fuzzy AHP-TOPSIS method to analyze the effect of induced disturbances on the selection of natural fibers. There is a systematic breakdown of the processes involved in the subsequent section.

3.2.1 Data Assemblage and Precursory Scrutiny

Twelve natural fibers' mechanical properties were collected from the most recent research published in this area (Abdollah et al., 2015; Alkbir et al., 2016; M. George et al., n.d.; Misnon et al., 2014; Petrone and Meruane, 2017). Since using the average values for the parameters could lead to false conclusions, we avoided doing so. The most available physical properties of different variant of various natural fibers are shown in Table 2.5, which includes their density, tensile strength, Young's modulus, and the elongation at break.

Exploratory data analysis, shown by the box plot in Fig 3.1, can be used to see patterns in the data of various parameters. Each variant's data can be seen clearly in the accompanying figures. Fig 3.1(a) depicts overall density variation of various fiber variants. The density of banana fiber is the lowest of any fiber studied so far. Pineapple fiber is the densest and most diverse of all fibers. The range in tensile strength among fiber types is depicted in Fig 3.1(b). Tensile strength decreases from highest (flax) to lowest (coir). Furthermore, flax

fiber has the greatest variance in tensile strength while coir fiber has the least. Fig 3.1(c) displays that the Young's modulus varies the most for pineapple fiber and the least for coir fiber. Young's modulus of ramie fiber was found to be the highest of any fiber tested. As can be shown in Fig 3.1(d), coir fiber is the most resistant to shape change without fracture development. Except for pineapple fiber, which has the subsequent greatest ratio of elongation at break, all the other fibers exhibit nearly identical behaviors in this regard.

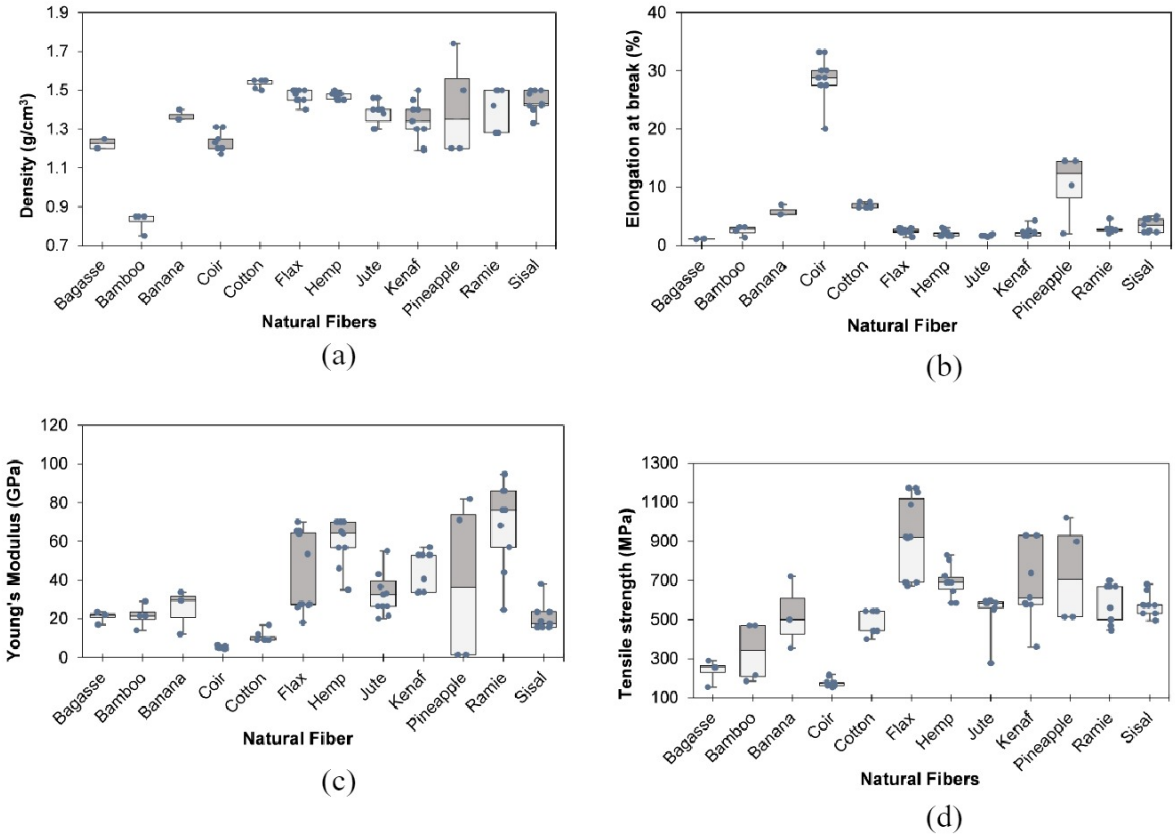

Fig 3.1: Significant variation shown from statistics collected of several natural fibers based on (a) density; (b) elongation at break; (c) Young's modulus; (d) tensile strength.

3.2.2 Fuzzy AHP Approach to Measure the Criteria Weightages

Prior to employing alternative approaches to compare the performance of various fibers, the Fuzzy AHP model was used to evaluate the relative weight of each feature. The following procedures were used to assess the weights of criteria employing fuzzy AHP:

Step 1: Establishing the analysis's goals and subdivide the MCDM problem into objectives, criteria, and alternatives.

The objective of this study was to select an optimum fiber based on its mechanical properties. Higher tensile strength, higher Young's modulus, higher elongation at break, and reduced density were the criteria for superior mechanical properties. The alternatives considered in this study included a total of twelve different types of fiber: bagasse, bamboo, banana, coir, cotton, flax, hemp, jute, kenaf, pineapple, ramie, and sisal.

Step 2: Developing a pairwise comparison matrix.

Triangular fuzzy numbers (TFN) were used to produce the pairwise comparison matrix because to their ease of implementation and practicality (Kaufmann and Gupta, 1988). The results of a translation of Saaty's nine-point scale into the TFN linguistic scale, which may be used to quantify the relative impact between one criterion over another, as shown in Table 3.1 (Zhu, Jing, and Chang, 1999).

Table 3.1: Pairwise comparison matrix

Linguistic Scale	Saaty's scale	Fuzzy Scale	Fuzzy reciprocal scale
Equally significant	1	(1, 1, 1)	(1, 1, 1)
Moderately significant	3	(2, 3, 4)	$(\frac{1}{4}, \frac{1}{3}, \frac{1}{2})$
Strongly significant	5	(4, 5, 6)	$(\frac{1}{6}, \frac{1}{5}, \frac{1}{4})$
Very strongly significant	7	(6, 7, 8)	$(\frac{1}{8}, \frac{1}{7}, \frac{1}{6})$
Extremely significant	9	(8, 9, 9)	$(\frac{1}{9}, \frac{1}{9}, \frac{1}{8})$
Intermediate values	2	(1, 2, 3)	$(\frac{1}{3}, \frac{1}{2}, 1)$
	4	(3, 4, 5)	$(\frac{1}{5}, \frac{1}{4}, \frac{1}{3})$
	6	(5, 6, 7)	$(\frac{1}{7}, \frac{1}{6}, \frac{1}{5})$
	8	(7, 8, 9)	$(\frac{1}{9}, \frac{1}{8}, \frac{1}{7})$

The values of the TFN linguistic scale for each condition are shown in Eq. (3.1) through (3.3). Using the TFN linguistic scale, the minimum, median, and maximum values of a fuzzy number are represented by l_{ij}, m_{ij}, u_{ij} represents a fuzzy number's minimum, average, and maximum values using TFN linguistic scale. Eq. (3.4) was used to compile values for use in selecting choices (Buckley, 1985).

$$\tilde{a}_{ij} = (l_{ij}, m_{ij}, u_{ij}) \ ; l_{ij} \le m_{ij} \le u_{ij} \quad (3.1)$$

$$l_{ij} = \min(\tilde{a}_{ij}) \quad (3.2)$$

$$m_{ij} = \left(\sqrt[n]{\prod_{i=1}^{n} \tilde{a}_{ij}} \right) \quad (3.3)$$

$$u_{ij} = \max(\tilde{a}_{ij}) \quad (3.4)$$

Step 3: Assessing the criteria weights.

The relative weights of fuzzy criteria were determined using the Eq. (3.5) through (3.7) (Ayhan, 2013). The criteria average weights were determined using Eq. (3.8). The method used was a center-of-area de-fuzzification of the criteria weights approach (Balmat et al., 2011). Eq. (3.9) was applied to determine the adjusted criteria weights, where ω is the criteria weights, n is the total number of criteria, and m is the total number of possible solutions.

$$\tilde{r}_i = \left(\prod_{i=1}^{n} (\tilde{a}_{ij}) \right)^{\frac{1}{n}} \quad (3.5)$$

$$\left(\sum_{i}^{n} \tilde{r}_i \right)^{-1} = (\tilde{r}_{i1} \oplus \tilde{r}_{i2} \oplus \dots \oplus \tilde{r}_{in})^{-1} \quad (3.6)$$

$$\tilde{\omega}_j = \tilde{r}_i \otimes (\tilde{r}_{i1} \oplus \tilde{r}_{i2} \oplus \dots \oplus \tilde{r}_{in})^{-1} = l\tilde{\omega}_j, m\tilde{\omega}_j, u\tilde{\omega}_j \quad (3.7)$$

$$M_i = \frac{l\tilde{\omega}_j \oplus m\tilde{\omega}_j \oplus u\tilde{\omega}_j}{3} \quad (3.8)$$

$$f_i = \frac{M_i}{\sum_{i=1}^{n} M_i} \quad (3.9)$$

Step 4: Analyzing the performance of the matrix by calculating its consistency ratio.

The consistency ratio of the matrix can be calculated by finding the largest eigenvalue (λ_{max}) applying Eq. (3.10). After that, Eq. (3.11) and (3.12) were used for measuring the Consistency Index (CI) and Consistency Ratio (CR). Results of the criteria weights were evaluated using measures of Mean Square Error (MSE), Root Mean Square Error (RMSE), Mean Absolute Error (MAE), Percentage Error (PE), and Accuracy were calculated using Eq. (3.13) to (3.17).

$$\lambda_{max} = \sum_{i=1}^{n} \frac{\sum_{j=1}^{a} a_{ij} \times \omega_j}{\omega_j} \; ; \; i = 1, 2, 3, ..., m \text{ and } j = 1, 2, ..., n \tag{3.10}$$

$$CI = \frac{\lambda_{max} - n}{n - 1} \tag{3.11}$$

$$CR = \frac{CI}{RI} \; ; \; RI = \text{Random matrix index} \tag{3.12}$$

$$MSE = \frac{\sum_{i=1}^{n} (x_i - \bar{x})^2}{n}; \; n = \text{total number of criteria} \tag{3.13}$$

$$RMSE = \sqrt{\frac{\sum_{i=1}^{n} (x_i - \bar{x})^2}{n}}; \; n = \text{total number of criteria} \tag{3.14}$$

$$MAE = \frac{\sum_{i=1}^{n} |x_i - \bar{x}|}{n}; \; n = \text{total number of criteria} \tag{3.15}$$

$$PE = \frac{|x_i - \bar{x}|}{x_i} \tag{3.16}$$

$$Accuracy = (1\text{-}PE) \times 100\% \tag{3.17}$$

3.2.3 Fuzzy TOPSIS Approach to Determine the Fiber Rankings

The Fuzzy Technique for Order of Preference by Similarity to Ideal Solution (TOPSIS) method was used to assess the performance ratings of various natural fibers and their variations. The natural fiber's performance rating is a function of its mechanical properties. TOPSIS analysis was utilized to choose the optimal fiber variant in the first step. In the second phase, the data were analyzed with TOPSIS method again to determine which of several possible natural fibers was superior. Techniques utilized during both phases include the following steps.

Step 1: Generating the decision matrix.

With the help of Eq. (3.18) the decision matrix in TOPSIS method was generated. Natural fiber alternatives (or variants) are denoted in the equation by the letters A_1, A_2, …., A_m. C_1, C_2, …., C_n are the numerical representations of the criteria including density, tensile strength, Young's modulus, and elongation at break. Each alternative's criterion values are denoted by x_{ij}.

$$D = \begin{array}{c} \\ A_1 \\ A_2 \\ \vdots \\ A_m \end{array} \begin{array}{c} \begin{array}{cccc} C_1 & C_2 & \cdots & C_n \end{array} \\ \begin{bmatrix} x_{11} & x_{12} & \cdots & x_{1n} \\ x_{21} & x_{22} & \cdots & x_{2n} \\ \vdots & \vdots & \vdots & \vdots \\ x_{m1} & x_{m2} & \cdots & x_{mn} \end{bmatrix} \end{array} \tag{3.18}$$

Step 2: Constructing the standardized and fuzzy weighted standardized decision matrix.

When conducting the TOPSIS analysis, the standardized decision matrix was created using Eq. (3.19). Each standardized term's values are denoted by $\tilde{n}_{ij}$. Using Eq. (3.20) the weighted standardized decision matrix was formed where ω_i represents the fuzzy weightages derived from AHP method, N_D represents the standardized decision matrix and V represents the fuzzy weighted standardized decision matrix.

$$n_{ij} = \frac{x_{ij}}{\sqrt{\sum_{i=1}^{m} x_{ij}^2}} \; ; \; i = 1, 2, 3, \ldots, m \text{ and } j = 1, 2, \ldots\ldots, n \tag{3.19}$$

$$\tilde{V} = N_D \otimes \tilde{\omega}_j = \begin{bmatrix} \tilde{V}_{1i} & \cdots & \tilde{V}_{1j} & \cdots & \tilde{V}_{1n} \\ \vdots & & \vdots & & \vdots \\ \tilde{V}_{m1} & \cdots & \tilde{V}_{mj} & \cdots & \tilde{V}_{mn} \end{bmatrix} \tag{3.20}$$

Step 3: Calculating the positive and negative ideal solutions.

To find the positive and negative ideal reference solutions Eq. (3.21) and (3.22) were used. The ideal solutions, denoted by A^+ and A^- are shown here also. Here, we see that the tensile strength, Young's modulus, and elongation at break are all connected to the I term, whereas the density of all plant fabrics is related to the J term. A weighted standardized matrix, created in the previous phase, is denoted by the symbols V_{ij}, which represent its individual members.

$$A^+ = \left\{ \left(\max_j \tilde{V}_{ij}; I \in I \right) \left(\min_j \tilde{V}_{ij}; I \in J \right) ; I = 1, 2, 3, \ldots, m \right\} \tag{3.21}$$

$$A^- = \left\{ \left(\min_j \tilde{V}_{ij}; I \in I \right) \left(\max_j \tilde{V}_{ij}; I \in J \right) ; I = 1, 2, 3, \ldots, m \right\} \tag{3.22}$$

Step 4: Calculating the performance score.

To obtain the performance score, the Euclidean distances between the options and the optimal solution were computed. Si^+ is defined as is the Euclidean distance from a positive ideal solution, whereas Si^- is the Euclidean distance from a negative ideal solution. Eq.

(3.23) to Eq. (3.25) were utilized to calculate the performance score. Based on the performance score, rankings were determined.

$$S_i^+ = \sum_{j=1}^{n} \left(v_{ij} - v_j+\right)^{1/2} \; ; i = 1, 2, 3, ..., m \tag{3.23}$$

$$S_i^- = \sum_{j=1}^{n} \left(v_{ij} - v_j-\right)^{1/2} ; i = 1, 2, 3, ..., m \tag{3.24}$$

$$PS = \frac{S_i^-}{S_i^+ + S_i^-} \tag{3.25}$$

3.2.4 Experimenting Sensitivity of the Obtained Weights for Different Criteria

To evaluate the sensitivity of the TOPSIS assessment, varying the weightages of the criteria was performed. This was carried out by initiating a disruption in the criteria weights $\widetilde{\omega}_j$; where, j = 1, 2, 3, …, n and $\widetilde{\omega}_j$ is transformed into $\widetilde{\omega}_j^*$. The interrelation between the variables $\widetilde{\omega}_j$ and $\widetilde{\omega}_j^*$ is declared as the unitary ratio β_j and represented in Eq. (3.26).

$$\beta_j = \frac{\omega^*_j}{\omega_j} \tag{3.26}$$

Any disruption to ω_j would change the other weights concurrently since the aggregate of the weights is 1. So, the other weights were altered according to Eq. (3.27).

$$\omega^*_j = \frac{\omega_j}{1 + (\gamma_k - 1)\, \omega_j} \tag{3.27}$$

The term γ_j is designated as the preliminary variation ratio and the expression is represented in Eq. (3.28).

$$\gamma_j = \frac{\beta_j - \beta_j \omega_j}{1 - \beta_j \omega_j} \tag{3.28}$$

In this study, nine values of β_j were applied, i.e., β_j = 0.01, 0.02, 0.05, 0.1, 0.2, 0.5, and 1. Once this weights were adjusted owing to the implementation of β_j, the performance scores and rankings were measured and assessed again against one another. Subsequently, disturbances were introduced to each of the criterion weights, and the variance in each case's ranks was documented.

3.3 Fabrication of Natural Fiber Reinforced Epoxy Nanocomposite

These selected natural fibers underwent an alkaline treatment, a method pivotal for fibrillation, which effectively reduced the fiber bundles into smaller entities. This process also mitigated the hydrophilic properties of the fibers, thereby enhancing their resistance to moisture absorption and improving the interface between the fibers and the epoxy matrix. In parallel, a meticulous preparation of the epoxy/MWCNT mixture was undertaken, followed by a sedimentation test to assess the stability of the dispersed CNTs. The final phase involved the careful fabrication of the nanocomposite, where the treated fibers and the epoxy/MWCNT mixture were combined using the hand lay-up technique. This thorough and multi-stage process is described in the following subsections.

3.3.1 Materials

This study employed Pineapple, coir and sisal fiber as a reinforcement and multi-walled carbon nanotubes (MWCNT) as a filler material with Epoxy resin as a matrix material. Araldite Epoxy Resin AW106, a bisphenol-A-based resin containing some percentage of bisphenol-F, was procured from Epoxy Resin BD Ltd. This grade is used explicitly as adhesive, especially in the furniture industry. Also, hardener HV 953 IN was procured from the same source. This combination of resin and hardener is commonly applied for hand lay-up fabrication. Multi-walled carbon nanotubes CNT-3080 were procured from Dongguan Gelon Lib Co. Ltd, China. Untreated pineapple and coir fibers were procured from a local supplier in Dhaka, Bangladesh. Sisal fiber was procured from Ravi Exports, Mumbai, India.

Table 3.2 represents the experimental conditions for the materials and conducted experiments.

Table 3.2: Experimental conditions

Item	Conditions	Temperature and Humidity
MWCNT	1,2, 3 and 4 wt.% with 99% purity, 30-80 nm diameter, and length less than 20 μm	Average 30-34°C temperature with, 80-88% humidity
Natural fibers	30 wt.% and 40 wt.%, randomly oriented	
Epoxy resin	Epoxy and hardener ratio 10:8	

Table 3.3 represents the supplier provided data for each of the component materials. The table presented elucidates the supplier provided specific properties of the various materials used in the experimental analysis of the epoxy natural fiber CNT composites. Four critical physical properties were detailed: Density, Young's modulus, tensile strength, and Poisson's ratio.

Table 3.3: Properties of each of the component (Ref: supplier data)

Material Name	Density (g/cm^3)	Young's modulus (GPa)	Poisson's ratio	Tensile Strength (MPa)
Matrix	1.16	1.2	0.33	27
MWCNT	1.3	1000	0.31	60000-63000
Pineapple fiber	1.5	35	0.41	800-1050
Sisal fiber	1.45	9	0.45	400-450
Coir fiber	1.2	4	0.4	100-150

3.3.2 Alkaline Treatment

Alkaline treatment was applied as a benchmark chemical modification approach to eliminate the hydroxyl group from the chemical structure of the cellulose fibers (B. Wang et al., 2007). This process involved the deconstruction of the fiber bundle into smaller, individual fibers, a phenomenon known as fibrillation. The alkaline treatment aimed to improve the interfacial adhesion between the fibers and the matrix, thus enhancing the overall performance of the composite. Fig 3.2 illustrates the alkaline treatment process of natural fibers.

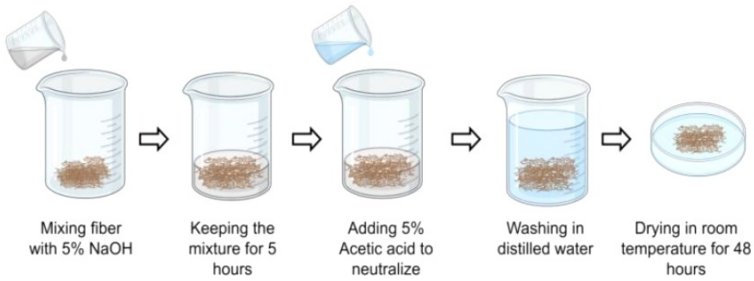

Fig 3.2: Illustration of alkaline treatment process on fibers (Panyasart et al., 2014).

To improve the adhesive property between the natural fiber and the epoxy resin, it was subjected to an alkalization with 5% NaOH for 5 hours to fix any imperfections.

Subsequent to the neutralization step, the fiber mixture was thoroughly rinsed in distilled water. This was done to remove any remaining traces of the alkaline and acidic solutions from the fibers. Next, the treated fibers were air-dried for 48 hours at room temperature.

This ensured that the fibers were completely free of moisture prior to their incorporation into the epoxy matrix. Moisture-free fibers are crucial for preventing any undesirable reactions between the fibers and the matrix material during the composite fabrication process.

3.3.3 Preparation of Epoxy/MWCNT Mixture

In this study, the procedure followed by other research that documented a good dispersion as well as a significant aspect ratio ($\lesssim 500$) of MWCNT was followed to carry out the dispersion process of MWCNT (Fan and Advani, 2007). To begin, MWCNT was mixed in acetone in a 200 mg: 100 ml ratio, then sonicated for one hour in an ultrasonic bath. The purpose of this step was to break down clusters of MWNTs into smaller aggregates. After that, epoxy resin was added with the MWCNT, followed by ultrasonication for one hour again. Subsequently, the mixture was placed into a hot plate, and the degassing procedure was carried out to evaporate the acetone. Fig 3.3 illustrates the step-by-step procedure of MWCNT dispersion.

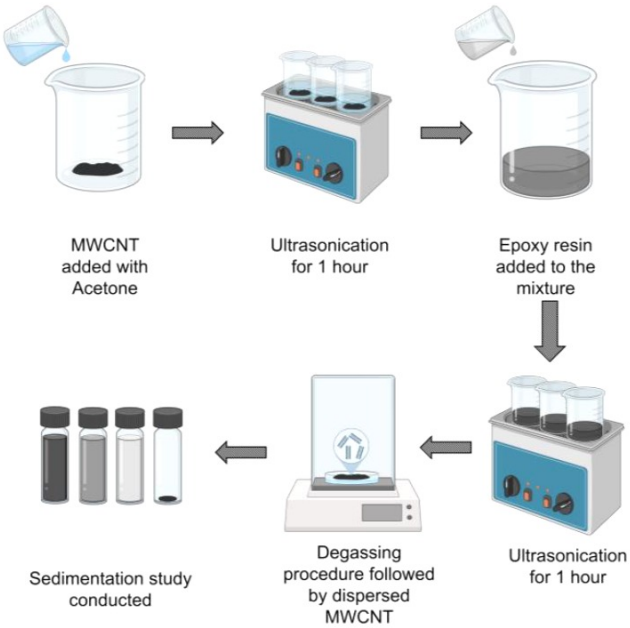

Fig 3.3: Schematic diagram of a step-by-step procedure of MWCNT dispersion (Fan and Advani, 2007).

The stability of MWCNT was assessed using the same procedure that has been employed in many other studies, where the stability of nanoparticles in the base fluid was examined using the sedimentation technique (Politowski et al., 2021; Velzeboer et al., 2011; Yadav, Gupta, and Sharma, 2022). The MWCNT specimens were each subjected to

ultrasonication. The ultrasonication duration ranged from 30 minutes to 90 minutes. Prior to a visual evaluation, these tubes were left undisturbed for periods of 12 hours, 24 hours, and 48 hours. The aim of this process was to observe any potential changes in the sedimentation behavior of MWCNT within these specified time frames.

3.3.4 Fabrication of Nanocomposite

In the methodology, fibers derived from pineapple, sisal, and coir were allocated into distinct molds, following a predetermined weight ratio scheme, as specified in Table 3.2. This process was carried out with precision to ensure an accurate representation of the varied weight ratios in the final composite material.

The next step involved the even application of a thoroughly mixed solution of epoxy resin, carbon nanotubes (CNT), and hardener onto the surface of the randomly oriented fibers within each mold. The epoxy/CNT mixture served as the matrix, binding the individual fibers together, while the hardener was introduced to initiate the curing process of the epoxy resin. The uniform spreading of this mixture over the fibers was a critical step in ensuring an even distribution of the matrix material, thereby contributing to the overall structural integrity of the final composite. Fig 3.4 represents the schematic overview of the fabrication process step by step.

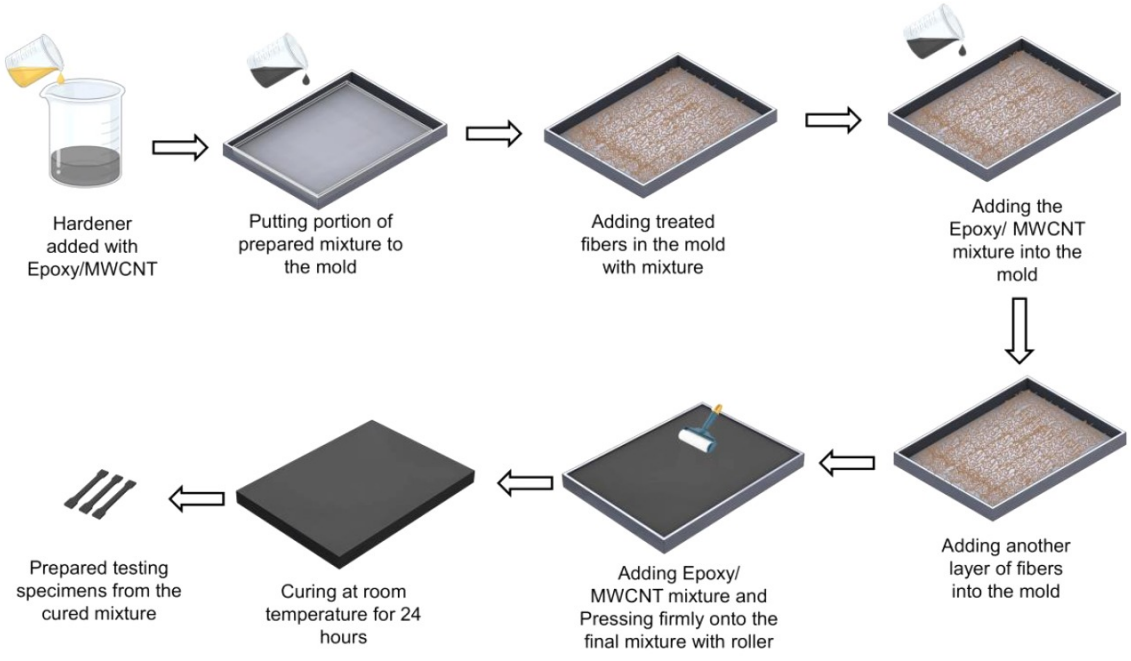

Fig 3.4: Schematic diagram of step-by-step procedure of nanocomposite fabrication.

Finally, the fabrication process concluded with the curing of the composite. The composite-laden mold was left undisturbed at room temperature for a period of 24 hours (Ratna and Misra, 2018). During this time, the hardener triggered a chemical reaction with the epoxy resin, transforming it from a liquid state into a solid, thereby securing the fibers and CNT within a hardened matrix.

3.4 Experimental Characterization

Various methods were utilized to characterize the mechanical and physical properties of the composites, including measuring density, void content, water absorption, tensile strength, Young's modulus, elongation at break, flexural strength, and Rockwell Hardness. Scanning Electron Microscopy (SEM) and Fourier-Transform Infrared (FTIR) spectroscopy were used to examine the composites' microstructure and chemical interactions. Additionally, Finite Element Method (FEM) analyses modeled the behavior of various composite components. This comprehensive characterization strategy as provided below ensured a detailed understanding of the material's behavior.

3.4.1 Density and Void Content

The composite density was measured to elicit the physical property of the composite material. Three samples according to the ASTM D1895 standard were taken for each composite type to report the average value of density. An analytical balance was employed to measure the prepared samples' mass, followed by the determination of volumes applying digital vernier calipers. All the samples were oven-dried at 80°C for 8 hours and cooled at room temperature for 24 hours before the procedure (Salman et al., 2015).

The theoretical density of the composite was calculated based on the rule of mixtures, using the densities of the individual components (epoxy, natural fiber, CNT) and their respective weight percentages. Eq. (3.29) and (3.30) were applied to evaluate the void content.

$$\text{Void Content} = \frac{\rho_{theory} - \rho_{experiment}}{\rho_{theory}} \times 100\% \quad (3.29)$$

$$\rho_{theory} = \frac{1}{\frac{W_m}{\rho_m} + \frac{W_r}{\rho_r} + \frac{W_f}{\rho_f}} \quad (3.30)$$

where, W_m = matrix wt%, W_r = reinforcement of fiber wt%, W_f = filler of CNT wt%, ρ_m= theoretical matrix density, ρ_r= theoretical fiber density and ρ_f= theoretical CNT density. The supplier provided data in Table 3.3 was used as the theoretical density value.

3.4.2 Water Absorption Test

To account for the water absorption properties, the samples dried up at 80°C temperature for 6 hours followed by cooling for 24 hours at room temperature (Khalil et al., 2013). This process was repeated several times to ensure that the weight of the samples with ASTM D570 standard was constant. After that, the samples were submerged in water for 24 hours followed by removing and weighing them in an analytical balance soon after being dried with a dry cloth. Subsequently, the weighing process was continued for 240 hours (10 days) at an interval of 24 hours and weight gains of the composites were evaluated for each observation using the formula from Eq. (3.31).

$$\text{Weight gain} = \frac{m_t - m_o}{m_0} \times 100\% \quad (3.31)$$

where, m_t = mass at time t, m_o = initial mass before immersion of the composite product.

The Fickian water absorption model as shown in Eq. (3.32), illustrates the time-dependent weight of the sample of a fully immersed thin plate (Espert, Vilaplana, and Karlsson, 2004).

$$\frac{M_t}{M_\infty} = 1 - \frac{8}{\pi^2} \sum_{j=1}^{\infty} \frac{1}{(2j+1)^2} e^{-\left[\frac{(2j+1)^2 \pi^2}{h^2} Dt\right]} \quad (3.32)$$

where M_t is the weight of the water at time t, M_∞ is the weight of the maximum amount of water that material can absorb i.e., water weight at equilibrium, D is the diffusion coefficient and h is the thickness of the sample. Diffusion coefficient can be expressed as Eq. (3.33).

$$D = \pi \left[\left(\frac{M_2 - M_1}{\sqrt{t_2} - \sqrt{t_1}} \right) \frac{h}{4M_\infty} \right]^2 \quad (3.33)$$

The infinite aggregate in the solution may necessitate computing effort, even though Eq. (3.32) is an utterly effective method for characterizing the moisture absorption behavior. It has been noticed that as the number of terms, j, increases, the impact of each term on the final sum reduces. In this study, the value of j was taken as 10. Water absorption with Fickian model was compared with the experimental water absorption values.

3.4.3 Tensile Test

The tensile test was conducted with applying a 1000 kN load capacity INSTRON Universal Testing Machine 1000HDX in accordance with ASTM D638 standard procedures. The test samples were prepared in a dog-bone shape, as prescribed by the standard. Each sample was placed in the grips of the tensile testing machine. The test was performed at a uniform rate of crosshead movement until the sample broke. The force exerted on the sample and the corresponding elongation were continuously recorded by the Bluehill software integrated with the universal testing machine.

3.4.4 Flexural Test

The flexural test was conducted with applying a 1000 kN load capacity Fatigue testing machine model HST PLS100, in line with ASTM D790 standard procedures. The test samples were prepared with the appropriate dimensions as outlined by the standard.

Each sample was subjected to a three-point bending test in the testing machine. The test was conducted at a consistent rate of crosshead movement until the sample broke. The force applied to the sample and the corresponding deflection were continuously recorded by the Maxtest software integrated with the fatigue testing machine. Each test was repeated on three samples to ensure the accuracy and repeatability of the results, and the middle value of the three was recorded. The variations in fiber content and CNT concentration were considered, and the effects of these variations on the flexural properties of the composites were thoroughly analyzed. Eq. (3.34) and (3.35) represents the flexural stress and flexural modulus equation used in the analysis.

$$\text{Flexural Stress} = \frac{3PL}{2bd^2} \tag{3.34}$$

$$\text{Flexural Modulus} = \frac{mL^3}{4bd^3} \tag{3.35}$$

where, L = length of the support span = 150 mm, b= width of the test beam = 12 mm, d = depth of the test beam = 10 mm, P = applied load and m = slope of load-deflection curve.

3.4.5 Rockwell Hardness Test

The Rockwell hardness test was performed using the ASTM D785 standard procedure for plastics. The testing was carried out on a Brooks Rockwell hardness tester in B scale. The Rockwell method involved the application of a preliminary minor load (10 kg), followed by a larger major load (90 kg) that was applied for a set period. The depth of indentation from the major load, beyond the indentation from the minor load, was then used to calculate the Rockwell hardness number.

During the test, the sample was placed on the anvil of the tester, and the indenter (a steel ball, with 1/16-inch diameter) was brought into contact with the sample. The minor load was applied first, followed by the major load. Upon removal of the major load, the hardness number was read directly from the tester's scale. The reading of the Rockwell Hardness Number (RHN) was directly obtained from the dial reading of the tester.

3.4.6 Charpy Impact Test

The pendulum-type impact tester namely, Universal Impact Tester, model AIT300EN was utilized, with samples being prepared as per the ASTM D6110 standard procedure.

To begin, specimens of suitable dimensions as per the ASTM standard were prepared from the cured composites. The samples were prepared with a notch, the presence of which significantly influences the failure mechanism and the measured impact energy. The sample was positioned horizontally across the supports of the machine, with the notched face facing the striking pendulum. When released from a known height of 1.439 m (at an angle of 140°), the pendulum swung down with a velocity 5.35 m/s and broke the sample. The blow was struck on the face opposite to the notch. The energy absorbed by the sample to cause fracture was calculated from the loss of kinetic energy of the pendulum, as indicated by the height to which the pendulum rose after fracturing the sample.

3.4.7 FTIR Test

The Fourier Transform Infrared Spectroscopy (FTIR) analysis of the developed epoxy composites reinforced with natural fibers and carbon nanotubes (CNTs) was conducted, offering valuable insights into the chemical interactions within the composite materials.

In the first instance, each sample was prepared for FTIR analysis by grinding it into a fine powder. This powdered form enabled better interaction of the sample with the infrared radiation during the analysis. The FTIR spectrometer used in this study was a Shimadzu IR 470 spectrophotometer, which could provide high-quality spectral data for FTIR analysis. To collect the FTIR spectra, the ground composite sample (3 mg) was mixed with potassium bromide (KBr, 200 mg), a standard method for sample preparation in FTIR analysis (Sarkar and Adhikari, 2001). This mixture was then compressed to form a thin, transparent pellet.

The FTIR spectra were collected in the mid-infrared range (4000 - 400 cm^{-1}) at a resolution of 4 cm^{-1}. Each spectrum was recorded by averaging several scans to ensure the accuracy and repeatability of the spectral data.

The collected spectra were then analyzed to identify and interpret the characteristic absorption peaks. These peaks corresponded to the specific vibrational modes of the chemical bonds present in the composite material, thereby offering insights into the chemical structure and interactions within the composite.

3.4.8 Morphology Test Using the SEM

Scanning Electron Microscopy (SEM) was employed using a TESCAN VEGA Scanning Electron Microscope to examine the morphology of the formulated composites. Operating under high vacuum conditions, the microscope could capture detailed and high-resolution images of the sample surfaces with 3 nm resolution at 30 keV and 8 nm resolution at 3 keV. The SEM imaging was carried out at different magnifications to examine both the composite structure and the fine details of the fiber-matrix interfaces.

Initially, composite samples consisting of fractured tensile, flexural and impact specimens was placed in liquid nitrogen to achieve a fresh and clean surface, which is a crucial step to reveal the internal structure of the composites. The fractured samples were then sputter-

coated with a thin layer of gold (Au) to make them electrically conductive, a prerequisite for SEM imaging.

The acquired SEM images were then analyzed for the distribution and dispersion of natural fibers and CNTs within the epoxy matrix. Special attention was paid to the fiber-matrix and CNT-matrix interfaces, as these regions significantly influence the mechanical properties of the composites. Furthermore, the presence of any voids, cracks, or other defects in the composite structure was also noted, as these could potentially impact the composite performance. The collected SEM images were then compared to discern any changes in the composite microstructure with the variation in fiber and CNT content.

3.5 Finite Element Modeling

In this research, a particular methodology known as the Microstructure-Free Finite Element Modeling (MF-FEM) was utilized. MF-FEM is advantageous in that it does not require detailed microstructural information, making it suitable for a wide range of applications.

The initial step in the process was to develop the Representative Volume Element (RVE) model. This involved constructing a geometric model that adequately represented the composite material structure. The RVE was designed to include the matrix, reinforcements, and fillers, as required by the specific composite under investigation.

Once the RVE model was established, the next stage involved the application of appropriate boundary conditions. These conditions were carefully chosen to reflect the actual physical constraints under which the composite material operates. Alongside these boundary conditions, the governing equations describing the behavior of the composite material were also defined and integrated into the model.

After that, the model was further refined through a mesh independence test. This test was designed to identify the optimal element-to-RVE size ratio that would provide accurate results without excessive computational expense. Three RVE ratios were considered: 0.1, 0.04, and 0.025. The standard deviations and error bars associated with the results obtained at each of these ratios were examined, and the ratio that minimized these measures was selected as the optimal value. Following that, a validation study with experimental results was carried out.

3.5.1 Development of Finite Element Model

The "Representative Volume Element" (RVE) approach or the "homogenization" approach represents the idea that if a volume of material is large enough to be statistically representative of the whole material but small enough so that the material's properties can be assumed to be uniform across the volume, then this volume can be treated as a homogeneous and isotropic material at a certain scale. This simplifies analysis significantly because it allows the use of simpler equations and models that assume homogeneity and isotropy. To maintain this arrangement, three factors were ensured for the MF-FEM. These factors were:

(1) The inclusions' geometric aspect ratio was low,

(2) Their distribution and direction are statistically homogeneous, and

(3) Their characteristic dimensions are appropriately tiny relative to the size of the RVE.

The process for development of RVE model is explained as follows:

- In the study, the Representative Volume Element (RVE) was conceived as a cube, maintaining a dimensionless side length of L = 100 units, which can be ranged from nanometer unit to even meter unit because only the reinforcement-to-RVE size ratio is of relevance for this model. The reinforcements were embodied as finite elements.

- The Representative Volume Element (RVE) was initially designed as a uniform mesh made up of cubic elements, devoid of any reinforcements. This means that a uniform mesh of brick components was initially created without any reinforcements, which did not yet account for the variable properties of reinforcements that would be incorporated later.

- After that, some of the elements quantified by specific vol.% were randomly chosen and given reinforcement properties, while the remainder of the elements were configured to have matrix properties. The material properties were defined in Table 3.3, where the Young’s modulus and poisons ratio were considered. In all the developed RVE models, 25 vol.% and 34 vol.% natural fibers were taken as reinforcements corresponding to 30 wt.% and 40 wt.% respectively, in the

experimental analysis. 0,1,2 and 3 vol.% CNT were taken as filler material to corresponding to 0,1,2 and 3 wt.% of CNTs in experimental analysis. The intended vol% of reinforcements and the volume of each element were used to calculate the number of the chosen elements.

- The first n elements in the finite element mesh of the RVE were identified as reinforcements. This selection was based on the volume these elements represented within the mesh, ensuring a realistic representation of the volume of reinforcements within the actual composite. From the known densities of the matrix, fibers and MWCNT, weight fractions were converted into volume fractions.

- It was essential that the total volume of these selected elements was equal to the volume of the reinforcements. This volume was determined by the preferred volume fraction of the reinforcements in the actual composite, ensuring that the model accurately reflected the material's composition.

- The MATLAB function randperm(N) was used to create a random permutation of integers from 1 to N. This function ensured that the selection of elements to represent reinforcements was genuinely random, with no repeating sequences.

- The distribution of reinforcements within the RVE was not constrained by any periodic arrangement, reflecting the random distribution of reinforcements that typically occurs in real-world materials.

- To assess mesh independence, the element sizes of 10, 4, and 2.5 units were employed respectively. As such, the resulting ratio between the elements and the RVE was noted as 1:10, 1:25, and 1:40 respectively, providing diverse granularity levels for comparative analysis.

Fig 3.5 displays the detailed RVE model used in this study. The red element indicates 3vol.% CNT, the black elements indicates 25vol.% fiber and the rest of the element in grey color indicates epoxy resin. The element to RVE ratio was taken as 1:25 in this figure.

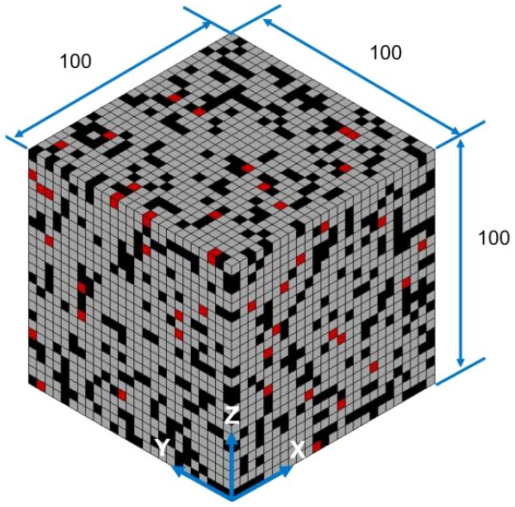

Fig 3.5: Developed RVE model for FEM analysis with side length 0f 100 units.

3.5.2 Boundary Conditions and Finite Element Analysis

In theory, the representative volume element (RVE) of the composite should display isotropic elastic properties, provided that the previously stated assumptions in section 3.5.1 3.5.1are met. Nonetheless, the actual dispersion of reinforcements within the matrix might not adhere strictly to a uniform and random pattern, potentially leading to slight anisotropy in the RVE properties (Luo, 2022a). To mitigate this residual anisotropy, the properties along the x, y, and z axes were averaged, ensuring a more consistent estimation of the composite's behavior. The boundary conditions are listed for each face of the RVE, corresponding to x = 0, y = 0, z = 0, x = 100, y = 100, and z = 100. The conditions, defining the Young's modulus of the RVE when subjected to certain constraints or loads were outlined in the designated Table 3.4.

Table 3.4: Boundary conditions in the RVE

RVE surface	Young's modulus in X direction $\overline{E}_x$	Young's modulus in Y direction $\overline{E}_y$	Young's modulus in Z direction $\overline{E}_z$
x=0	$u_x = 0$	$u_x = 0$	$u_x = 0$
y=0	$u_y = 0$	$u_y = 0$	$u_y = 0$
z=0	$u_z = 0$	$u_z = 0$	$u_z = 0$
x=100	$u_x = 1$	Homogeneous u_x	Homogeneous u_x
y=100	Homogeneous u_y	$u_y = 1$	Homogeneous u_y
z=100	Homogeneous u_z	Homogeneous u_z	$u_z = 1$

Here's the summary of the boundary conditions:

- For x = 0: The displacement in the x-direction (u_x) is fixed to zero, regardless of the material properties. This means the left face of the RVE is not allowed to move in

the x-direction. The shear deformation is also restrained, with no displacement allowed in any direction.

- For y = 0: The displacement in the y-direction (u_y) is fixed to zero, regardless of the material properties. This means the bottom face of the RVE is not allowed to move in the y-direction.

- For z = 0: The displacement in the z-direction (u_z) is fixed to zero, regardless of the material properties. This means the front face of the RVE is not allowed to move in the z-direction.

- At x=100, the displacement in the x-direction (u_x) is set to 1, and the displacements in the y and z directions are set to vary homogeneously. This means that all nodes on this face move in the x direction by an amount of 1, and the y and z displacements of these nodes are not fixed, but they change uniformly across the face.

- At y=100, the displacement in the y-direction (u_y) is set to 1, and the displacements in the x and z directions are set to vary homogeneously. This means that all nodes on this face move in the y direction by an amount of 1, and the x and z displacements of these nodes are not fixed, but they change uniformly across the face.

- At z=100, the displacement in the z-direction (u_z) is set to 1, and the displacements in the x and y directions are set to vary homogeneously. This means that all nodes on this face move in the z direction by an amount of 1, and the x and y displacements of these nodes are not fixed, but they change uniformly across the face.

The term "homogeneous" here referred to the fact that the displacement varied uniformly across the face of the RVE.

The properties of the representative volume element (RVE), specifically the effective Young's moduli ($\overline{E}_x$) were derived from the average stresses (σ_i) and average strains (ε_i) along the three axial directions, given by the Eq. (3.36), for i = x, y, z.

$$\overline{E}_i = \frac{\overline{\sigma}_i}{\overline{\varepsilon}_i} \tag{3.36}$$

The computation of these average stresses and strains was facilitated through the integration of the finite element stresses σ_i and strains ε_i over the volume of the RVE, denoted as V, given by Eqs. (3.37) and (3.38).

$$\overline{\sigma}_i = \frac{1}{V} \int_V \sigma_i \, dV \tag{3.37}$$

$$\overline{\varepsilon}_i = \frac{1}{V} \int_V \varepsilon_i \, dV \tag{3.38}$$

Ultimately, the effective Young's modulus of the RVE were calculated as the arithmetic mean of the respective values in the x, y, and z directions, as given by Eq. (3.39).

$$\overline{E} = \frac{\overline{E}_x + \overline{E}_y + \overline{E}_Z}{3} \tag{3.39}$$

$$SD = \sqrt{\frac{(\overline{E}_x - \overline{E})^2 + (\overline{E}_y - \overline{E})^2 + (\overline{E}_z - \overline{E})^2}{3}} \tag{3.40}$$

In this study, the element chosen for the analysis was the 20-node solid186 model. For every RVE model, calculations were made to obtain the average (denoted as $\overline{E}$) and the standard deviation (represented by SD) of the Young's moduli, which were characterized from the three loading orientations, as given by Eq. (3.40).

Commercial software ANSYS Mechanical APDL (2020 R1), was employed to carry out all finite element analyses in this study.

3.5.3 Validation Study

A validation study was conducted with the experimental Young's modulus to validate the result of the developed FE model.

Fig 3.6 shows the developed RVE model for the validation study of finite element model. Here, the element in black color indicates 30 vol% reinforcements and rest of the elements in grey color indicates matrix material.

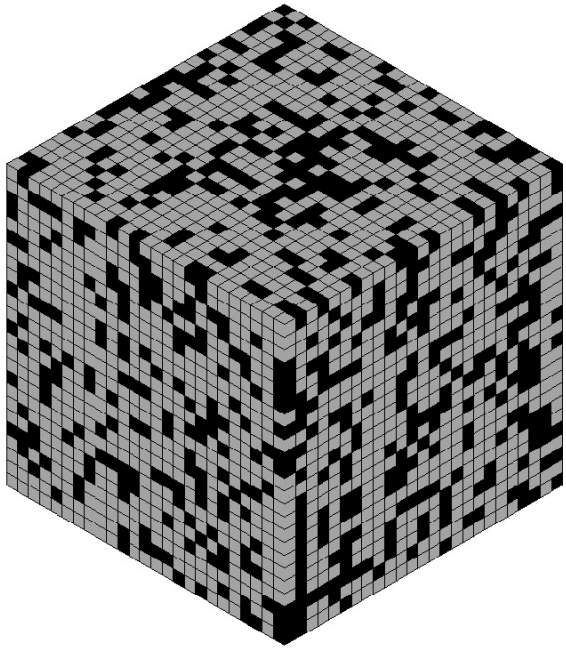

Fig 3.6: Developed RVE model for validation study of FEM analysis

3.5.4 Mesh Independency

The mesh independence test was performed by studying the influence of the element-to-RVE size ratio on the predicted Young's modulus derived from the Microstructure Free Finite Element Method (MF-FEM). The composite under consideration was either a two-phase Epoxy pineapple fiber composite or a three-phase Epoxy pineapple fiber CNT composite. The volume fraction of the reinforcing elements was set at 25%, which corresponded to 30 wt.% of pineapple fibers and 3 vol.% CNTs.

The mesh independence testing commenced with the creation of an initial finite element model with a specific element-to-RVE size ratio 0.1. This model was then subjected to simulated mechanical testing via ANSYS software, and the predicted Young's modulus was noted.

Subsequently, the element-to-RVE size ratio was systematically altered to 0.04, and 0.025, and the mechanical testing simulation was repeated for each alteration. During each iteration, the Young's modulus was recorded. The volume fraction of the reinforcing elements remained constant at 25%. Fig 3.7 represents the developed RVE model with two and three materials, where the elements in black color indicate pineapple fiber, the elements in red color indicate CNT and the rest of the elements in grey color indicate epoxy resin. The RVEs in Fig 3.7 are indicative of: (a) two materials with element to RVE ratio 0.1, (b)

two materials with element to RVE ratio 0.04, (c) two materials with element to RVE ratio 0.025, (d) three materials with element to RVE ratio 0.1, (e) three materials with element to RVE ratio 0.04, and (f) three materials with element to RVE ratio 0.025..

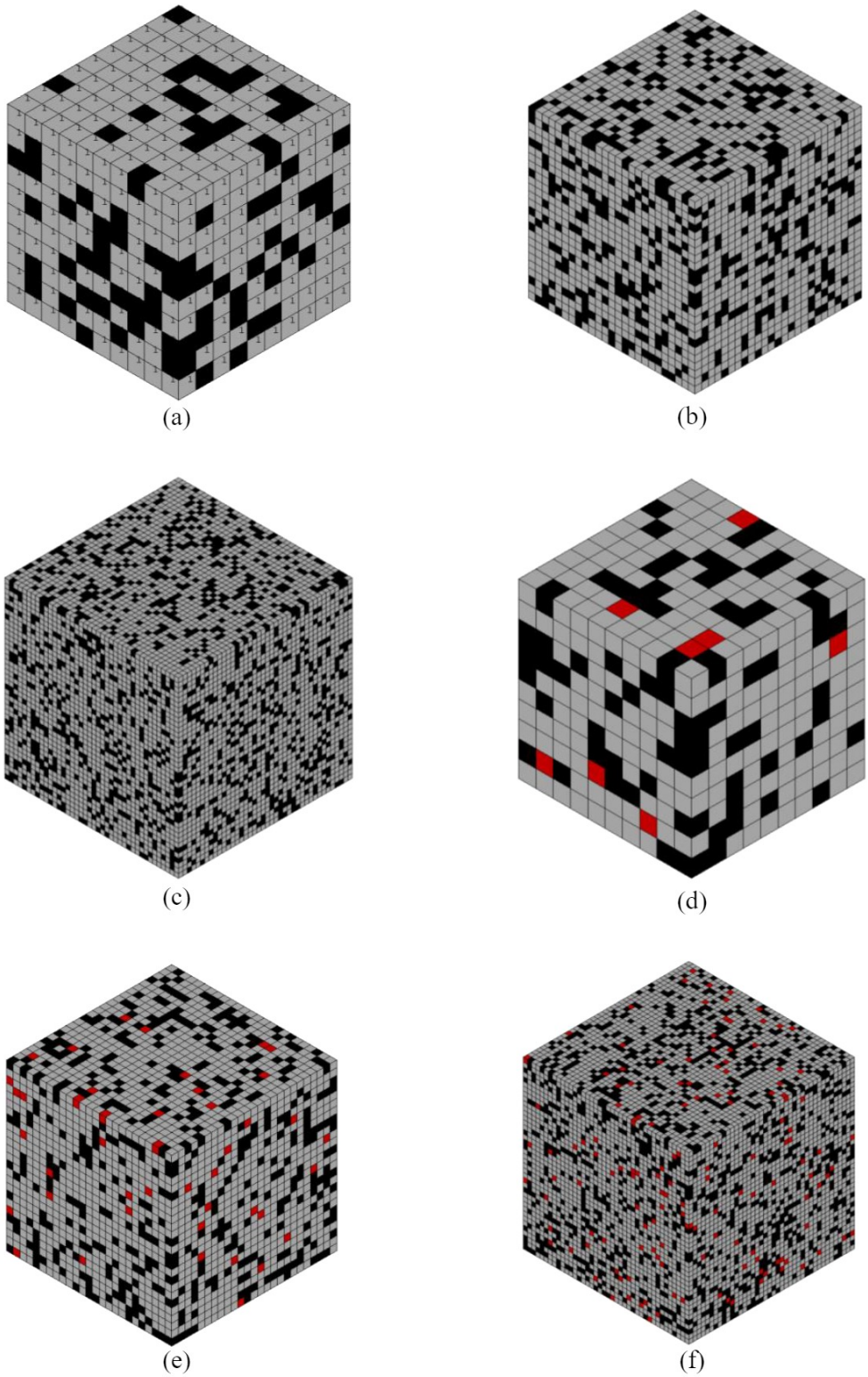

Fig 3.7: Developed RVE models for mesh independency test

The average Young's modulus and its standard deviation were calculated for each of the three element-to-RVE size ratios. Error bars, derived from the standard deviation values, were plotted to visually represent the degree of anisotropy. The length of these error bars served as an indicator of the variation in the predicted Young's modulus for the different size ratios.

3.6 Uncertainty Analysis

For the study's uncertainty analysis, a procedure was employed that utilized the average values and standard deviation calculations. It was understood that all experimental results are subject to uncertainty and this analysis was critical to estimate the precision of the obtained results. The steps of the methodology are as follows:

1. Initially, the mean value (μ) for a set of measurements for each sample was calculated using standard statistical methods using Eq. (3.41) where, E_1, E_2 and E_3 were the values for three measurements.

$$\mu = \frac{E_1 + E_2 + E_3}{3} \tag{3.41}$$

2. Subsequently, the standard deviation (σ) was computed, which is a measure of the spread of data values from their mean value using Eq. (3.42). It gave an indication of the variability or dispersion present in the data set.

$$\sigma = \sqrt{\frac{(\mu - E_1)^2 + (\mu - E_2)^2 + (\mu - E_3)^2}{3}} \tag{3.42}$$

3. Once both the mean and standard deviation were obtained, the percentage uncertainty was determined. This was computed by dividing the standard deviation by the mean and multiplying by 100, giving the relative uncertainty in percentage form.

$$\text{Uncertainty} = \frac{\sigma}{\mu} \times 100\% \tag{3.43}$$

4. This process was repeated for each of the experimental data sets corresponding to different conditions of the study.

5. Ultimately, the calculated percentage uncertainties were graphed to present a visual depiction of the variation in uncertainty under different conditions or parameters. This helped identify any patterns or outliers that might exist, providing further insight into the reliability of the data.

3.7 Regression Equations

The methodology for developing quadratic regression equations for each of the studied properties - tensile strength, Young's modulus, elongation at break, flexural strength, flexural modulus, Rockwell hardness number, impact energy, density, void content, and water absorption - in the epoxy natural fiber CNT composites was executed as follows:

After the collection of the relevant mechanical properties, quadratic regression analyses were conducted. In these analyses, the weight percentages of the fibers and CNTs served as independent variables (represented by A and B respectively), while the respective property in question was the dependent variable for three different fiber types (denoted by Y). The general form of the quadratic regression equation employed was:

$$Y = a + bA + cB + dAB + eBB$$

In this equation, 'a' was the y-intercept of the regression parabola, 'b', 'c', 'd', and 'e' were the regression coefficients that indicated the degree of change in Y for a unit change in the corresponding independent variable, A or B. BB represented the squared terms necessary for quadratic regression, and AB was the interaction term. These quadratic regression equations were derived using statistical software Minitab that determined the coefficients 'a', 'b', 'c', 'd', and 'e' in order to minimize the sum of the squared residuals (the differences between the observed and predicted values of Y).

As in any statistical modeling, the validity of these quadratic regression models needs to be examined using appropriate statistical checks. These may include inspection of the residuals for normality and homoscedasticity, and calculation of the coefficient of determination (R^2) to estimate the proportion of the variance in the dependent variable that can be predicted from the independent variables.

3.8 Optimization of Constituent Materials

The optimization of constituent materials for the Epoxy natural fiber CNT composites was performed using Grey Relational Analysis (GRA). The following physical properties were chosen as response variables for this study: tensile strength, Young's modulus, elongation at break, flexural strength, flexural modulus, Rockwell hardness number, Impact energy, density, void content, and water absorption. Among these, tensile strength, Young's modulus, elongation at break, flexural strength, flexural modulus, Rockwell hardness number, and Impact energy were identified as "larger-the-better" type responses. On the other hand, density, void content, and water absorption were considered as "smaller-the-better" type responses (Kuo, Yang, and Huang, 2008).

The first step in applying GRA was the normalization of the experimental data. Each of the response variables was normalized using the grey relational generation, which transforms the data series into a comparable scale. The procedure for the "larger-the-better" type was defined by the Eq. (3.44):

$$Z_{ij} = \frac{Z_j - \min Z_j}{\max Z_j - \min Z_j} \tag{3.44}$$

And for "smaller-the-better" type was defined by the Eq. (3.45):

$$Z_{ij} = \frac{\max Z_j - Z_j}{\max Z_j - \min Z_j} \tag{3.45}$$

where Z_{ij} is the performance score of property j of alternative i and Z_j is the experimental value of each composite for each test. The resultant normalized values were within the interval of zero to one.

The second step involved the calculation of the grey relational coefficients, ξ_{ij}, which reflect the relationship between the desired and actual experimental data. The distinguishing coefficient or identification coefficient (ζ), which takes value between 0 and 1, was set as 0.5. The grey relational coefficient ξ_{ij} of property j of alternative i was then calculated as Eq. (3.46):

$$\xi_{ij} = \frac{\Delta_{min} + \zeta\Delta_{max}}{\Delta_{ij} + \Delta_{max}} \quad (3.46)$$

Where Δ_{min} and Δ_{max} are the smallest and the largest values of Δ_{ij}, and $\Delta_{ij} = |Z_{0j} - Z_{ij}|$, where Z_{0j} represents the reference sequence and Z_{ij} is the comparability sequence.

The third step in the GRA was the determination of the Grey Relational Grade (GRG), which was calculated by averaging the grey relational coefficients corresponding to each performance characteristic.

$$GRG = \frac{1}{n}\sum_{i=1}^{n} \xi_{ij} \quad (3.47)$$

Finally, the optimization of the composites' constituent materials was done by identifying the composition that yielded the highest grey relational grade, indicative of the most favorable combination of properties:

CHAPTER 4
RESULTS AND DISCUSSIONS

4.1 Selection of Natural Fiber as Constituent Materials

The task of selecting a suitable natural fiber to serve as a reinforcement in composites required an integrative approach involving both the Fuzzy Analytical Hierarchy Process (AHP) and Techniques for Order Preference by Similarity to an Ideal Solution (TOPSIS) method. These multiple criteria decision-making (MCDM) tools enabled a holistic evaluation of an array of fiber candidates, each distinguished by its unique set of properties. The potential fibers were rigorously examined and ranked based on their performance metrics. Emphasis was placed on characteristics higher tensile strength, higher Young's modulus, higher elongation at break and lower density. Following this systematic evaluation, the most promising fiber was selected, offering optimized performance within the specific constraints and requirements of aerospace composite fabrication. This integrative approach proved instrumental in ensuring an objective and comprehensive selection process, thereby maximizing the potential success of the resulting composite material.

4.1.1 Resultant Criteria Weightage from Fuzzy AHP Technique

Table 4.1 delineate the pairwise contrast matrix, comparative fuzzy criteria weightage and standardized non-fuzzy criteria weightages attained from the pairwise contrast matrix. It was noted that the tensile strength had the maximum weightage, and Young's modulus and the elongation at break had the minimum weightage, among the four criteria. The highest eigenvalue for the relationship from Eq. (3-10) was 4.0605, and the consistency index (CI) obtained from Eq. (3-11) was 0.0202. The consistency ratio (CR) gained from Eq. (3-12) was 0.0227 for this study, which was under 0.1 and indicated that the weightages obtained from the Fuzzy AHP method were satisfactory.

Table 4.1: Pairwise contrast matrix and fuzzy criteria weights attained from AHP

Criteria	Tensile Strength	Density	Young's Modulus	Elongation at Break
Tensile strength	(1, 1, 1)	(1, 2, 3)	(2, 3, 4)	(2, 3, 4)
Density	($^1/_3$, $^1/_2$, 1)	(1, 1, 1)	(2, 3, 4)	(2, 3, 4)

Criteria	Tensile Strength	Density	Young's Modulus	Elongation at Break
Young's modulus	(1/4, 1/3, 1/2)	(1/4, 1/3, 1/2)	(1, 1, 1)	(1, 1, 1)
Elongation at break	(1/4, 1/3, 1/2)	(1/4, 1/3, 1/2)	(1, 1, 1)	(1, 1, 1)
Relative fuzzy weight	(0.234,0.441,0.754)	(0.178,0.312,0.573)	(0.083,0.124,0.203)	(0.083,0.124,0.203)
Normalized non fuzzy weights	0.432	0.313	0.124	0.124

Table 4.2 represents the performance scrutiny of the derived standardized non fuzzy criteria weightages. Mean Square Error (MSE), Root Mean Square Error (RMSE), Mean Absolute Error (MAE), percentage error and accuracy were measured to evaluate the performance. It was observed that MSE, RMSE and MAE were miniscule for this assessment. The complete accuracy was more than 99%, demonstrating the acceptability of the obtained criteria weightages.

Table 4.2: Performance scrutiny of the derived standardised non fuzzy weightages

Criteria	Young's Modulus
Mean	0.25
MSE	0.01
RMSE	0.12
MAE	0.10
Percentage error	0.67%
Accuracy	99.33%

4.1.2 Assessment of Fiber Ranking with Fuzzy TOPSIS Approach

From the criteria weightages achieved from AHP, the fuzzy TOPSIS analysis was conducted for each of the alternatives of the twelve natural fibers. Table 4.3 exemplified the choice and performance result for the nine variations of coir fiber employing fuzzy TOPSIS technique.

Table 4.3 shows that the E6 variation has the maximum performance score because of the highest tensile strength, low density as well as good Young's modulus and elongation at break. Therefore, the variation ranked first compared to other fibers. Accordingly, similar analyses were carried out to select the best variants among the other fibers based on the performance score.

Table 4.3: Comparison of the selection of alternatives from coir fiber

Code	Performance Score	Rank
E1	0.716	2
E2	0.504	4
E3	0.304	6
E4	0.214	9
E5	0.271	8
E6	0.770	1
E7	0.498	5
E8	0.290	7
E9	0.563	3

After selecting the best alternatives from each fiber, the next step was to carry out TOPSIS analysis on the selected variant from each fiber. Table 4.4 represents the selected alternative and maximum performance score for each of the fibers.

Table 4.4: Selection of the best alternatives and order of preferences for all fibers

Code	Maximum Performance Score	Rank
Banana	0.320	6
Bagasse	0.087	12
Cotton	0.220	10
Ramie	0.357	5
Coir	0.513	2
Pineapple	0.562	1
Flax	0.420	3
Hemp	0.300	7
Jute	0.213	11
Sisal	0.239	8
Kenaf	0.391	4
Bamboo	0.233	9

Pineapple fiber and coir fiber were close competitors for the first position in the order of preference of fibers. However, due to the over-the-top tensile strength of the pineapple fibers, it ranked first, and coir fiber ranked second mainly because of its abundant elongation at break property compared to other fibers. However, bagasse fiber ranked last in the analysis mainly because of its poor tensile strength, Young's modulus and elongation at break properties.

4.1.3 Sensitivity Analysis by Inducing Disturbance on Fuzzy Criteria Weights

To carry out the sensitivity analysis of the TOPSIS method, an investigation was conducted varying the unitary ratio (β_k) of the fuzzy criteria weights.

Fig 4.1 shows the change in the rankings derived from AHP-TOPSIS method due to sequential induced disturbance on the criteria weights for (a) density; (b) tensile strength; (c) Young's modulus; and (d) elongation at break.

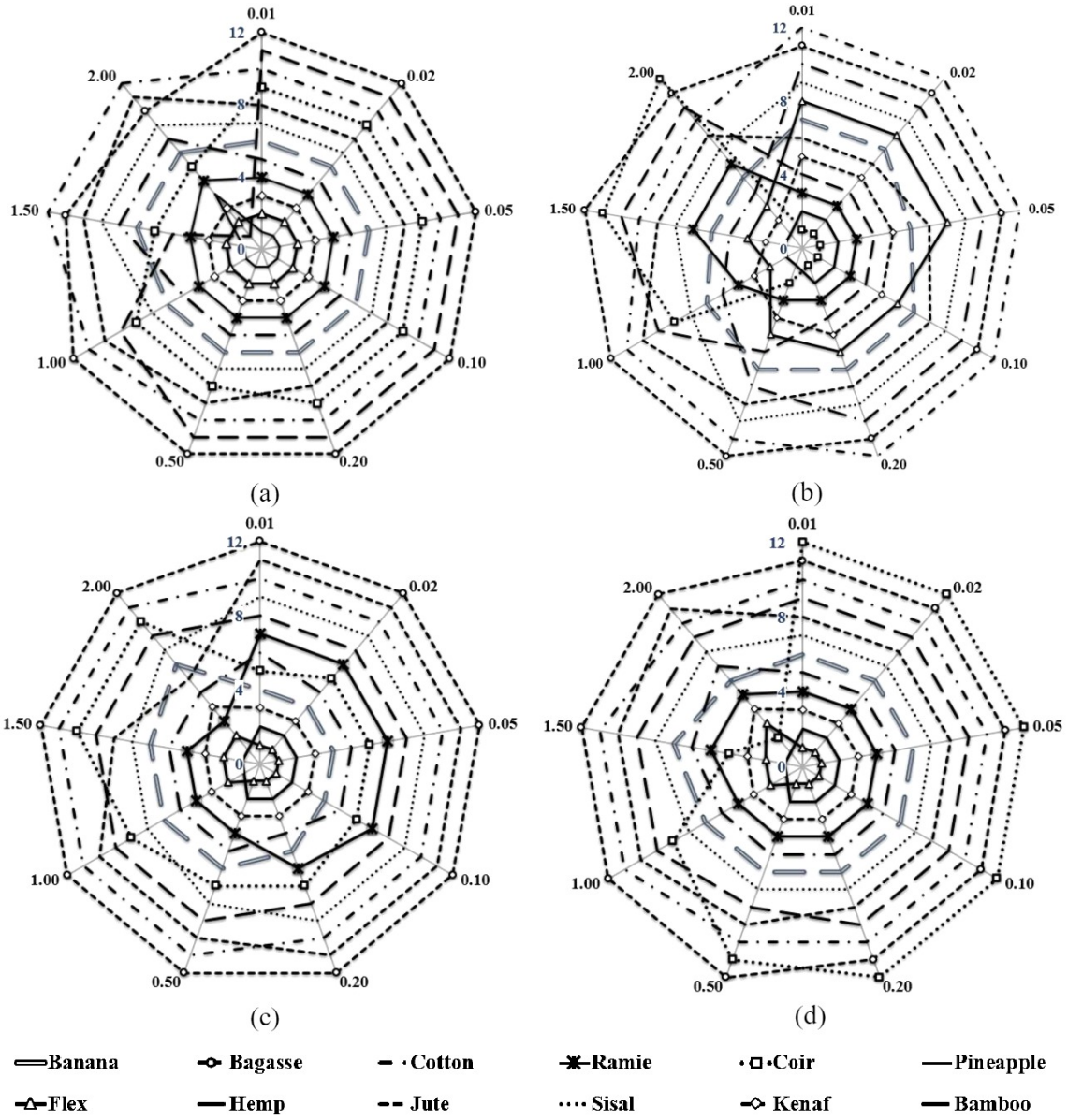

Fig 4.1: Deviation of ranking with induced disturbance on the weightages of mechanical properties.

Fig 4.1(a) shows that the ranks of all single natural fibers were altered after $\beta_1 = 0.2$ as the criteria weightage for density was changed. After $\beta_1 = 1.0$, the ranking change became more irregular as the criteria weights for density increased rapidly with β_1. No variation was observed for flax and kenaf fiber whereas, minor variations in the ranking were observed for ramie, and banana fiber. The rest of the fibers were largely sensitive to the variations of the weightage for density. A sharp change in the ranking of the bamboo fiber was observed

due to its relatively much lower density than other fibers and gradual increase in the weightage for density. Fig 4.1(b) reveals that due to the disturbance forced on the weights of tensile strength, the ranks of the fibers were consistent up to $\beta_2 = 0.02$. After that, there was only a slight change in the ranking of flax, jute, and banana fiber up to $\beta_2 = 0.20$. Notably, there was a noticeable alteration in the ranking score of bamboo, coir, and hemp fiber. The rest of the fibers were found to be sensitive also to the weight variation of tensile strength.

Fig 4.1(c) shows that the fibers were very less sensitive for the disturbance induced on the weights of Young's modulus whereas, bagasse fiber was not sensitive to the disturbance at all. The ranks of all the fibers were consistent up to $\beta_3 = 0.1$, and slight changes in the ranking were observed in flax, kenaf, bamboo, hemp, and pineapple fibers. No sharp alterations were observed for any of the fibers. Fig 4.1(d) demonstrates that all the fibers were sensitive to a certain extent by the disturbance induced on the weights of elongation at break. The ranks of all the fibers were unaffected up to $\beta_4 = 0.2$. After that, there was a gradual change in the rankings of the fibers due to the sharp change in only the rank of coir fiber. Coir fiber has a much higher percentage of elongation of break compared to other fibers. So, as the β_4 increased, the weightage for the elongation at break kept rising. As a result, an improvement in the ranking of coir fiber was detected.

Therefore, it can be observed that the derived ranking of the natural fibers was stable after 20% of change in weightages. However, large changes in the weightages, specially more than 20% resulted in large deviations of the derived rankings. So, the weightages obtained from the AHP analysis can be altered maximum up to 20% and the ranking would be almost same. This indicates the wide range of stability of the derived rankings from integrated fuzzy AHP-TOPSIS method.

4.2 Sedimentation Test Result

Fig 4.2 shows the effect of ultrasonication on matrix/ MWCNT mixture, where the MWCNT concentrations are marked in white font as 1, 2, 3 and 4 indicating 1,2,3 and 4 wt.% MWCNT respectively in the mixture. Table 4.5 represents the detailed information about Fig 4.2 including the ultrasonication time as well as observation time.

Table 4.5: Detailed description of each figure corresponding to Fig 4.2

Rows	Column 1 Observations after 24 hours	Column 2 Observations after 48 hours	Column 3 Observations after 48 hours
Row 1: No ultrasonication	(a)	(b)	(c)
Row 2: 30 min ultrasonication	(d)	(e)	(f)
Row 3: 60 min ultrasonication	(g)	(h)	(i)
Row 4: 90 min ultrasonication	(j)	(k)	(l)

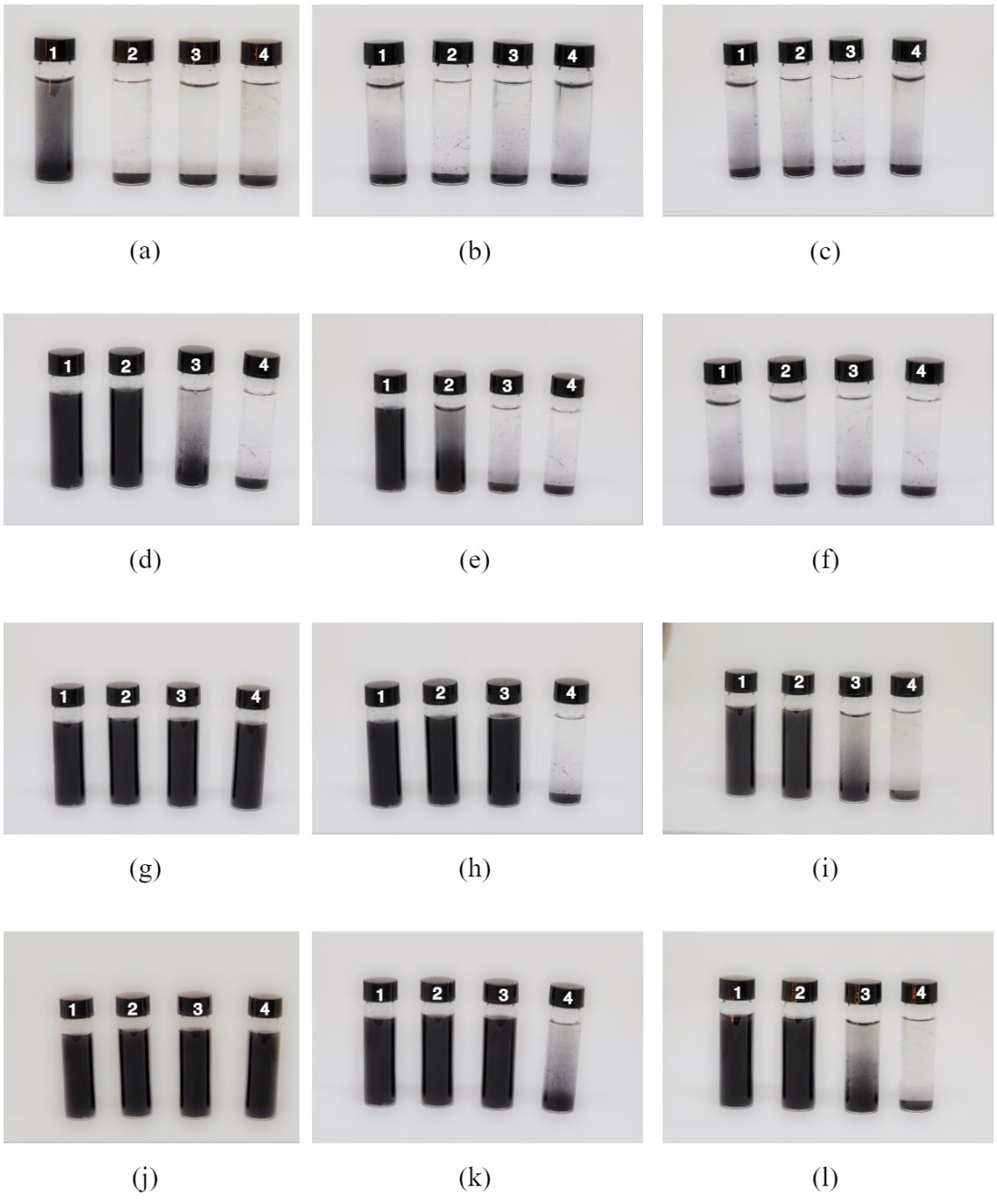

Fig 4.2: Photograph of MWCNT dispersion in epoxy.

Without ultrasonication, the dispersion stability was visibly poor. A modest degree of stability was observed in a 1 wt.% CNT mixture after 24 hours. However, after 48 and 72 hours, all samples demonstrated marked sedimentation. It was evident that without ultrasonication, the attractive forces between individual CNTs led to their agglomeration and eventual sedimentation.

Upon ultrasonication for 30 minutes, enhanced dispersion stability was observed in the 1 wt.% and 2 wt.% CNT mixtures after 24 hours. However, after 72 hours, all the samples were again heavily sedimented. This outcome suggested that a 30-minute ultrasonication period was insufficient to maintain the dispersion stability of the CNTs in the long term.

When the ultrasonication time was increased to 60 minutes, substantial improvements in dispersion stability were observed. After 24 hours, the 1 wt.%, 2 wt.%, and 3 wt.% CNT mixtures remained stable, while the 4 wt.% CNT mixture began to sediment after 48 hours. After 72 hours, the 1 wt.% and 2 wt.% CNT mixtures still maintained stability. A similar trend was observed for an ultrasonication time of 90 minutes, further corroborating these findings.

Consequently, it had been deduced that an ultrasonication time of 60 minutes was optimal for balancing experimental time, cost, and dispersion stability. The increased ultrasonication time evidently weakened the inter-CNT attractive forces and improved their dispersibility in the epoxy, thereby enhancing the physical and chemical interactions between the CNTs and the epoxy. The increase of ultrasonication time from 30 minutes to 60 minutes to the surfaces of CNTs not only weakened the strong attraction contacts between the CNTs, but also modified their dispersibility in epoxy and thus ensured better interfacial physical and chemical attraction between CNTs and epoxy. But with increasing wt.% of CNT to a certain quantity resulted in agglomeration as indicated by the settling out of CNT particles at the bottom of the vials

However, the findings also indicated that an increase in the wt.% of CNT beyond a certain threshold led to agglomeration, as demonstrated by the sedimentation of CNT particles at the bottom of the vials. This sedimentation was likely due to the increased CNT concentration overcoming the dispersion forces induced by ultrasonication, resulting in agglomeration and sedimentation.

4.3 Physical and Mechanical Properties

A comprehensive study on the properties of the developed epoxy composites, focusing on the physical and mechanical properties of the materials was conducted in this study. Table 4.6 represents the code of each composite in the figures of corresponding physical and mechanical properties determined.

Table 4.6: Code of each composite in the figures of physical and mechanical properties

Natural fiber reinforcement	Weight fraction of MWCNT			
	0 wt.%	1 wt.%	2 wt.%	3 wt.%
Sisal fiber	S0	S1	S2	S3
Pineapple fiber	P0	P1	P2	P3
Coir fiber	C0	C1	C2	C3
Epoxy-CNT Composite	EC			

4.3.1 Density and Void Content

The experimental density values of the composite specimens are exhibited in Fig 4.3. It was observed that, as the fibers being added have a higher density than the matrix material, increasing the fiber content increased the overall density of the composite. This is because the fibers were taking up a larger proportion of the composite's volume, and their higher density contributes more to the overall density of the material.

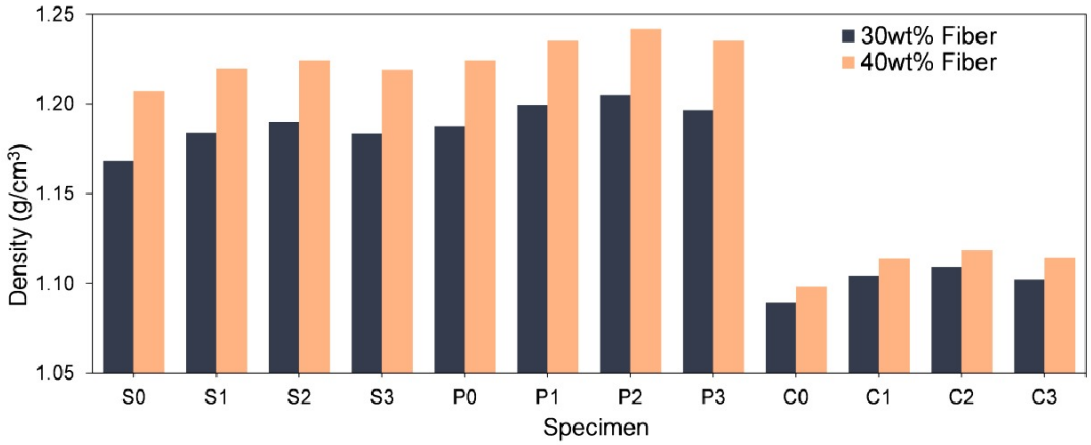

Fig 4.3: Experimental result for density with varying fiber contents.

It had been observed that pineapple fiber composites consistently yielded the highest experimental density across all weight percentages, followed by sisal and then coir fiber reinforced composites. The higher cellulose content in pineapple and sisal fibers, as compared to coir fibers, as evident in Table 2.1 contributed to the higher densities of these composites. This finding is aligned with existing literature also (Mehdikhani et al., 2019).

Fiber with a high cellulose content tends to have a denser structure due to the arrangement of cellulose molecules. When these fibers are embedded in a matrix material to form a composite, they contribute to the overall density of the composite.

The incorporation of CNTs in the composite material generally led to an increase in experimental density. However, it appears that there is an optimal CNT weight percentage (2 wt.%) for each fiber type, beyond which the density starts to decrease. Carbon nanotubes have a higher density compared to the Epoxy resin. When CNTs were added to the composite material, they increased the overall density of the composite due to their high-density nature. However, the slight decrease in density observed at 3% CNT across all fiber types and both fiber content levels might be attributed to the agglomeration of CNTs, leading to the formation of voids within the matrix. Such voids would reduce the overall density of the composites. The similar observation has been documented in other researches also (Ciecierska et al., 2013).

Fig 4.4 exhibits the comparison of theoretical and experimental densities of the composites. As shown in Fig 4.4, the experimental and theoretical density values of the composites increased with the increasing loading of nanofillers. Carbon nanotubes typically have a higher density compared to epoxy resin and as the proportion of CNTs in the composite increased, the overall density of the composite increased due to this higher density.

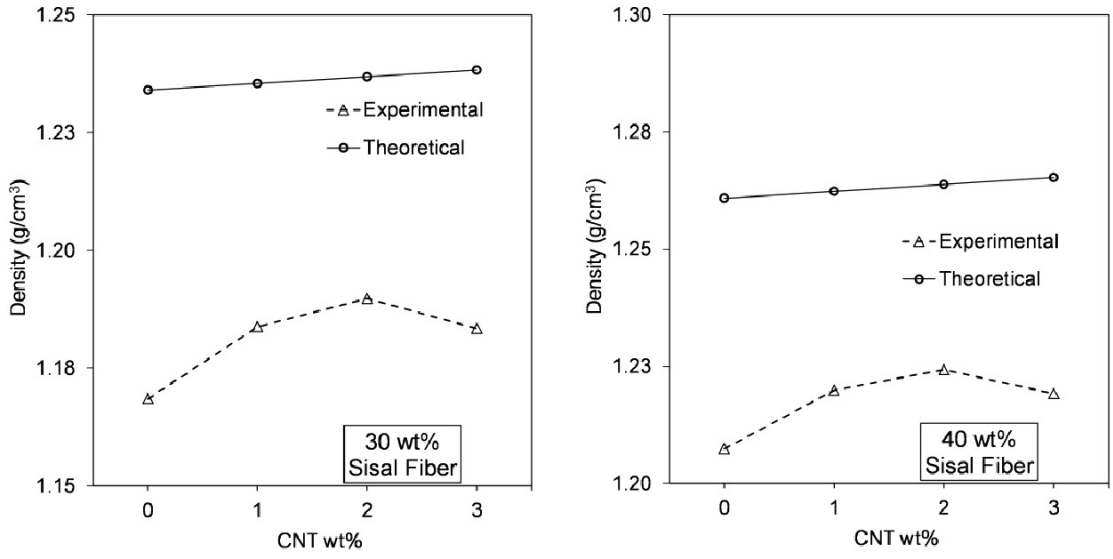

(a) (b)

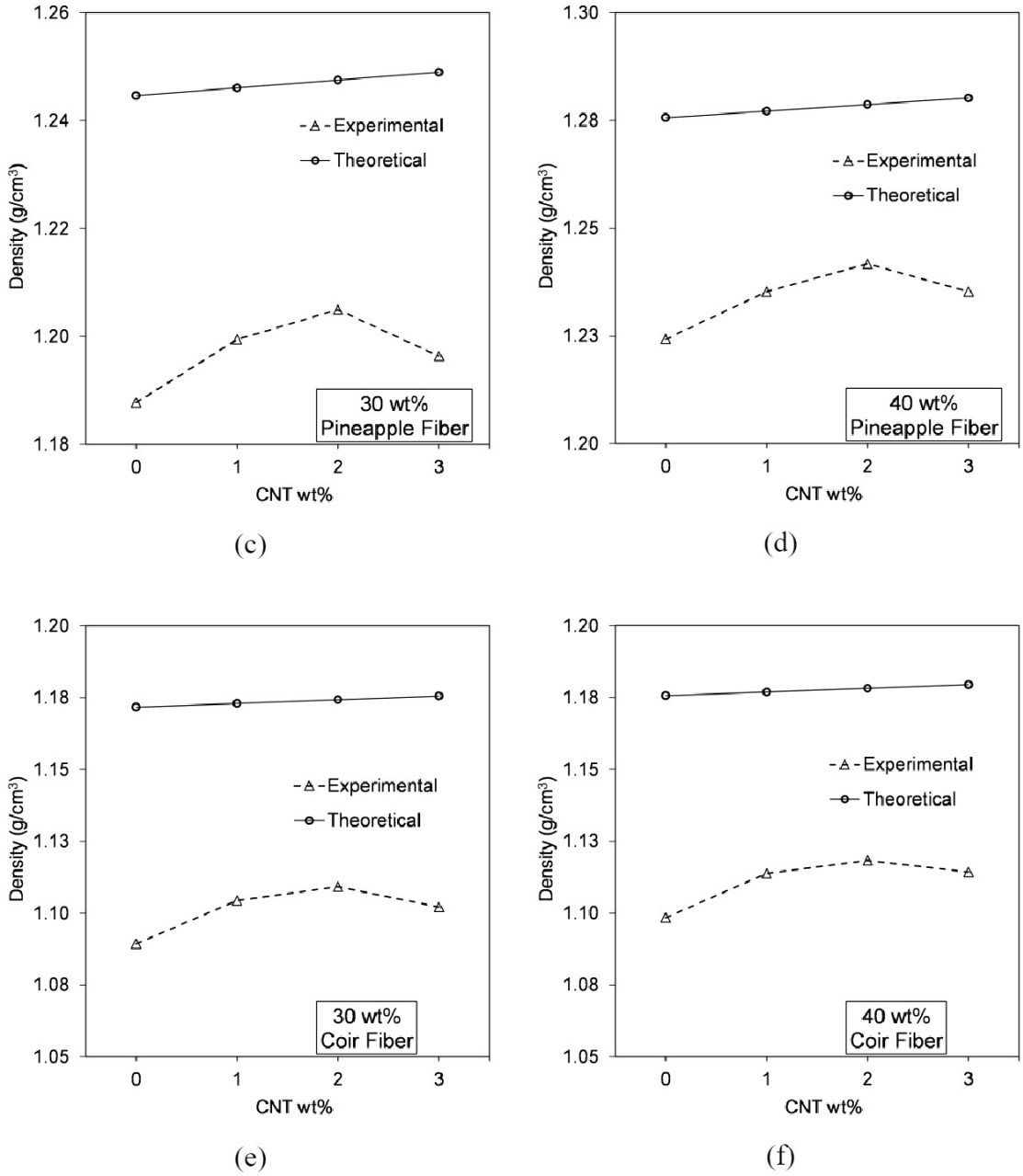

Fig 4.4: Variation of experimental and theoretical density among composites.

However, Fig 4.4 also indicates that the density values determined experimentally for composites are commonly lower than the corresponding theoretical values. For 3 wt.% of CNT, the voids were more significant than the other weight percentages of CNTs. As a result, lower density values were observed than composites with 1 wt.% and 2 wt.% CNT. The differences between the experimental and theoretical densities could have been due to several factors. For one, the theoretical densities were calculated based on the assumption of perfect dispersion and adhesion of the fibers and CNT within the epoxy matrix. However, during the actual fabrication process, several factors such as the presence of voids, imperfect fiber dispersion, and sub-optimal fiber-matrix adhesion could have resulted in

lower experimental densities. Additionally, natural fibers possess inherent variability in their properties, including density, which could have contributed to the observed discrepancy. Similar observations had been reported in other literature also (Mohan and Rajmohan, 2017).

Fig 4.5 demonstrates the void content properties of the prepared composite specimens. As the fiber content increased, there had been less space available within the composite for voids to form, resulting in a reduction in void content. The fibers had essentially filled up the space that might have otherwise been occupied by voids. The denser packing of fibers could have led to a more compact structure, which in turn might have restricted the formation of voids. For this reason, a smaller number of voids had been formed in 40wt.% fiber reinforced composites than 30wt.% fiber reinforced composites. The discovery was consistent with prior researches that had been documented in a scholarly review publication (Mehdikhani et al., 2019).

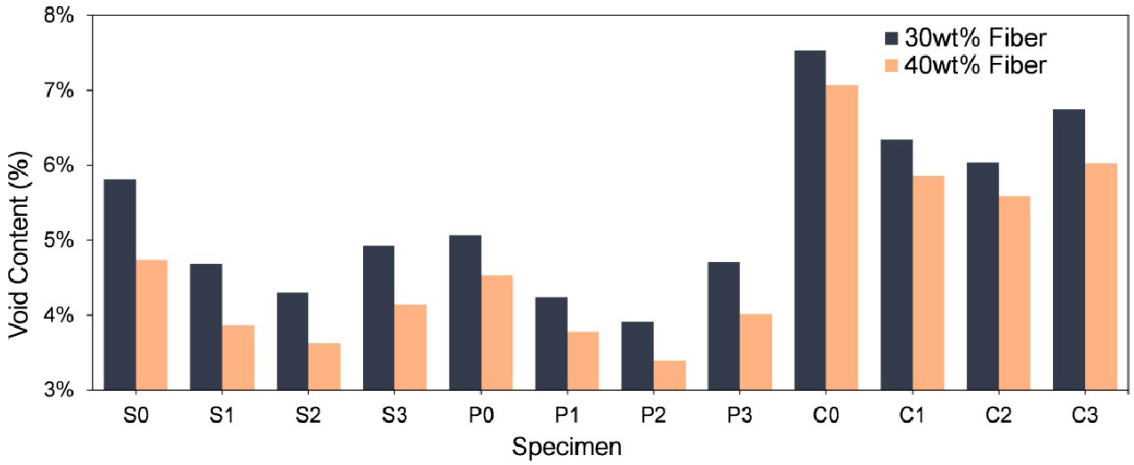

Fig 4.5: Variation of void contents among composite specimens.

High cellulose content in the fibers could have resulted in a denser packing within the composite, leaving less space for the formation of voids. As such, the void content in composites with higher cellulose content fibers like pineapple and sisal had been observed to be lower than that in composites with coir fibers, which have relatively lower cellulose content. Moreover, the cellulose in the fibers could have played a crucial role in the interaction between the fibers and the epoxy matrix. The hydroxyl groups in the cellulose molecule can form hydrogen bonds with the epoxy matrix, improving the fiber-matrix interfacial adhesion. Better adhesion could have reduced the chance of void formation at the interface, thereby reducing the overall void content (Franco and Valadez-González, 2005).

The addition of CNT had also been associated with a decrease in void content, up to a certain point. CNTs had been known for their high aspect ratio and good dispersion properties in the matrix, which could have resulted in a more homogeneous and densely packed composite structure. The CNTs could have also improved the interfacial adhesion between the fibers and the epoxy matrix, further reducing the void content. However, when the CNT content was increased to 3 wt%, an increase in void content had been observed. This rise in void content at higher CNT concentrations might have been due to agglomeration of the CNTs. At high concentrations, CNTs tend to form bundles or agglomerates due to van der Waals forces, leading to an uneven distribution of CNT in the matrix. These agglomerated areas could have created localized sites of stress concentration and resulted in void formation. This finding is consistent with the observations documented by other researchers (Nabinejad et al., 2018).

4.3.2 Water Absorption Results

A comprehensive set of data on water absorption in various composite materials had been measured and analyzed. The bar graph in Fig 4.6 displays the percentage of water absorption for different composites with varying natural fibers, their weight percentages and the weight percentages of Carbon nanotube. The x-axis shows the type of composites, while the y-axis shows the water absorption percentage.

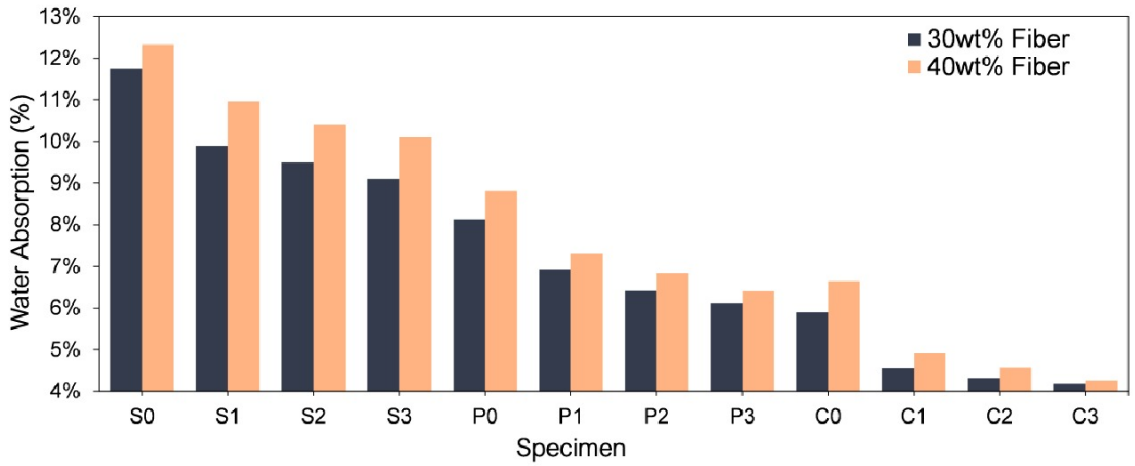

Fig 4.6: Variation of water absorption among composite specimens.

Comparing the results within each fiber type, it can be observed that increasing the fiber weight percentage from 30% to 40% led to an increase in water absorption for sisal and pineapple composites, while coir composites experienced a slight increase. This suggests that higher fiber content in sisal and pineapple composites results in increased

hydrophilicity. This could be attributed to the hydrophilic nature of fibers, particularly due to their hemicellulose content. More fibers meant more hydrophilic sites available for water molecules, resulting in higher absorption. This phenomenon is observed in other literature also (Mehdikhani et al., 2019).

Coir-based composites exhibited the lowest water absorption values among the three fiber types, followed by sisal and pineapple. This suggests that coir composites inherently have better hydrophobic properties followed by pineapple and sisal fiber. This can be attributed to the presence of lignin and hemicellulose of the coir fiber. Lignin is a hydrophobic component, whereas hemicellulose is a hydrophilic component (Deo and Acharya, 2010).

In a general sense, an increase in CNT weight percentage across all fiber types and contents corresponded to a decrease in water absorption percentages. This behavior could be related to the innate hydrophobic properties of CNTs. As the CNT content increased, a more pronounced protective layer of these hydrophobic CNTs might have formed around the fibers, as seen in the SEM image. This, in turn, could have minimized the overall water absorption of the composites by repelling water at the fiber surface (Prolongo, Gude, and Ureña, 2012).

The graph in Fig 4.7 represents the relationship between water absorption and time for composites over a period of ten days. The vertical axis of the graph represents the water absorption in percentage, while the horizontal axis represents the square root of time in hours.

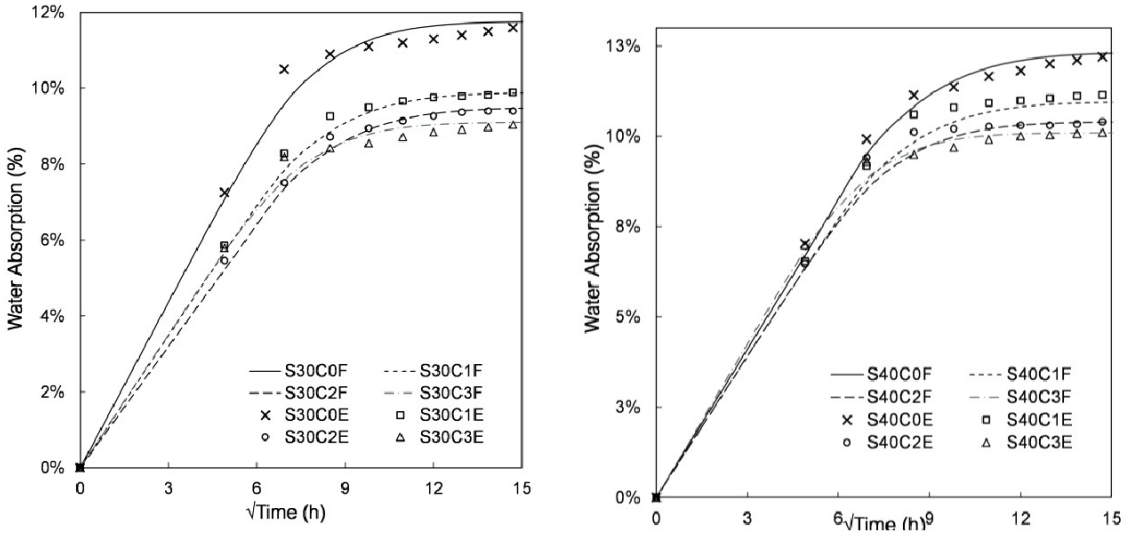

(a) (b)

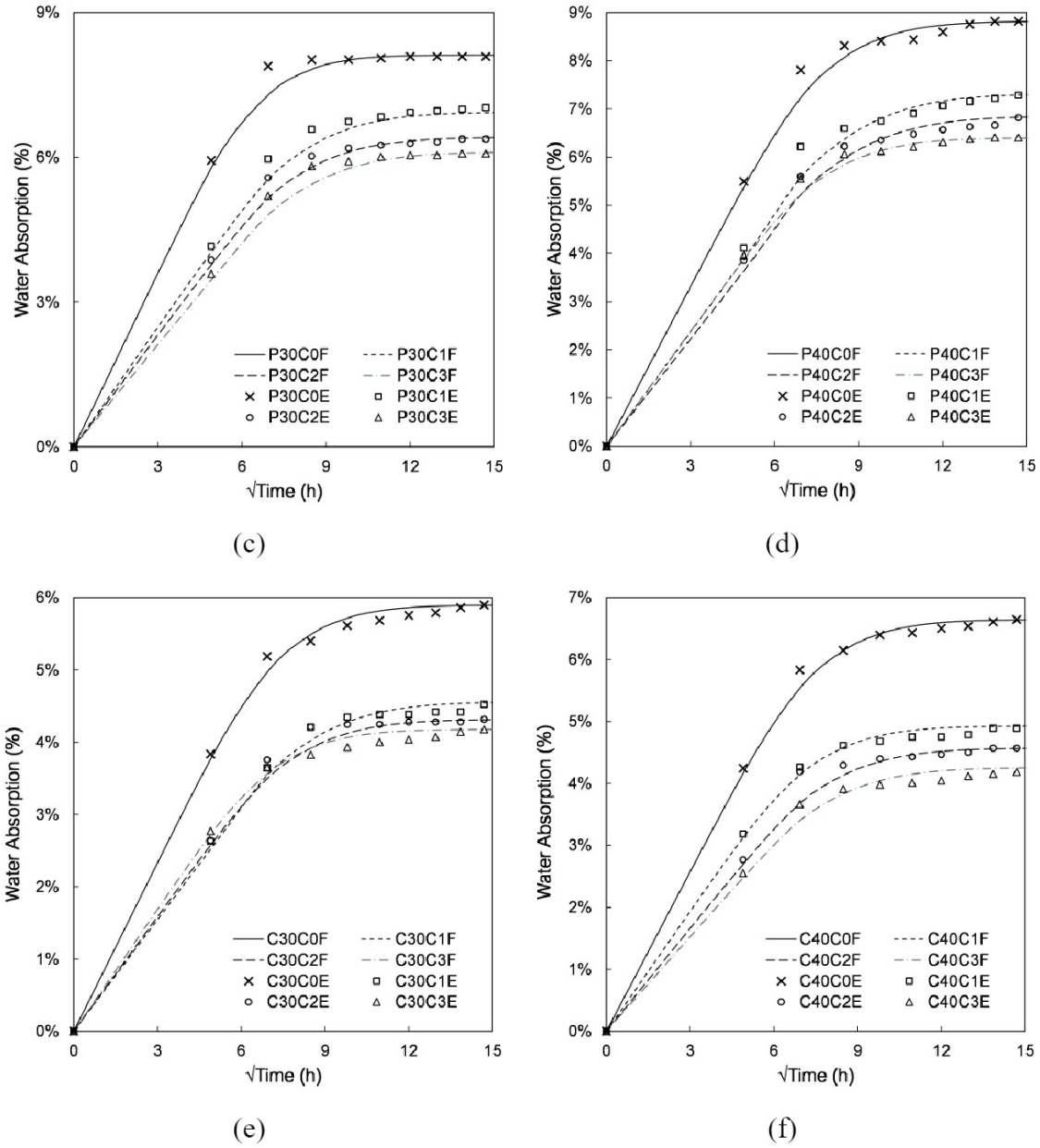

Fig 4.7: Experimental and Fickian diffusion model values of water absorption.

The water absorption of the materials was also modeled using the Fickian diffusion model, which predicts the amount of water absorbed by a material based on its diffusion coefficient and the concentration gradient of water across the material. The predicted values from the Fickian model are plotted on the same graph, shown as lines. As the graph is examined, it can be noticed that both the experimental data and the Fickian model predictions showed an initial increase in water absorption as time progressed, followed by a slowing down of the absorption rate. The experimental data and the Fickian model predictions displayed close correspondence, as both of them followed a similar trend and reached similar saturation levels.

It was observed that the experimental values diverged from those predicted by the Fickian model in some cases. A possible explanation for this discrepancy was that the Fickian model assumes the diffusion process to be the only mechanism affecting water absorption, which may not always hold true. Real-life materials, especially natural fibers like the ones under study, often exhibit more complex behavior due to their inherent heterogeneity and the presence of various components like cellulose, hemicellulose, and lignin, each with distinct properties, as outlined in literature (Ibrahim et al., 2017). For instance, the water absorption process in these fibers could also be influenced by swelling, capillary action, or reactions between water molecules and functional groups present in the fiber. The Fickian model, in its basic form, failed to account for these complex phenomena, potentially leading to the observed discrepancy between experimental and predicted values (Muñoz and García-Manrique, 2015).

4.3.3 Tensile Test Results

Fig 4.8 represents the stress-strain curves which had been generated from the obtained dataset from the tensile test, representing the relationship between tensile strength and tensile strain for a specific composite. For all of the composites, initially, the curve had shown a linear region where the tensile strength had been proportional to the tensile strain. In this region, the composite material had followed Hooke's law, and the slope of the curve had been indicative of the material's stiffness, or Young's modulus.

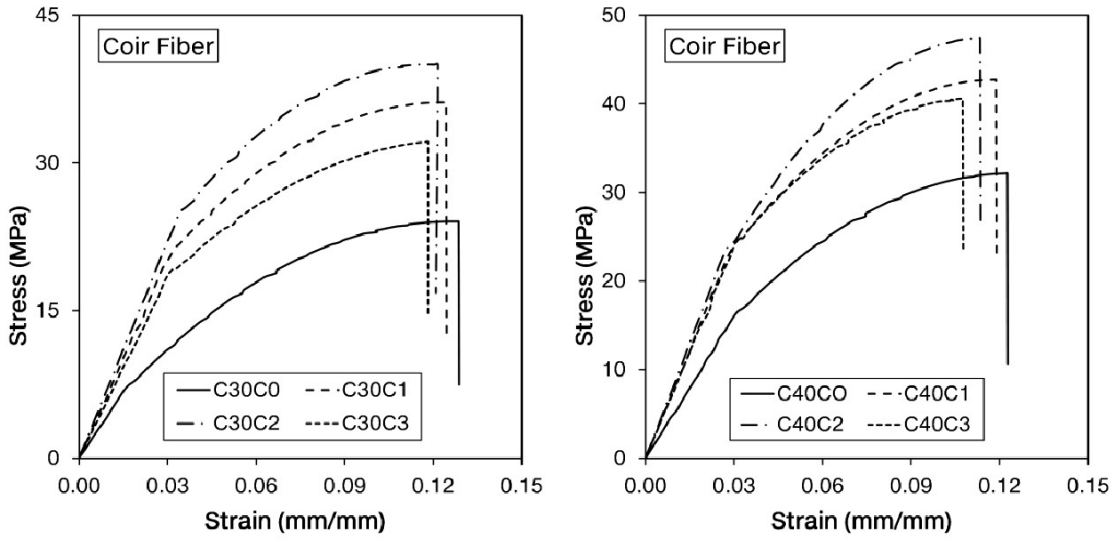

(a) (b)

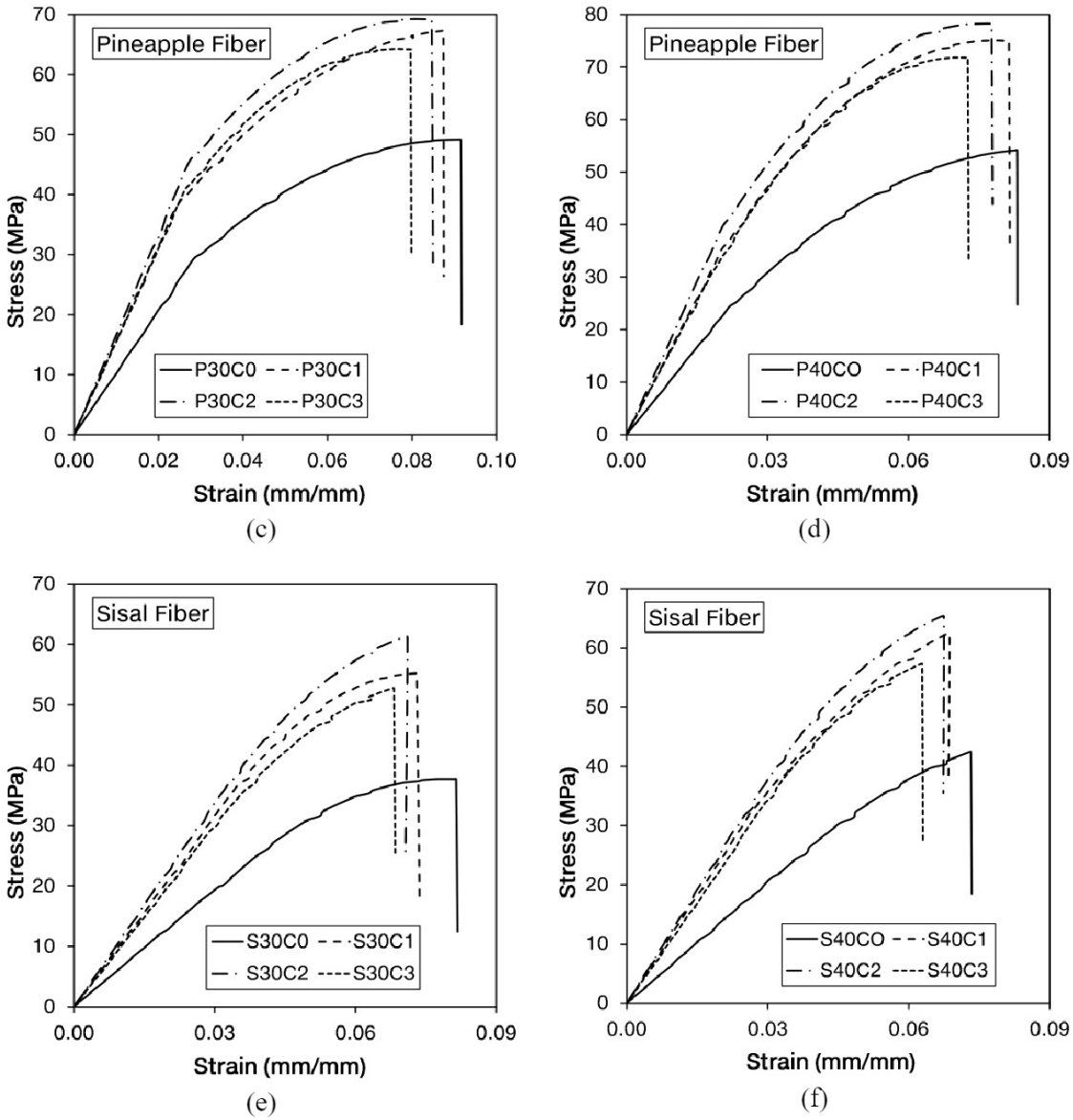

Fig 4.8: Tensile strength-strain curve for developed composites.

As the tensile strain had increased, the material had reached a point beyond which the linear relationship between stress and strain no longer held. At this stage, plastic deformation had commenced, and the curve had begun to deviate from the linear region. The material had continued to deform plastically as the stress had increased, eventually reaching a maximum tensile strength value. This point on the curve had represented the ultimate tensile strength of the material.

Upon reaching the peak stress value, the stress experienced a sudden drop, suggesting that the material exhibited little to no necking or localized deformation. The curve ultimately reached a point where the material fractured or broke, marking the end of the stress-strain

relationship for this material. The elongation at break, a measure of the material's ductility, could be determined from the tensile strain value at the point of fracture.

This abrupt decrease in stress and the absence of necking indicated that the material's behavior leaned more towards brittleness, with the fracture occurring rapidly and without significant plastic deformation. From the graph, it can also be noticed that coir fiber composites displayed more ductility followed by pineapple fiber composites and sisal fiber composites.

The bar graph in Fig 4.9 displays the tensile strengths for different composites, where the X-axis shows the type of composites, while the Y-axis shows the tensile strengths from the experimental analysis. The bar graph in Fig 4.10 displays the Young's modulus for different composites where X-axis shows the type of composites, while the Y-axis shows the Young's modulus from the experimental analysis. The bar graph in Fig 4.11 displays the elongation at break for different composites where X-axis shows the type of composites, while the Y-axis shows the elongation at break percentages from the experimental analysis. The results for Epoxy/MWCNT composites (1wt.% MWCNT) were obtained from literature (Roy, Petrova, and Mitra, 2018).

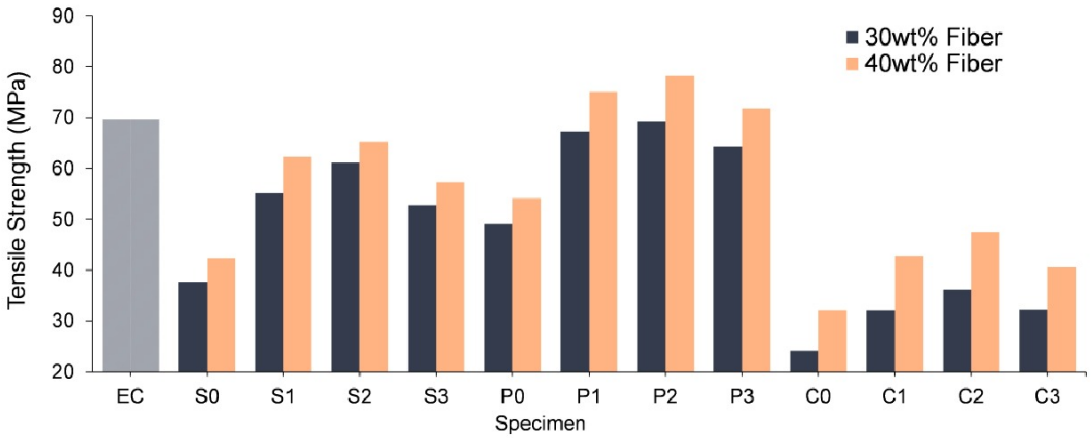

Fig 4.9: Experimental result for Tensile strength with varying fiber contents.

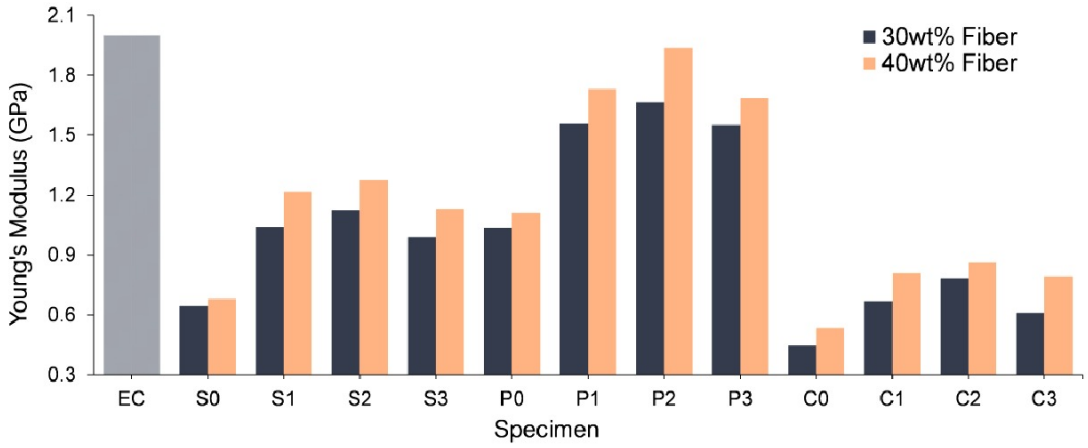

Fig 4.10: Experimental result for Young's modulus with varying fiber contents.

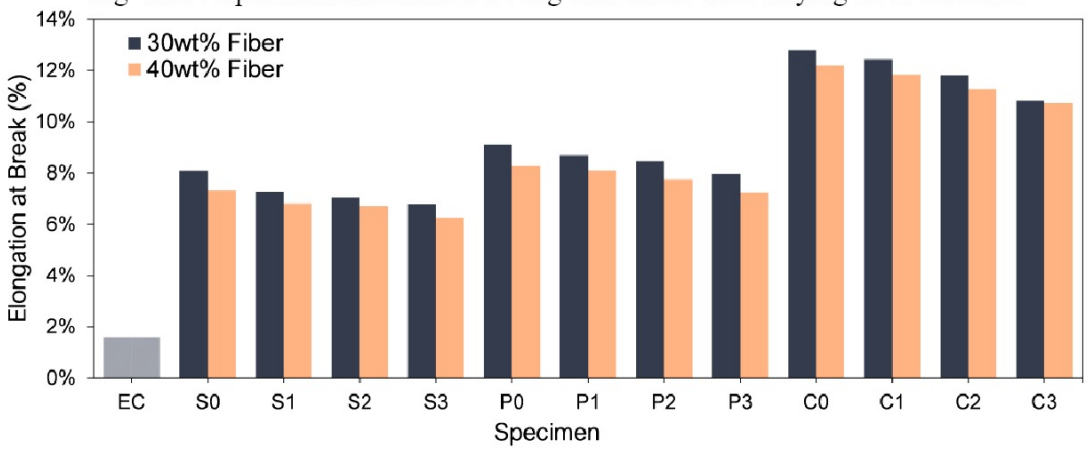

Fig 4.11: Experimental result for Elongation at break with varying fiber contents.

The effect of fiber type had been evident in the variation of tensile strength, Young's modulus, and elongation at break properties. The tensile strength and Young's modulus values had been the highest for pineapple fiber composites, followed by sisal and coir composites. However, the elongation at break had shown an inverse relationship, with coir composites exhibiting the highest values, followed by pineapple and sisal composites. This is due to the individual fiber properties, resulting from the high tensile strength and low elongation properties in pineapple and sisal fibers and opposite for coir fiber. Because of the high cellulose content in the pineapple fiber, additional tensile strength was observed for pineapple fiber reinforced composites (La Mantia and Morreale, 2011).

The influence of fiber content had been observed by comparing composites with 30% and 40% fiber weight percentages for each fiber type and CNT content. It had been found that the tensile strength and Young's modulus had generally increased with the higher fiber content. This increase had been consistent across all fiber types and CNT concentrations. As fibers possess more tensile strength compared to epoxy resin, therefore this phenomenon

can be observed. On the contrary, the elongation at break had decreased as the fiber content increased from 30% to 40%, because the fibers are brittle in nature compared to Epoxy resin. Therefore, increasing fiber content resulted in reduction of elongation at break properties. This trend had indicated that higher fiber content had contributed to greater material strength and stiffness but reduced ductility (CW Nguong S Debnath, 2013).

The tensile strength and Young's modulus had generally increased with increasing CNT content, albeit with some fluctuations after a certain limit of 2 wt.%. But when the CNT was increased to 3 wt.%, then agglomeration of the CNT particles took place and void content increased. Thus, the composite was subjected to inferior performance compared to 2 wt.% CNT. This trend had been consistent across all fiber types and fiber weight percentages, suggesting that CNTs had enhanced the mechanical properties of the composites. However, the elongation at break had generally decreased with increasing CNT content, as CNTs are highly brittle material. These observation are in alignment with reports from other literature (Thakur et al., 2018).

Epoxy/CNT composites provide moderate tensile strength, but very high Young's modulus because of the brittle nature of CNTs. However, they have much lower elongation at break properties compared to developed composites in this study.

4.3.4 Flexural Test Results

The bar graph in Fig 4.12 displays the flexural strengths for different composites where x-axis shows the type of composites, while the y-axis shows the flexural strengths from the experimental analysis. The bar graph in Fig 4.13 displays the flexural modulus for different composites where x-axis shows the type of composites, while the y-axis shows the flexural modulus from the experimental analysis. The results for Epoxy/MWCNT composites (1wt.% MWCNT) were obtained from literature (Kesavan Pillai and Ray, 2011).

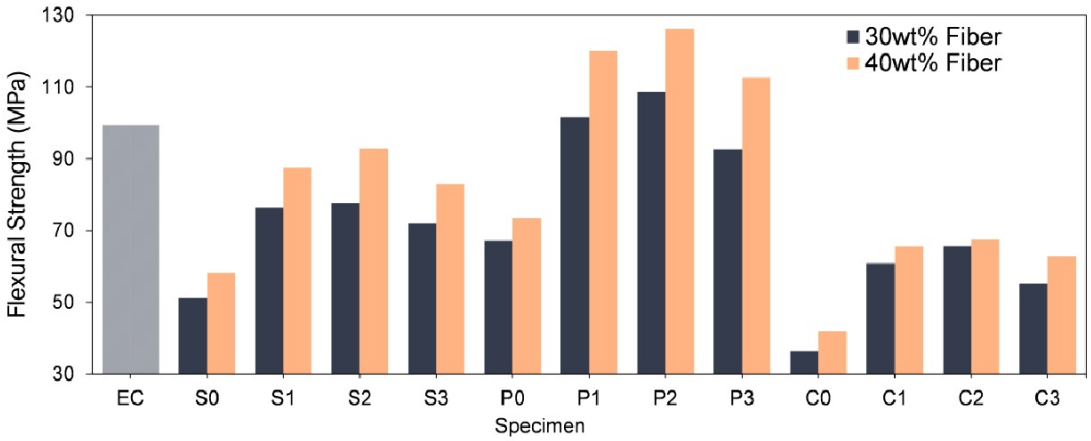

Fig 4.12: Experimental result for flexural strength with varying fiber contents.

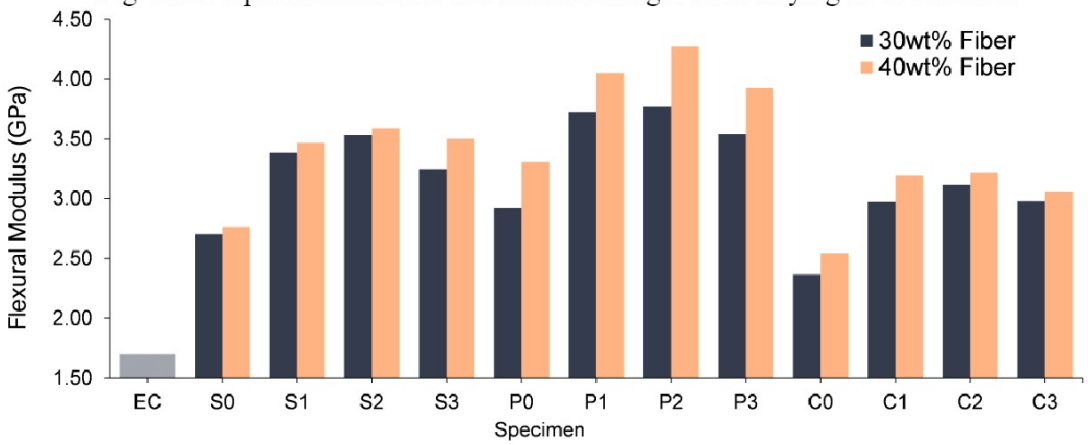

Fig 4.13: Experimental result for flexural modulus with varying fiber contents.

The analysis had revealed distinct differences based on fiber type. Sisal fiber composites, with their cellulose content ranging from 65 to 74%, and relatively low lignin content, had consistently outperformed coir in terms of flexural strength and modulus. Pineapple leaf fiber composites, boasting the highest cellulose content between 70 and 82%, and lowest lignin content, had demonstrated the highest flexural strength and modulus across the board. This suggested that the high cellulose content and lower lignin content contributed to superior flexural performance in composites (Alemayehu et al., 2020).

The flexural strength and modulus had shown a clear dependency on fiber content. An increase in fiber weight percentage from 30% to 40% had consistently resulted in improved flexural strength and modulus across all fiber types and CNT levels. This trend had suggested that an increased fiber content, and therefore, a higher content of cellulose, which provided strength and stiffness, enhanced the composite's flexural properties (Maurya et al., 2015).

The CNT content had also played a significant role in the flexural properties of the composites. The introduction of CNTs had generally resulted in an increase in both flexural strength and modulus for all fiber types and fiber contents. However, an optimum was typically observed at 2% CNT, with a decrease in values at 3% CNT. This was due to the agglomeration effect present in case of 3 wt.% CNT which created much void contents as observed from previous section. This indicates that an optimal CNT content exists for maximizing the flexural properties of the composites (Sapiai, Jumahat, and Mahmud, 2018).

Epoxy/CNT composites provide moderate flexural strength, but much lower flexural modulus properties compared to developed composites in this study.

4.3.5 Hardness Test Results

The bar graph in Fig 4.14 displays the Rockwell hardness number for different composites where x-axis shows the type of composites, while the y-axis shows the hardness number from the experimental analysis. The results for Epoxy/MWCNT composites (1wt.% MWCNT) were obtained from literature (Felisberto et al., 2012)

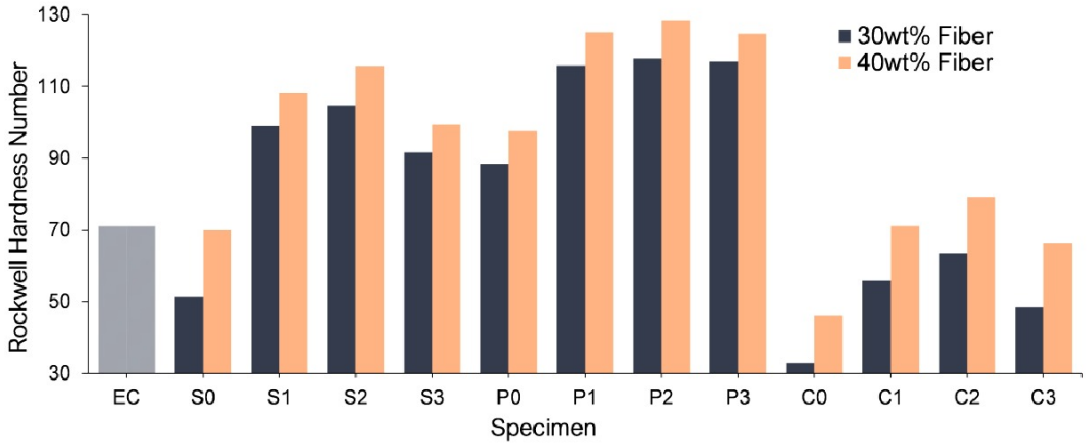

Fig 4.14: Experimental result for Rockwell hardness number with varying fiber contents.

A comprehensive analysis had been conducted on the Rockwell hardness numbers of different composites. The Rockwell hardness numbers had indicated that the composites with pineapple fibers had typically demonstrated the highest hardness, followed by sisal and then coir.

The analysis had revealed distinct differences based on fiber type. The fiber type had appeared to play a substantial role in the hardness of the composites. Composites with

pineapple leaf fibers had generally exhibited the highest Rockwell Hardness Numbers, which could be ascribed to their high cellulose content (70-82%). This had been followed by sisal (65-74% cellulose) and then coir (42.1% cellulose). Therefore, it was observed that the fibers with higher cellulose content, such as pineapple leaf and sisal, had consistently displayed higher hardness numbers compared to coir fiber composites and it had been one of the key factors contributing to the hardness of the composites (Faruk et al., 2014b).

When examining fiber content, an increase from 30% to 40% in fiber weight percentage had typically correlated with an increase in the Rockwell hardness number for each fiber type. This had indicated that higher fiber content, and therefore, a higher content of cellulose tended to augment the hardness of the composites. Cellulose, a complex carbohydrate that forms the primary structural component of plant cell walls, is known for its rigidity and durability. Therefore, as the proportion of cellulose-rich fibers within the composite increased, the hardness of the material had been observed to improve (Fuqua, Huo, and Ulven, 2012).

The CNT content had also demonstrated a noticeable impact on the hardness of the composites. In most cases, an increase in CNT content had corresponded with an increase in the Rockwell Hardness Number, reaching a peak at 2 wt.% CNT. However, at 3wt.% CNT, a slight decrease in hardness had been observed, which might have indicated an optimal CNT concentration for hardness enhancement. In terms of the agglomeration effect, up to a certain CNT concentration, the CNTs can be well dispersed and contribute significantly to the hardness enhancement by providing additional reinforcement and bridging between the matrix and fibers. This had been observed up to 2wt.% CNT content, where the Rockwell Hardness Number consistently increased with the CNT content. However, beyond this optimal concentration, it appeared that the CNTs started to agglomerate, resulting in clusters of CNTs rather than a uniform dispersion. These clusters could create weak zones in the composite, reducing the load transfer efficiency from the matrix to the fibers and thus leading to a slight decrease in hardness. This agglomeration effect was likely the cause of the observed reduction in hardness at 3wt.% CNT content. Therefore, while CNTs can significantly enhance the hardness of composites, their concentration needs to be carefully controlled to avoid agglomeration and ensure optimal performance (Mohan and Rajmohan, 2017).

Epoxy/CNT composites provide moderate hardness compared to developed composites in this study.

4.3.6 Impact Test Results

The bar graph in Fig 4.15 displays the Rockwell hardness number for different composites where x-axis shows the type of composites, while the y-axis shows the absorbed impact energy in KJ/m² from the experimental analysis. The results for Epoxy/MWCNT composites (1wt.% MWCNT) were obtained from literature (Kesavan Pillai and Ray, 2011).

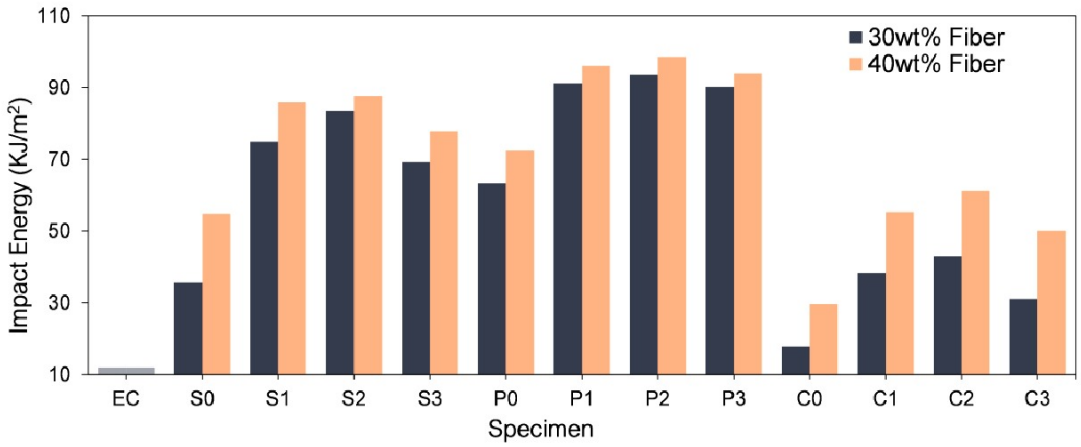

Fig 4.15: Experimental result for absorbed impact energy with varying fiber contents.

The impact energy data of the composite specimens had been meticulously examined. Among the composites, those reinforced with pineapple fibers had shown the highest impact energy, regardless of the fiber content and the presence or absence of CNT. This had been followed by the sisal fiber composites, with coir fiber composites trailing behind. This trend had been consistent at both the 30% and 40% fiber weight percentages.

The analysis had revealed distinct differences based on fiber type. The fiber type had appeared to play a substantial role in the absorbed impact energy by the composites. In terms of fiber type, a clear hierarchy had emerged in the impact energy data. Pineapple leaf fiber composites, with their high cellulose content (70-82%), had consistently exhibited the highest impact energy, followed by sisal fiber composites (with 65-74% cellulose), and then by coir fiber composites (42.1% cellulose). The high cellulose content in pineapple leaf and sisal fibers had contributed to their superior mechanical properties, since cellulose is a primary contributor to fiber strength and stiffness (Chand and Fahim, 2021b).

When examining fiber content, an increase from 30% to 40% in fiber weight percentage had typically correlated with an increase in the impact energy absorbed for each fiber type. This had indicated that higher fiber content, and therefore, a higher content of cellulose tended to augment the absorbed limit of impact energy of the composites. Cellulose, a complex carbohydrate that forms the primary structural component of plant cell walls, is known for its rigidity and durability. Therefore, as the proportion of cellulose-rich fibers within the composite increased, the impact energy of the material had been observed to improve (Franco and Valadez-González, 2005).

The CNT content had also demonstrated a noticeable impact on the absorbed impact energy of the composites. The addition of CNT to the composites had also played a significant role in the observed impact energy. At both fiber contents of 30% and 40%, the inclusion of 1-2% CNT had resulted in an increase in impact energy for all fiber types. This could be attributed to the strong mechanical properties of CNT and their ability to improve the interface bonding between the fibers and the matrix, leading to efficient load transfer under impact. Interestingly, at 3% CNT, a decrease in impact energy had been noted across all fiber types and fiber contents. This could be explained by the potential agglomeration of CNT at higher concentrations, leading to stress concentration points and premature failure of the composites, thereby reducing their impact energy (P. K. Kushwaha, Pandey, and Kumar, 2014).

Epoxy/CNT composites provide much lower impact energy compared to developed composites in this study, because of their brittleness.

4.4 Regression Equations

Regression models had been developed for each fiber type, and the coefficient of determination (R^2) had been employed to evaluate the models' goodness of fit. The regression equation for the physical and mechanical properties are as follows:

Experimental density (with R^2 value of 94.98%)

For coir fiber composites, density (g/cm^3) = 1.06036 + 0.000966 Fiber wt.% + 0.01890 CNT wt.% - 0.004947 CNT wt.%×CNT wt.% + 0.000020 Fiber wt.%×CNT wt.%.

For pineapple fiber composites, density (g/cm^3) = 1.07696 + 0.003669 Fiber wt.% + 0.01768 CNT wt.% - 0.004947 CNT wt.%×CNT wt.% + 0.000020 Fiber wt.%×CNT wt.%.

For sisal fiber composites, density (g/cm^3) = 1.06174 + 0.003602 Fiber wt.% + 0.01866 CNT wt.% - 0.004947 CNT wt.%×CNT wt.% + 0.000020 Fiber wt.%×CNT wt.%.

Void contents (with R^2 value of 95.10%)

For coir fiber composites, Void Content (%) = 0.08563 - 0.000515 Fiber wt.% - 0.01482 CNT wt.% + 0.004040 CNT wt.%×CNT wt.% - 0.000009 Fiber wt.%×CNT wt.%.

For pineapple fiber composites, Void Content (%) = 0.06255 - 0.000541 Fiber wt.% - 0.01347 CNT wt.% + 0.004040 CNT wt.%×CNT wt.% - 0.000009 Fiber wt.%×CNT wt.%.

For sisal fiber composites, Void Content (%) = 0.07682 - 0.000825 Fiber wt.% - 0.01431 CNT wt.% + 0.004040 CNT wt.%×CNT wt.% - 0.000009 Fiber wt.%×CNT wt.%.

Water absorption (with R^2 value of 98.64%)

For coir fiber composites, Water Absorption (%) = 0.04540 + 0.000470 Fiber wt.% - 0.01285 CNT wt.% + 0.002965 CNT wt.%×CNT wt.% - 0.000072 Fiber wt.%×CNT wt.%.

For pineapple fiber composites, Water Absorption (%) = 0.06540 + 0.000555 Fiber wt.% - 0.01351 CNT wt.% + 0.002965 CNT wt.%×CNT wt.% - 0.000072 Fiber wt.%×CNT wt.%.

For sisal fiber composites, Water Absorption (%) = 0.08499 + 0.000992 Fiber wt.% - 0.01418 CNT wt.% + 0.002965 CNT wt.%×CNT wt.% - 0.000072 Fiber wt.%×CNT wt.%.

Tensile strength (with R^2 value of 94.64%)

For coir fiber composites, Tensile strength (MPa) = -4.39 + 0.885 Fiber wt.% + 17.52 CNT wt.% - 5.568 CNT wt.%×CNT wt.% + 0.0488 Fiber wt.%×CNT wt.%.

For pineapple fiber composites, Tensile strength (MPa) = 29.74 + 0.660 Fiber wt.% + 20.17 CNT wt.% - 5.568 CNT wt.%×CNT wt.% + 0.0488 Fiber wt.%×CNT wt.%.

For sisal fiber composites, Tensile strength (MPa) = 25.91 + 0.440 Fiber wt.% + 19.92 CNT wt.% - 5.568 CNT wt.%×CNT wt.% + 0.0488 Fiber wt.%×CNT wt.%.

Young's modulus (with R^2 value of 94.74%)

For coir fiber composites, Young's Modulus (GPa) = 0.145 + 0.00833 Fiber wt.% + 0.4131 CNT wt.% - 0.1440 CNT wt.%×CNT wt.% + 0.00260 Fiber wt.%×CNT wt.%.

For pineapple fiber composites, Young's Modulus (GPa) = 0.683 + 0.01250 Fiber wt.% + 0.5206 CNT wt.% - 0.1440 CNT wt.%×CNT wt.% + 0.00260 Fiber wt.%×CNT wt.%.

For sisal fiber composites, Young's Modulus (GPa) = 0.374 + 0.00870 Fiber wt.% + 0.4675 CNT wt.% - 0.1440 CNT wt.%×CNT wt.% + 0.00260 Fiber wt.%×CNT wt.%.

Elongation at break (with R^2 value of 98.95%)

For coir fiber composites, Elongation at Break (%) = 0.14675 - 0.000597 Fiber wt.% - 0.00828 CNT wt.% - 0.000238 CNT wt.%×CNT wt.% + 0.000092 Fiber wt.%×CNT wt.%.

For pineapple fiber composites, Elongation at Break (%) = 0.11706 - 0.000855 Fiber wt.% - 0.00608 CNT wt.% - 0.000238 CNT wt.%×CNT wt.% + 0.000092 Fiber wt.%×CNT wt.%.

For sisal fiber composites, Elongation at Break (%) = 0.09907 - 0.000667 Fiber wt.% - 0.00622 CNT wt.% - 0.000238 CNT wt.%×CNT wt.% + 0.000092 Fiber wt.%×CNT wt.%.

Flexural strength (with R^2 value of 90.94%)

For coir fiber composites, Flexural Strength (MPa) = 30.2 + 0.180 Fiber wt.% + 32.79 CNT wt.% - 10.189 CNT wt.%×CNT wt.% + 0.122 Fiber wt.%×CNT wt.%.

For pineapple fiber composites, Flexural Strength (MPa) = 25.8 + 1.360 Fiber wt.% + 37.55 CNT wt.% - 10.189 CNT wt.%×CNT wt.% + 0.122 Fiber wt.%×CNT wt.%.

For sisal fiber composites, Flexural Strength (MPa) = 23.1 + 0.852 Fiber wt.% + 33.47 CNT wt.% - 10.189 CNT wt.%×CNT wt.% + 0.122 Fiber wt.%×CNT wt.%.

Flexural modulus (with R^2 value of 96.51%)

For coir fiber composites, Flexural Modulus (GPa) = 1.780 + 0.01824 Fiber wt.% + 0.783 CNT wt.% - 0.2088 CNT wt.%×CNT wt.% + 0.00100 Fiber wt.%×CNT wt.%.

For pineapple fiber composites, Flexural Modulus (GPa) = 1.889 + 0.03463 Fiber wt.% + 0.810 CNT wt.% - 0.2088 CNT wt.%×CNT wt.% + 0.00100 Fiber wt.%×CNT wt.%.

For sisal fiber composites, Flexural Modulus (GPa) = 2.368 + 0.01025 Fiber wt.% + 0.829 CNT wt.% - 0.2088 CNT wt.%×CNT wt.% + 0.00100 Fiber wt.%×CNT wt.%.

Rockwell hardness number (with R^2 value of 94.49%)

For coir fiber composites, Rockwell Hardness Number = -17.4 + 1.573 Fiber wt.% + 39.20 CNT wt.% - 10.731 CNT wt.%×CNT wt.% - 0.025 Fiber wt.%×CNT wt.%.

For pineapple fiber composites, Rockwell Hardness Number = 57.8 + 0.940 Fiber wt.% + 41.29 CNT wt.% - 10.731 CNT wt.%×CNT wt.% - 0.025 Fiber wt.%×CNT wt.%.

Lastly, for sisal fiber composites, Rockwell Hardness Number = 24.2 + 1.149 Fiber wt.% + 44.43 CNT wt.% - 10.731 CNT wt.%×CNT wt.% - 0.025 Fiber wt.%×CNT wt.%.

Impact energy (with R^2 value of 93.49%)

For coir fiber composites, Impact Energy (KJ/m^2) = -39.5 + 1.805 Fiber wt.% + 35.26 CNT wt.% - 9.021 CNT wt.%×CNT wt.% - 0.077 Fiber wt.%×CNT wt.%.

For pineapple fiber composites, Impact Energy (KJ/m^2) = 45.9 + 0.586 Fiber wt.% + 37.96 CNT wt.% - 9.021 CNT wt.%×CNT wt.% - 0.077 Fiber wt.%×CNT wt.%.

For sisal fiber composites, Impact Energy (KJ/m^2) = 10.2 + 1.113 Fiber wt.% + 38.74 CNT wt.% - 9.021 CNT wt.%×CNT wt.% - 0.077 Fiber wt.%×CNT wt.%.

Upon examining the regression equations, it was evident that all the properties had been affected by fiber weight percentage, CNT content, and the interaction between these two factors. The positive coefficients of fiber wt.% and CNT content had suggested that increasing either variable would result in an increase in all physical and mechanical properties. The negative coefficient of CNT wt.% × CNT wt.% had indicated that the positive effect of CNT content on mechanical properties had weakened as the CNT content increased. The negative coefficient of fiber wt.%×CNT in some cases, had demonstrated that there had been an antagonistic effect between the fiber weight percentage and CNT content on composite properties, making this effect significant compared to the individual effects of fiber weight percentage and CNT content. Moreover, a high R^2 value of 90% and

above had denoted that the model had accurately depicted the relationship between the independent variables (fiber weight percentage and CNT content) and the dependent variable (physical and mechanical properties).

4.5 Uncertainty Analysis

Fig 4.16 to Fig 4.23 represent the percentage uncertainty in measuring the physical and mechanical properties of the developed composites. The data had shown variations in uncertainty values based on the type of fiber used, the fiber weight percentage, and the CNT weight percentage.

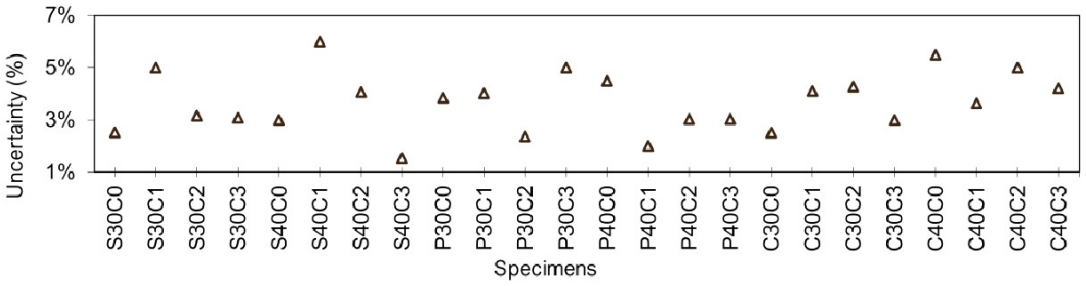

Fig 4.16: Percentage uncertainty in measuring density.

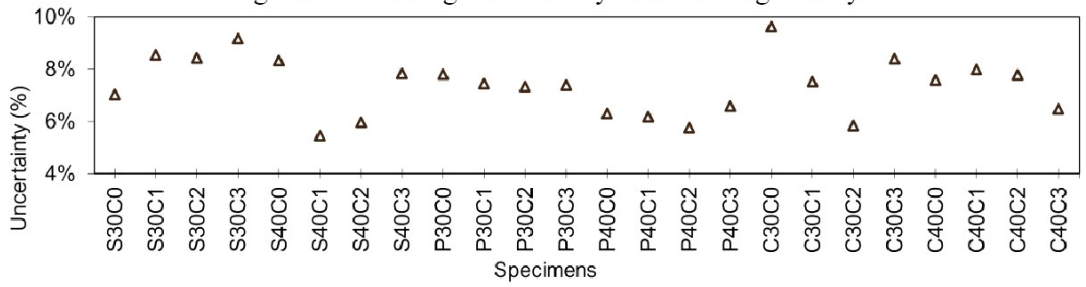

Fig 4.17: Percentage uncertainty in measuring tensile strength.

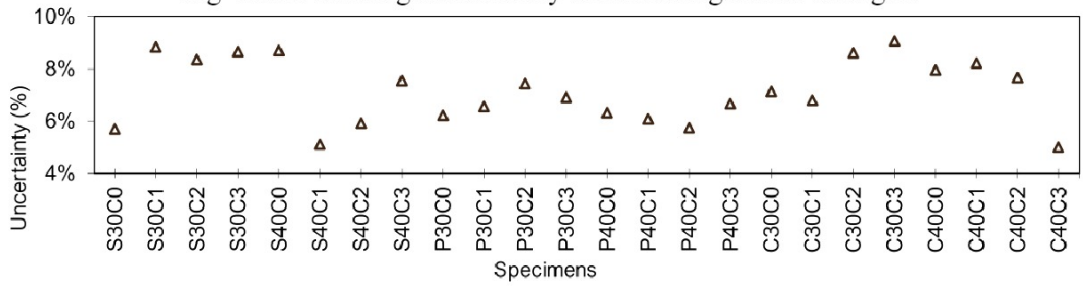

Fig 4.18: Percentage uncertainty in measuring Young's modulus.

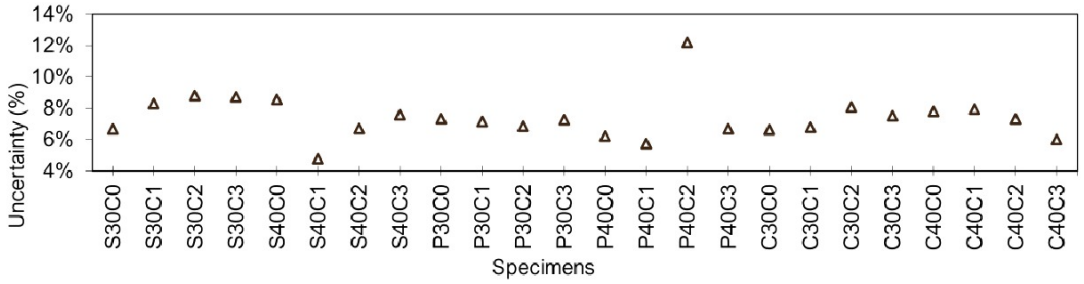

Fig 4.19: Percentage uncertainty in measuring elongation at break.

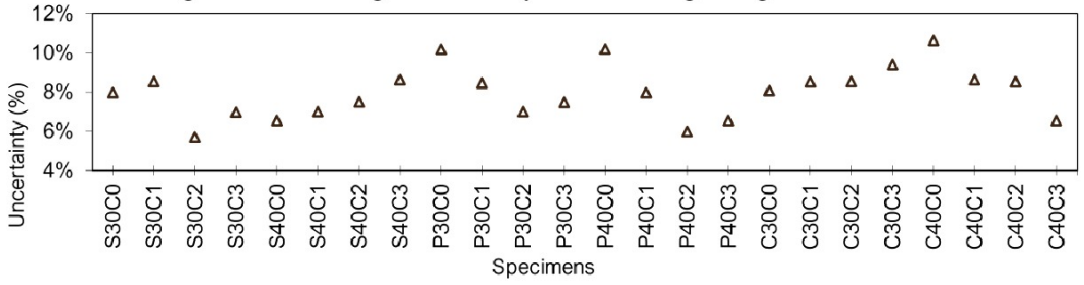

Fig 4.20: Percentage uncertainty in measuring flexural strength.

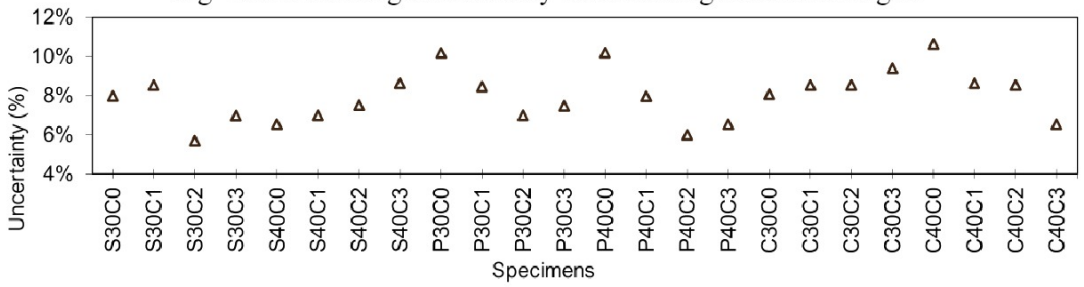

Fig 4.21: Percentage uncertainty in measuring flexural modulus.

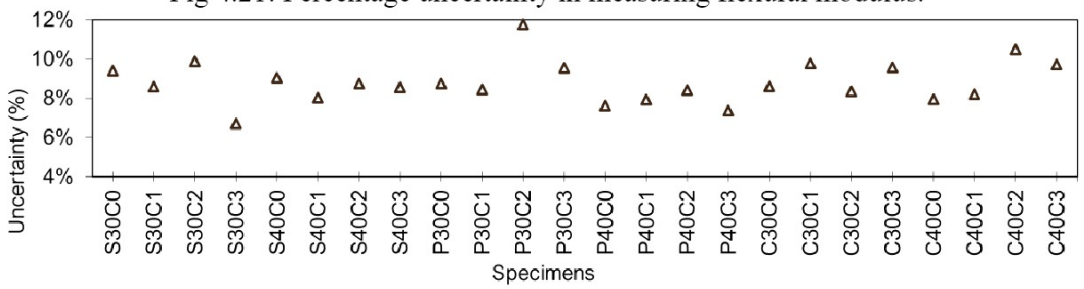

Fig 4.22: Percentage uncertainty in measuring Rockwell hardness number.

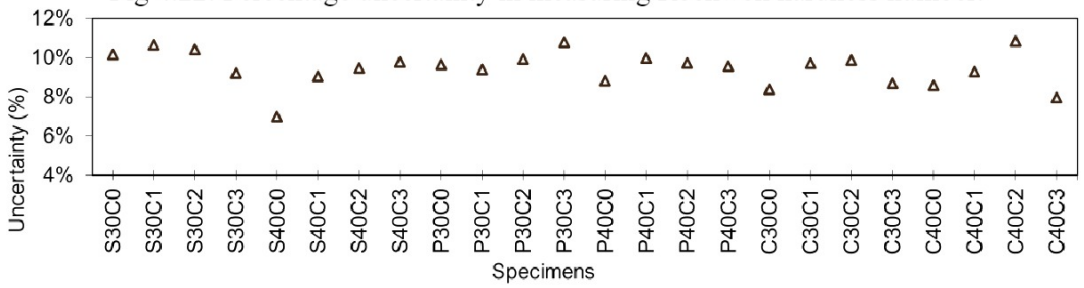

Fig 4.23: Percentage uncertainty in measuring impact energy.

It had been noteworthy that, despite the observed variations, the uncertainty percentages for almost all cases were less than 10%. This indicated that the experimental results were generally reliable and the variations in uncertainty could be considered within an acceptable

range. However, the slight increase in uncertainty above 10% for a few data points had suggested that there could be some factors introducing additional variability into the results. These factors could include variations in material properties, inconsistencies in sample preparation, or fluctuations in the testing environment. Nonetheless, the fact that most uncertainty values were below the 10% threshold suggested that the overall quality of the data was satisfactory.

4.6 Fourier Transform InfraRed (FTIR) Spectroscopy Result

Because of the presence of different constituent materials, the developed composites underwent noteworthy alterations in their molecular characteristics, vividly captured through the FTIR analysis. The examination allowed for an exhaustive depiction of the composite's molecular vibrations, unmasking the existence of functional groups and elucidating interfacial interactions within. Therefore, the outcomes of the FTIR test not only enlightened the composite material's intricate structure but also signaled towards potential enhancements in their fabrication process.

Fig 4.24 represents the FTIR result for Pineapple fiber reinforced Epoxy composite and Pineapple fiber and CNT reinforced Epoxy composite. Initially, the presence of hydroxyl groups (-OH) had been identified, as evidenced by the characteristic peaks at around 3300-3400 cm^{-1}. These groups had likely resulted from the interaction between the pineapple fiber and epoxy resin. However, when CNT was introduced, this peak had been diminished, indicating less possibility of water absorption.

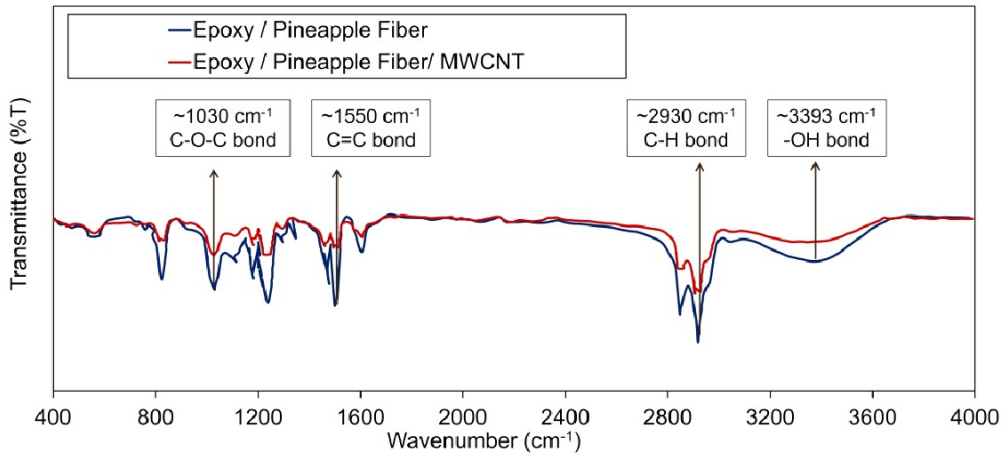

Fig 4.24: FTIR result for Pineapple fiber reinforced Epoxy composite and Pineapple fiber and CNT reinforced Epoxy composite.

The absorption bands observed at around 2930 cm^{-1} and 2850 cm^{-1} had indicated the presence of aliphatic C-H stretching vibrations, which had been attributed to the epoxy resin and pineapple fibers in both the composites. A peak at approximately 1710 cm^{-1} had been associated with the carbonyl group (C=O) stretching vibrations, further confirming the presence of the epoxy resin in both the composites.

The presence of CNTs as nanofillers had been supported by the observation of a peak at around 1620 cm^{-1}, which had corresponded to the C=C stretching vibrations in the graphitic structure of CNTs. This peak had demonstrated the successful incorporation of CNTs into the composite material, which was absent in case of Epoxy pineapple fiber composite.

Furthermore, peaks at around 1260 cm^{-1} and 1170 cm^{-1} had been indicative of epoxy ring-opening reactions, confirming that the epoxy resin had successfully reacted and cured within both the composite material.

The peak around 1030 cm^{-1} in both the composites had been attributed to the C-O-C stretching vibrations, indicating the formation of ether linkages between the pineapple fibers and epoxy resin. This observation had provided evidence of the chemical bonding occurring between the composite components, contributing to the improved mechanical properties of the material.

Fig 4.25 represents the FTIR result for Sisal fiber reinforced Epoxy composite and Sisal fiber and CNT reinforced Epoxy composite. Initially, the presence of hydroxyl groups (-OH) had been identified, as evidenced by the characteristic peaks at around 3300-3400 cm^{-1}. These groups had likely resulted from the interaction between the pineapple fiber and epoxy resin. However, when CNT was introduced, this peak had been diminished, indicating less possibility of water absorption.

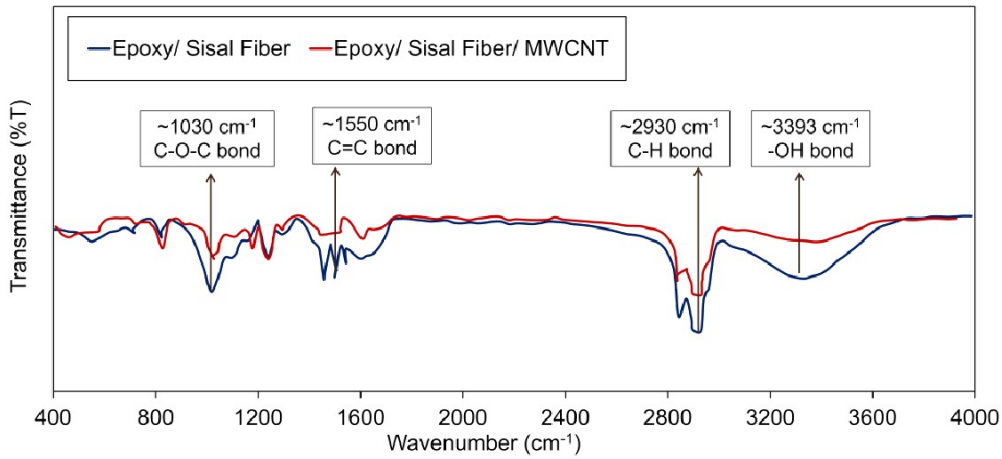

Fig 4.25: FTIR result for sisal fiber reinforced Epoxy composite and sisal fiber and CNT reinforced Epoxy composite.

The absorption bands observed at around 2930 cm^{-1} and 2850 cm^{-1} had indicated the presence of aliphatic C-H stretching vibrations, which had been attributed to the epoxy resin and sisal fibers in both the composites. A peak at approximately 1710 cm^{-1} had been associated with the carbonyl group (C=O) stretching vibrations, further confirming the presence of the epoxy resin in both the composites.

The presence of CNTs as nanofillers had been supported by the observation of a peak at around 1620 cm^{-1}, which had corresponded to the C=C stretching vibrations in the graphitic structure of CNTs. This peak had demonstrated the successful incorporation of CNTs into the composite material, which was absent in case of Epoxy sisal fiber composite.

Furthermore, peaks at around 1260 cm^{-1} and 1170 cm^{-1} had been indicative of epoxy ring-opening reactions, confirming that the epoxy resin had successfully reacted and cured within both the composite material.

The peak around 1030 cm^{-1} in both the composites had been attributed to the C-O-C stretching vibrations, indicating the formation of ether linkages between the sisal fibers and epoxy resin. This observation had provided evidence of the chemical bonding occurring between the composite components, contributing to the improved mechanical properties of the material.

Fig 4.26 represents the FTIR result for coir fiber reinforced Epoxy composite and coir fiber and CNT reinforced Epoxy composite. Initially, the presence of hydroxyl groups (-OH) had been identified, as evidenced by the characteristic peaks at around 3300-3400 cm^{-1}. These

groups had likely resulted from the interaction between the pineapple fiber and epoxy resin. However, when CNT was introduced, this peak had not been diminished to a greater extent, indicating lesser but significant possibility of water absorption.

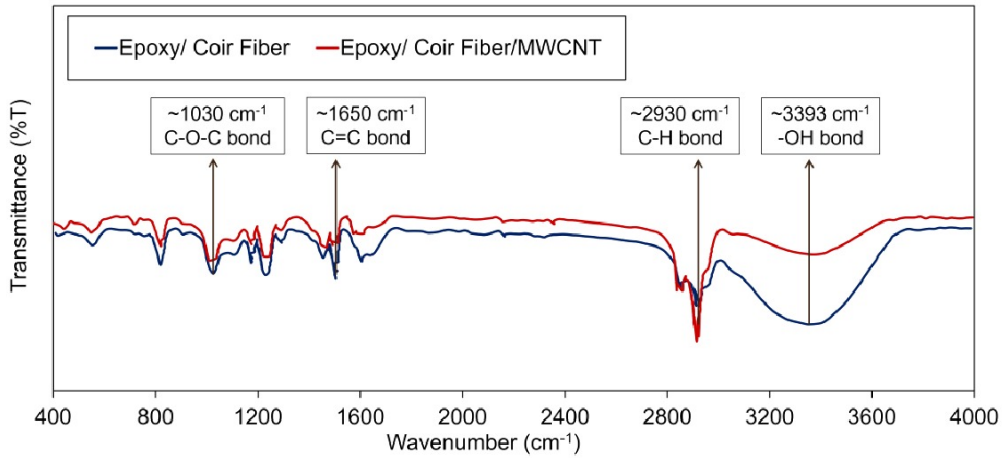

Fig 4.26: FTIR result for coir fiber reinforced Epoxy composite and coir fiber and CNT reinforced Epoxy composite.

The absorption bands observed at around 2930 cm^{-1} and 2850 cm^{-1} had indicated the presence of aliphatic C-H stretching vibrations, which had been attributed to the epoxy resin and coir fibers in both the composites. A peak at approximately 1710 cm^{-1} had been associated with the carbonyl group (C=O) stretching vibrations, further confirming the presence of the epoxy resin in both the composites.

The presence of CNTs as nanofillers had been supported by the observation of a peak at around 1620 cm^{-1}, which had corresponded to the C=C stretching vibrations in the graphitic structure of CNTs. This peak had demonstrated the successful incorporation of CNTs into the composite material, which was absent in case of Epoxy coir fiber composite.

Furthermore, peaks at around 1260 cm^{-1} and 1170 cm^{-1} had been indicative of epoxy ring-opening reactions, confirming that the epoxy resin had successfully reacted and cured within both the composite material.

The peak around 1030 cm^{-1} in both the composites had been attributed to the C-O-C stretching vibrations, indicating the formation of ether linkages between the coir fibers and epoxy resin. This observation had provided evidence of the chemical bonding occurring between the composite components, contributing to the improved mechanical properties of the material.

4.7 Scanning Electron Microscopic Image and Micrographic Image Result

Observations from the scanning electron microscope (SEM) for tensile, flexural, and impact specimens of epoxy natural fiber composites and epoxy natural fiber CNT composites had offered significant insights into the morphological aspects of these materials. The SEM images were captured within 2 weeks after fabrication. Different magnification level ranging from 30x to 200x was applied for this analysis.

Fig 4.27(a) represents the SEM image showing adherence of 2wt.% CNTs to the surface of the pineapple fiber, conforming the contours of the fiber surface and indicating a solid adhesion. This adhesion was because of the significant surface area and the existence of functional groups on the CNTs, which interacted with the cellulose molecules in the pineapple fibers to form hydrogen bonds. This interaction led to the formation of a well-integrated network of CNTs and pineapple fibers, which was likely to contribute to improved mechanical and thermal properties of the composite.

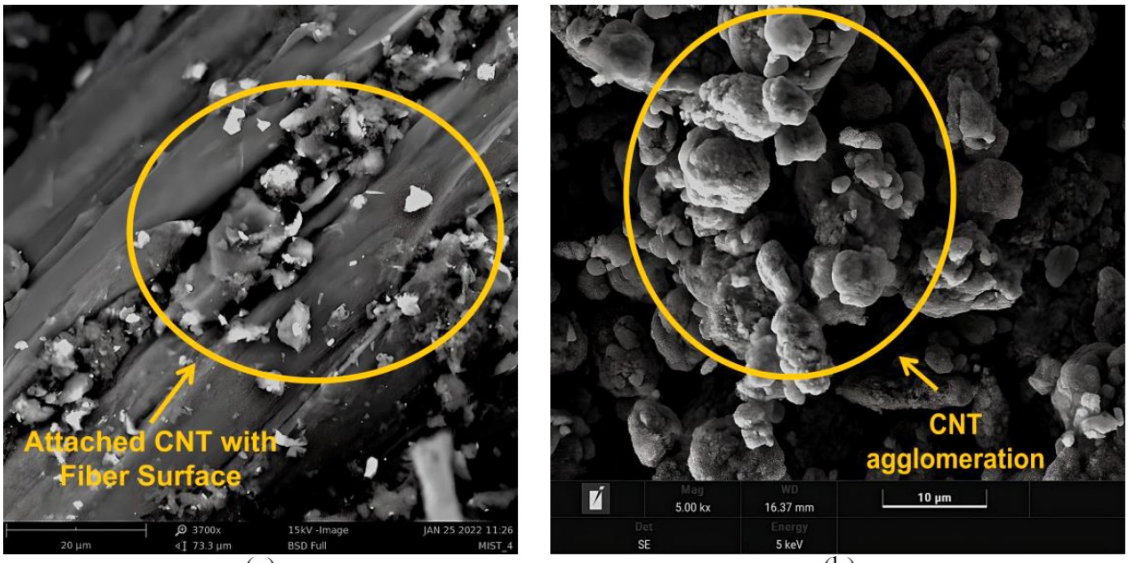

(a) (b)

Fig 4.27: Scanning Electron Microscope (SEM) image of developed composites

The surface of the fibers had been seen covered with CNTs, which had appeared as brighter, delicate structures adhered to the darker, more bulky fibers in the SEM image. This distribution of CNTs across the fiber surface indicated a successful dispersion of CNTs during the composite preparation process.

However, the SEM image of Fig 4.27(b) revealed a different scenario. In this image, the phenomenon of 3wt.% CNT agglomeration has been observed. Clusters of CNTs, appearing

as bright, dense patches, were dispersed throughout the image. The agglomerations had deviated from the desired uniform distribution of CNTs and were likely to create stress concentration regions within the composite, potentially conceding its overall performance.

Fig 4.28 represents the microscopic image showing the microstructural characteristics of sisal fiber, both before and after alkaline treatment, which was conducted through an optical microscope. A thorough examination of two distinct micrographs was conducted; one represented the state before alkaline treatment and the other depicted the aftermath of the same process. A striking difference was observed in the surface morphology and characteristics of the fiber between the two states.

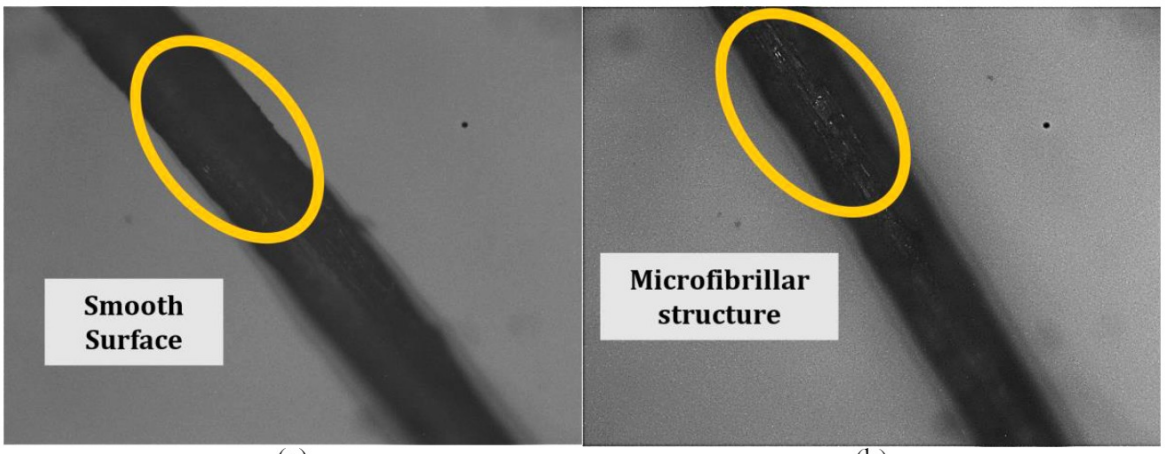

(a) (b)

Fig 4.28: Optical microscope image of sisal fiber (a) before alkaline treatment and (b) after alkaline treatment

In the initial micrograph, prior to the alkaline treatment as shown in Fig 4.28(a), the fiber exhibited a relatively smooth surface, and its diameter was measured to be larger. This state presented a lower aspect ratio, indicating a weaker interfacial interaction between the fiber and the matrix.

However, the micrograph taken after the alkaline treatment, as shown in Fig 4.28(b) showed a significantly altered morphology. The fiber diameter was noticeably reduced due to the action of the alkaline treatment, resulting in an increased aspect ratio. Additionally, the surface topography of the fiber became rougher and more irregular.

This modification in the fiber's surface characteristics, as evidenced by the micrographs, was conducive to an improved fiber-matrix interface adhesion. The rougher surface facilitated better mechanical interlocking between the fiber and the matrix, thereby strengthening the bond between them. This enhanced interfacial adhesion consequently

improved the overall mechanical properties of the composite, rendering it more robust and durable.

Fig 4.29 represents the SEM image of the composite specimens subjected to tensile fracture for three different composites reinforced with (a) pineapple fiber, (b) sisal fiber and (c) coir fiber. The fracture surfaces had presented a mix of fiber breakage and fiber pull-out, demonstrating that the fiber-matrix interface had been sufficiently strong to resist pull-out in some cases but not always.

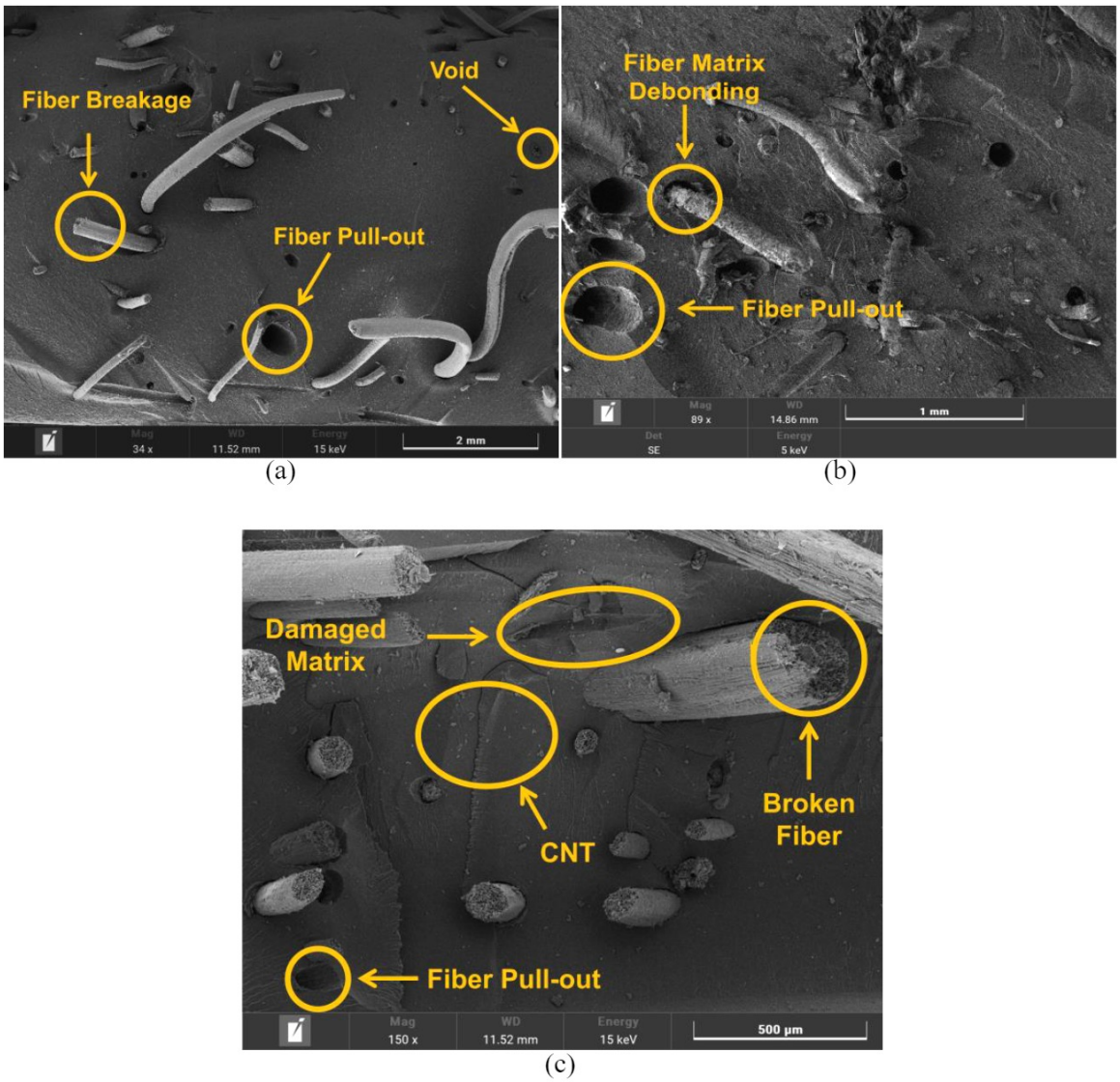

Fig 4.29: Scanning Electron Microscope (SEM) image of composites subjected to tensile failure

Instances of fiber pull-out implied an insufficient bond strength between the fibers and the matrix, leading to premature failure under tensile strength. Furthermore, the SEM images showed that the fibers were well distributed within the matrix, but the regions of fiber clustering were visible. These fiber clusters had acted as stress concentrators, potentially

leading to micro-cracks initiation under tensile loading. Also, the fractured fibers had generally been clean and smooth, suggesting that the failure had occurred at the fiber-matrix interface.

Fig 4.30 represents the SEM image of the composite specimens subjected to flexural fracture for different composites reinforced with (a) pineapple fiber, (b) and (c) sisal fiber and (d) coir fiber.. The flexural fractured specimens' SEM images showed a more complex failure mechanism. The fibers within the matrix displayed signs of both bending and fracture. The matrix had shown signs of plastic deformation, indicating the material's effort to resist the bending forces.

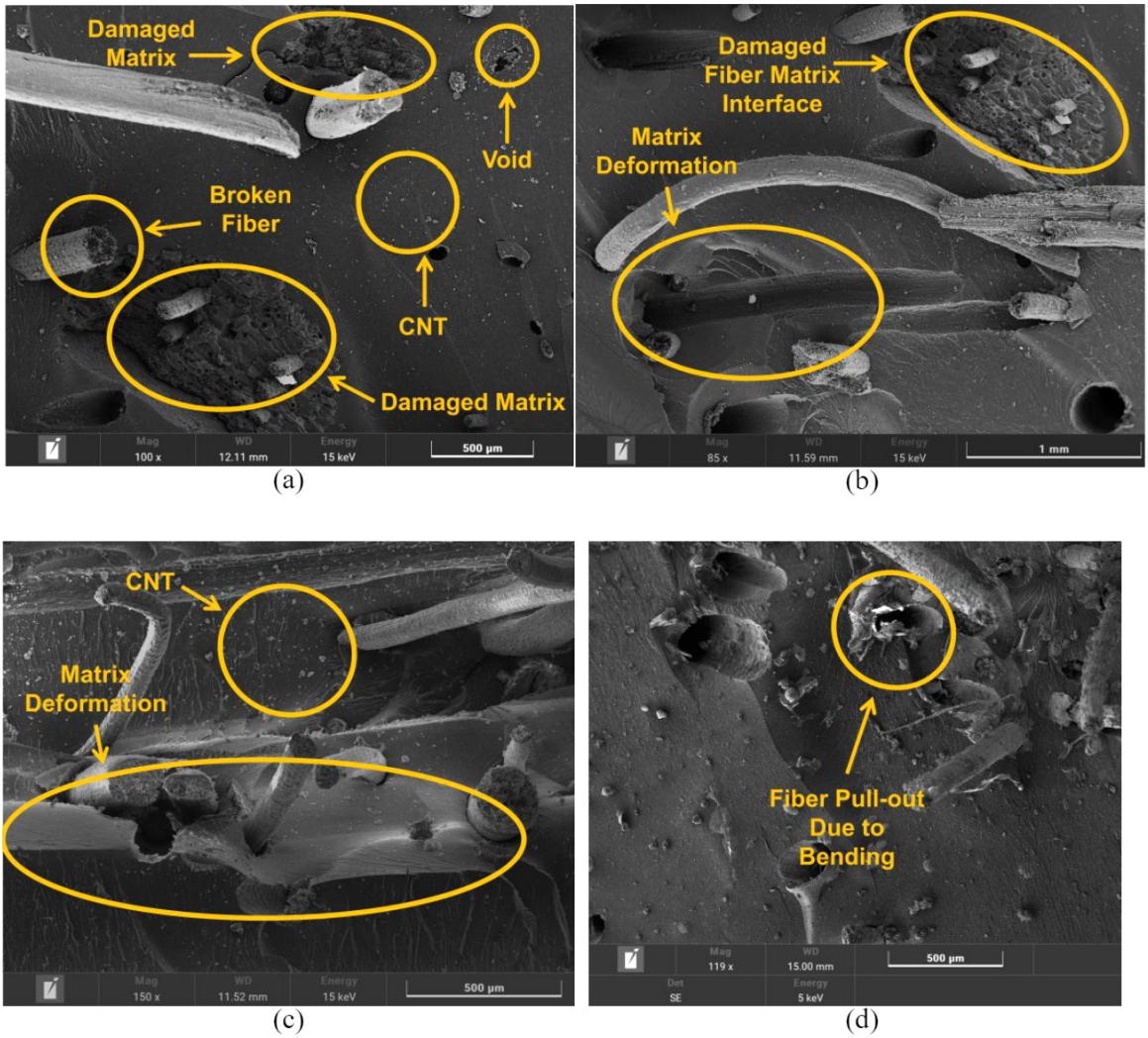

Fig 4.30: Scanning Electron Microscope (SEM) image of composites subjected to flexural failure

The SEM images showed the fracture surfaces to be marked by a combination of fiber breakage and fiber pull-out. This indicated varying bonding strength between the fibers and the matrix. The instances of fiber pull-out suggested weaker adhesion at some points, which

could have failed under flexural strength. Moreover, while the fibers seemed to be well dispersed within the matrix, areas of fiber clustering had been detected. These clusters could have acted as stress concentration points, which may have led to micro-cracks initiation when subjected to flexural strength.

Fig 4.31 represents the SEM image of the composite specimens subjected to impact fracture for different composites reinforced with (a) pineapple fiber, (b) sisal fiber and (c) coir fiber. The impact-fractured specimens displayed features that were markedly different. The region of the damaged matrix was visible in the SEM image. Also, the images revealed debonding, fiber pull-out, and the presence of voids and micro-cracks, suggesting the material's lower resistance to impact forces.

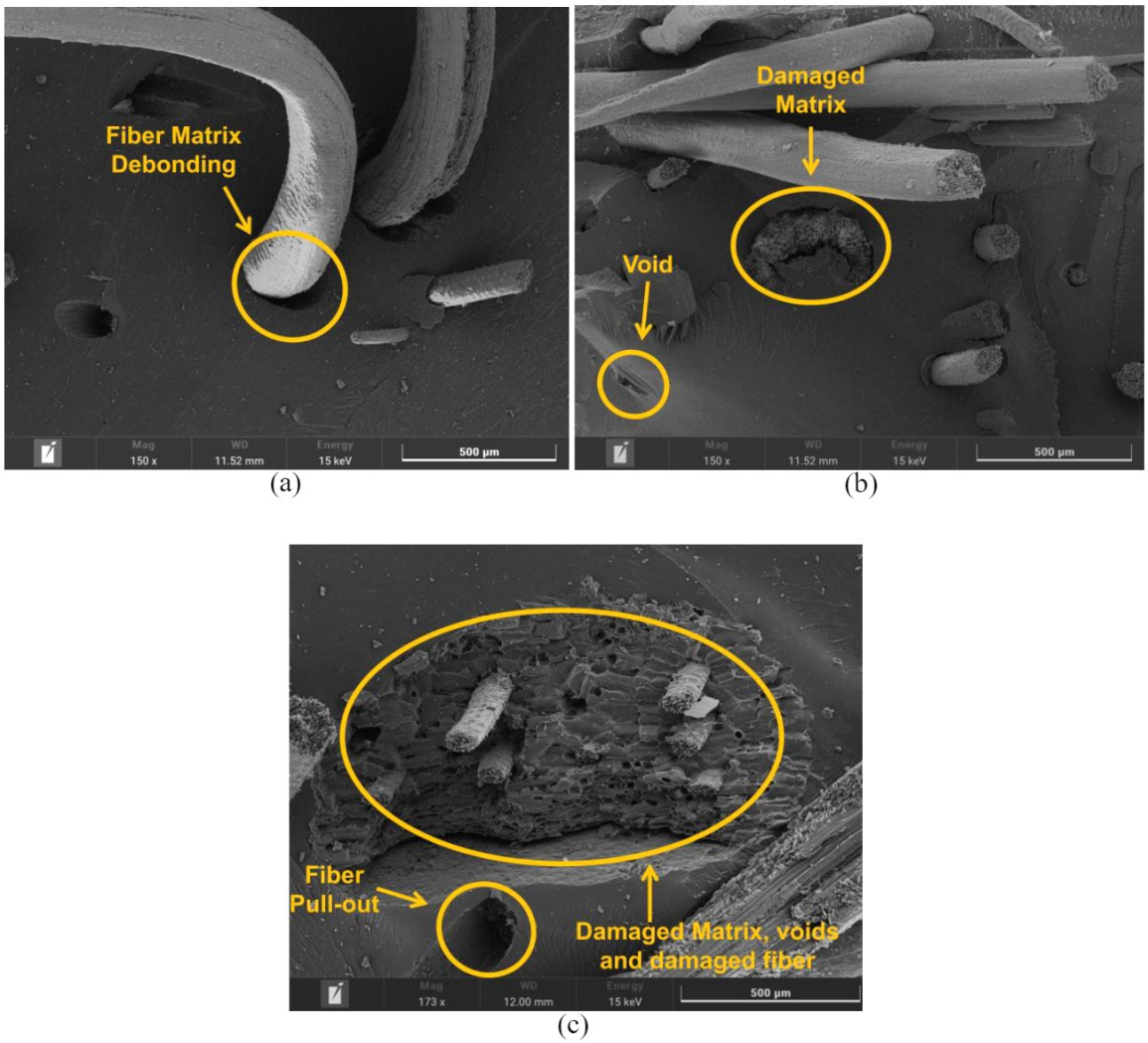

Fig 4.31: Scanning Electron Microscope (SEM) image of composites subjected to impact fracture

On closer inspection, the fibers within the matrix appeared to have fractured cleanly, suggesting a brittle failure mechanism. The fiber-matrix interface had shown signs of

debonding and fiber pull-out, indicating that the bond strength between the fiber and the matrix may not have been sufficient to withstand the impact forces. The presence of voids and micro-cracks on the fracture surfaces had also been noted, which may have acted as stress concentration points, initiating and propagating failure under impact loading.

4.8 Finite Element Modelling

In this study, the finite element method (FEM) is utilized as an essential computational tool for research. The FEM allows for the numerical examination and optimization of the composites developed, offering critical information about their mechanical properties. This section contains four subsections: (1) mesh independence, which delves into the influence of mesh refinement on the FEM outcomes, ensuring the dependability of the results; (2) results, in which the findings of the FEM simulations are presented, and the performance of the epoxy composites is explored; (3) validation study, where the approach used to confirm the precision of the FEM models is detailed through comparison with experimental findings and lastly, (4) analysis, where the outcomes are scrutinized, significant patterns are identified, and a comprehensive understanding of the mechanical traits of these innovative composite materials is offered.

4.8.1 Mesh Independence

The developed finite element model was tested at various inclusion-to-RVE (representative volume element) ratios to determine its mesh independence criteria. This test was focused on two key properties: Young's modulus and Shear modulus.

The mesh independence test was conducted across two different scenarios, involving a varying number of materials. In the first scenario, only two materials—epoxy and fiber—were considered. The second scenario involved three materials: epoxy, fiber, and carbon nanotubes (CNTs). The goal was to establish the optimal inclusion-to-RVE ratio that would yield the most accurate and reliable results without demanding excessive computational resources. Fig 4.32 shows the validation study results against the experimental and computational cases.

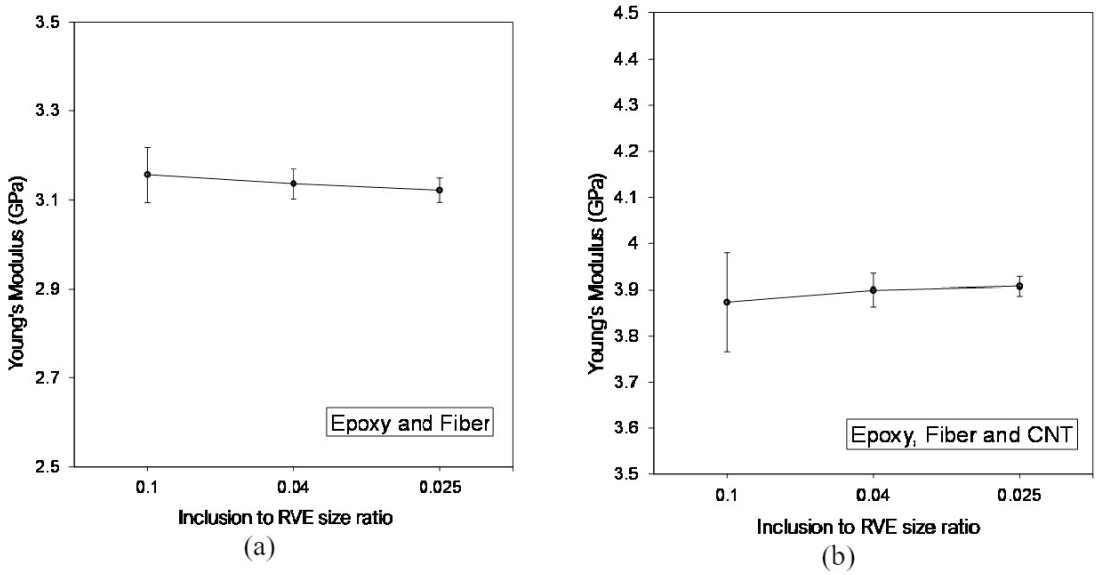

Fig 4.32: Mesh independence test for Young's modulus (a) consisting of 2 materials, and (b) consisting of 3 materials.

Upon analyzing the results, it was observed that for an inclusion-to-RVE ratio of 0.1, the standard deviation was relatively high, indicating a less accurate model. On the other hand, an inclusion-to-RVE ratio of 0.025 yielded the best standard deviation compared to the 0.04 ratio, suggesting a more precise and reliable representation of the composites' behavior. However, it can be noted that the 0.025 ratio necessitated a significantly higher amount of computational power and time.

After careful consideration, it was decided to use an inclusion-to-RVE ratio of 0.04 for conducting all subsequent analyses. While the standard deviation difference between the 0.025 and 0.04 ratios was marginal, the computational resources required for the latter were more manageable. This decision allowed for a balance between accuracy and computational efficiency, ensuring that the finite element model could effectively capture the mechanical properties of the epoxy composites reinforced with carbon nanotube and natural fiber.

Throughout the study, the finite element model played an essential role in understanding and predicting the performance of the developed composites. The mesh independence test served as a vital step in refining the model and ensuring its reliability in representing the complex interplay of materials in the composites. By identifying the optimal inclusion-to-RVE ratio, conducting further analyses with confidence was possible based on the model's accuracy and reliability.

In conclusion, the mesh independence test provided valuable insights into the performance of the finite element model and its ability to represent the mechanical properties of epoxy composites reinforced with carbon nanotube and natural fiber. By selecting the appropriate inclusion-to-RVE ratio of 0.04, it was possible to strike a balance between accuracy and computational efficiency, enabling more in-depth analyses and a better understanding of the composites' behavior.

4.8.2 FEM Results

Fig 4.33 represents the developed RVE models with varying fiber contents and CNT contents, where following compositions were applied (a) 30wt.% fiber, 0 wt.% CNT, (b) 40wt.% fiber, 0 wt.% CNT, (c) 30wt.% fiber, 1 wt.% CNT, (d) 40wt.% fiber, 1 wt.% CNT, (e) 30wt.% fiber, 2 wt.% CNT, (f) 40wt.% fiber, 2 wt.% CNT, (g) 30wt.% fiber, 3 wt.% CNT, and (h) 40wt.% fiber, 3 wt.% CNT. The elements in black color represent the fiber content (25vol.% and 34vol.%) and the elements in red color represent the CNT content (1,2 and 3vol.%).

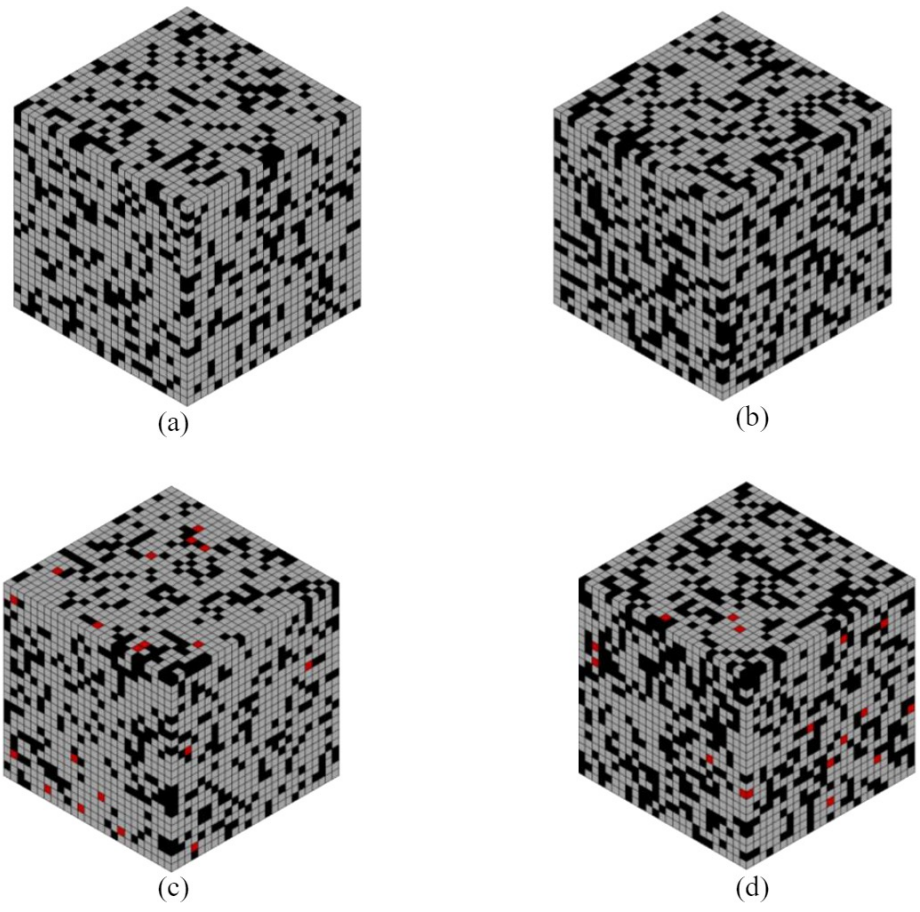

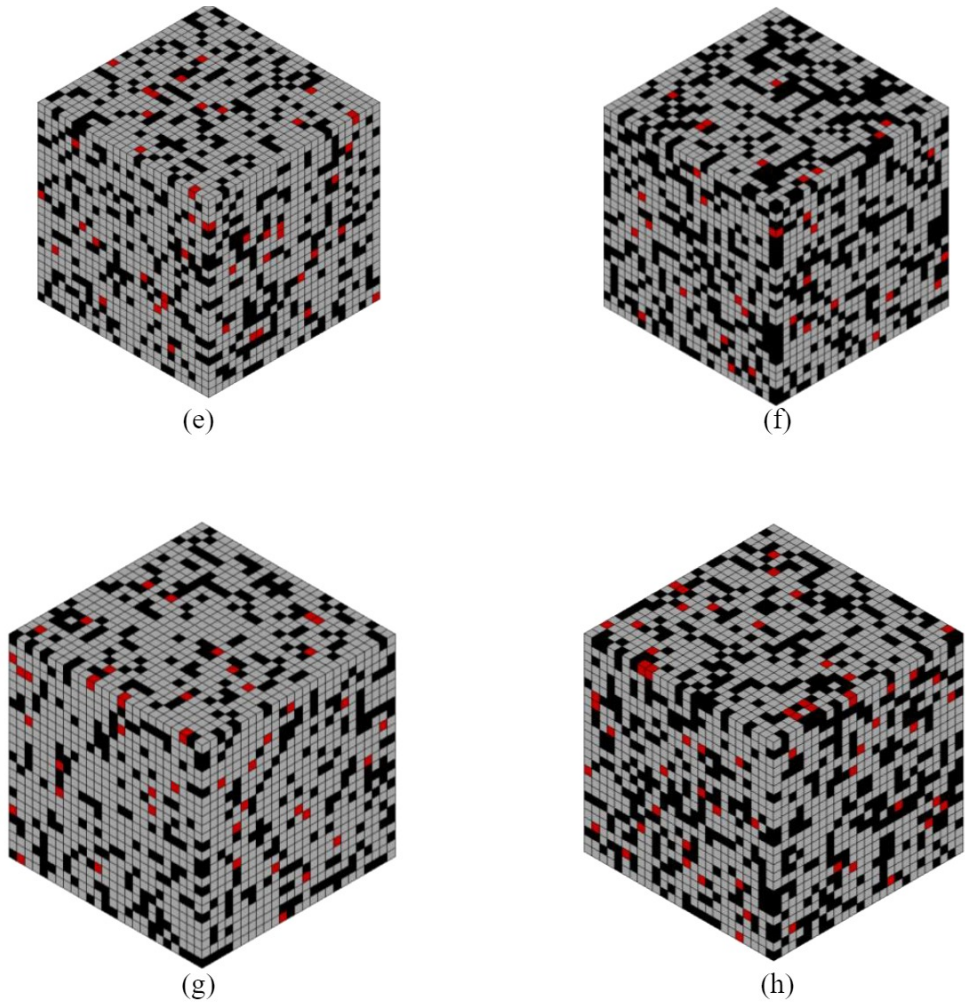

Fig 4.33: Developed RVE with varying fiber and CNT content.

The following data obtained from the FEM simulations represents the Young's modulus of the composites under various conditions. These conditions include different types of fibers (sisal, pineapple, and coir), varying fiber weight percentages (30% and 40%) corresponding to two volume percentages (25% and 34%), and the incorporation of carbon nanotubes (CNTs) at different volume percentages (0%, 1%, 2%, and 3%). Fig 4.34 shows the FEM simulation results for various scenarios, where where S0, S1, S2 and S3 indicates sisal fiber with 0wt.%, 1wt.%, 2wt.% and 3wt.% MWCNT respectively, P0, P1, P2 and P3 indicates pineapple fiber with 0wt.%, 1wt.%, 2wt.% and 3wt.% MWCNT respectively, and C0, C1, C2 and C3 indicates coir fiber with 0wt.%, 1wt.%, 2wt.% and 3wt.% MWCNT respectively.

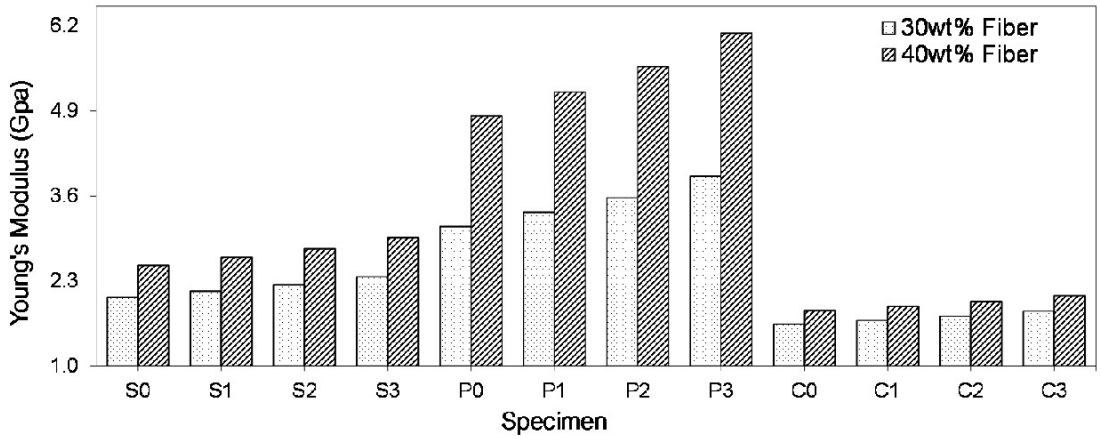

Fig 4.34: FEM result for Young's modulus with varying fiber contents.

From Fig 4.34, several trends become apparent, indicating the effects of each factor on the mechanical properties of the epoxy composites. First, a clear correlation between the type of fiber and the Young's modulus values can be observed. In general, pineapple fiber composites exhibit the highest values, followed by sisal and then coir. This suggests that the pineapple fiber is more effective in enhancing the stiffness of the epoxy composite compared to the other two fiber types.

Furthermore, as the fiber weight percentage increases from 30% to 40%, there is a noticeable increase in the Young's modulus for all three fiber types. This trend indicates that a higher fiber content leads to a stronger and stiffer composite material.

The addition of carbon nanotubes (CNTs) also seems to have a positive impact on the mechanical properties of the composites. As the CNT percentage increases from 0% to 3%, there is a consistent rise in the Young's modulus for all fiber types and fiber weight percentages. This demonstrates that CNTs have a synergistic effect when combined with natural fibers, further enhancing the mechanical performance of the epoxy composites.

4.8.3 Validation Study

The Microstructure Free Finite Element Model (MF-FEM) applied for this study was validated against experimental data in this study. From Fig 4.35 and Fig 4.36, first, it is essential to acknowledge that the FEM predictions for Young's modulus were generally higher than the experimental results. This discrepancy might arise due to simplifications in the finite element model, high phase contrast differences in material properties, or the

presence of voids and defects in the experimental specimens that were not accounted for in the FEM simulations.

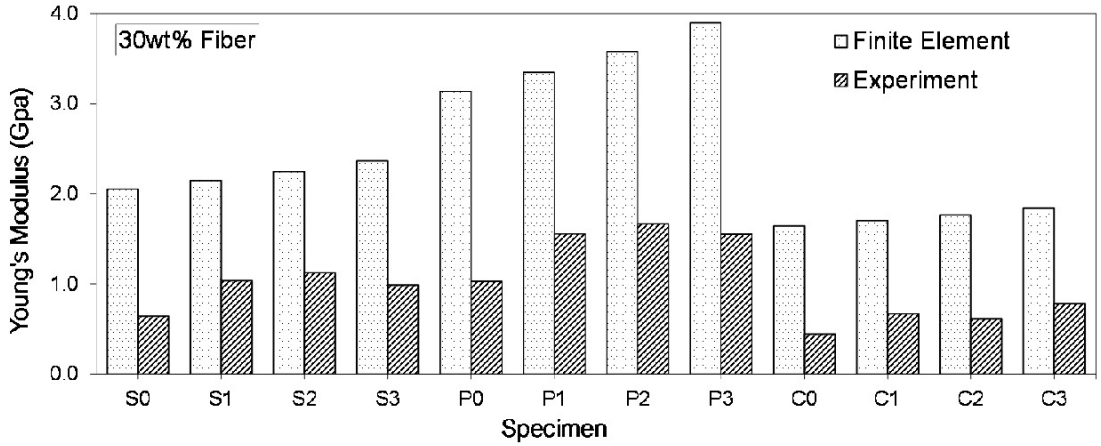

Fig 4.35: Comparison between FEM and experimental result of this study for Young's modulus with 30 wt.% fibers.

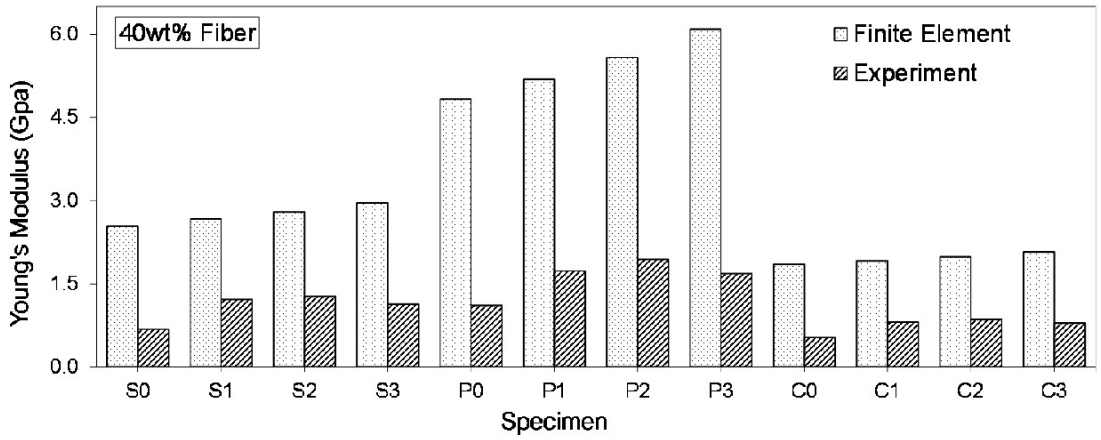

Fig 4.36: Comparison between FEM and experimental result of this study for Young's modulus with 40 wt.% fibers.

When analyzing the data for sisal fiber composites at 30% fiber weight, a noticeable trend emerges: as the CNT concentration increased, both the experimental and FEM-predicted Young's modulus values increased. This suggests that the addition of CNTs enhanced the mechanical properties of the composite. However, the FEM predictions consistently overestimated the Young's modulus compared to the experimental data. A similar trend can be observed for sisal fiber composites at 40% fiber weight.

For pineapple fiber composites at 30% fiber weight, the addition of CNTs also leads to an increase in both experimental and FEM-predicted Young's modulus values. The same pattern is seen in the 40% fiber weight case. It is worth noting that the discrepancy between the experimental and FEM-predicted values was slightly smaller for pineapple fiber

composites than for sisal fiber composites, indicating a better correlation between the FEM model and experimental data for the former.

In the case of coir fiber composites, the general trend of increasing Young's modulus with increasing CNT concentration is once again observed for both the experimental and FEM-predicted data. The ratio between the two datasets was relatively higher, especially at higher CNT concentrations. This suggests that the FEM model was inferior at predicting the mechanical properties of coir fiber composites compared to sisal and pineapple fiber composites.

Overall, the FEM model's performance in predicting the Young's modulus of the epoxy composites shows a reasonable correlation with experimental data, despite overestimating the values. The model is especially more accurate in predicting the mechanical properties

4.8.4 Analysis of the FEM Results

MF-FEM analysis was used to analyze epoxy composites reinforced with natural fibers and carbon nanotubes (CNTs). The FEM-predicted data exhibited discrepancies when compared to the experimental results. Several factors could potentially contribute to these differences. The analysis of the results are as follows:

a) Firstly, material properties can significantly impact the accuracy of FEM predictions. The mechanical properties used in the simulations may not accurately represent the properties of the actual materials used in the experiments. Variations in fiber orientation, inconsistencies in material production, and batch-to-batch variations could all contribute to differences between the assumed and actual material properties.

b) Secondly, the presence of voids and defects in the experimental specimens may not be adequately represented in the FEM model. Voids can result from manufacturing processes, such as incomplete resin impregnation or air entrapment during curing. These voids can significantly reduce the mechanical properties of composites, leading to lower experimental values than predicted by the FEM model, which assumes a perfect, non-porous material.

c) Thirdly, the finite element model's simplifications and assumptions could contribute to the difference between the experimental and FEM data. For example, the model assumed isotropic material properties for simplification, which might not be the case for the actual composite materials. For example, agglomeration of CNTs at higher concentration cannot be modeled by the FEM, therefore it led to a deviation from the experimental results.

d) Fourthly, when there was a larger phase contrast, the disparity in the mechanical properties of the constituent materials became more pronounced. With a larger phase contrast, the interfacial stress transfer and bonding between the constituents became increasingly important. This led to inaccuracies in the FEM model, as it could not effectively capture the complex interactions between the constituent materials.

e) Lastly, experimental errors and uncertainties can also contribute to the observed differences. Measurement inaccuracies, inconsistencies in specimen preparation, and variations in testing conditions can all lead to discrepancies between the experimental results and the FEM predictions

4.9 Assessment of Composite Ranking with GRA

The analysis of composite ranking with Grey Relational Analysis (GRA) was meticulously carried out to investigate the performance characteristics of Epoxy natural fiber CNT composites. The fiber types in consideration were pineapple, sisal, and coir, with fiber weight percentage ranging between 30 and 40 wt%, and CNT weight percentage varying from 0 wt% to 3 wt%. The Grey Relational Grade (GRG) was computed for each combination and was used to determine the rank of each composite. Table 4.7 represents the ranking of the composites based on GRG score.

Table 4.7: Composite ranking based on GRG score

Fiber	Fiber wt.%	CNT wt.%	GRG score	Rank	Fiber	Fiber wt.%	CNT wt.%	GRG score	Rank
Pineapple	40	2	0.833	1	Coir	30	1	0.543	13
Pineapple	40	1	0.741	2	Coir	40	3	0.534	14
Pineapple	40	3	0.701	3	Sisal	40	3	0.523	15
Pineapple	30	2	0.684	4	Coir	30	3	0.515	16
Pineapple	30	1	0.645	5	Sisal	30	1	0.509	17
Pineapple	30	3	0.620	6	Pineapple	40	0	0.507	18
Sisal	40	2	0.594	7	Coir	30	0	0.504	19

Fiber	Fiber wt.%	CNT wt.%	GRG score	Rank	Fiber	Fiber wt.%	CNT wt.%	GRG score	Rank
Sisal	40	1	0.559	8	Coir	40	0	0.488	20
Coir	40	2	0.559	9	Sisal	30	3	0.486	21
Coir	40	1	0.549	10	Pineapple	30	0	0.483	22
Sisal	30	2	0.545	11	Sisal	40	0	0.422	23
Coir	30	2	0.544	12	Sisal	30	0	0.400	24

The highest GRG score, at 0.833, corresponded to the composite containing pineapple fibers at a concentration of 40 wt% and CNTs at a concentration of 2 wt%. This composite secured the first rank, indicating its superior performance characteristics in the tested conditions. The second rank was also obtained by a composite with pineapple fiber, but with a lower CNT content of 1 wt%. Its GRG score was 0.741, a close second to the top performer. Composites with pineapple fiber consistently held the top six positions, with the CNT content and fiber concentration altering between the ranks, demonstrating the dominant performance of pineapple fiber-based composites.

In contrast, composites comprising sisal and coir fibers scored lower GRGs and therefore held lower ranks. The highest-ranked sisal composite, containing 40 wt% fiber and 2 wt% CNT, had a GRG score of 0.594 and was ranked seventh. The best-performing coir composite, containing 40 wt% fiber and 2 wt% CNT, had a GRG score of 0.559 and was ranked ninth. This indicated that composites based on sisal and coir fibers were less performant under the selected conditions compared to the pineapple fiber-based composites.

In terms of CNT content, it was observed that as the CNT content reduced, the rank of the composites, regardless of the type of fiber, significantly dropped. This was evident from the ranks of the composites with no CNT content. For instance, the pineapple fiber composite with 40 wt% fiber and 0 wt% CNT had a GRG score of 0.507 and was ranked 18th. The sisal fiber composite with similar compositions ranked even lower at 23rd position with a GRG score of 0.422. This trend implied that CNT played a crucial role in boosting the performance of the composites.

Interestingly, as the CNT content decreased or was absent (0 wt%), the rank of the composites, irrespective of the type of fiber used, significantly fell, hinting towards the important role CNTs play in the overall performance of the composites. From these rankings, it could be deduced that composites containing pineapple fibers at a concentration of 40 wt% and CNTs at 2 wt% yielded the best performance as per the tested conditions

and selected responses. Meanwhile, sisal fiber-based composites, especially those with lower CNT content, appeared to underperform in comparison to the other compositions. The results from the Grey Relational Analysis provided valuable insights into the multi-response optimization of the composites and helped in identifying the most promising composite composition.

CHAPTER 5
CONCLUSIONS AND RECOMMENDATIONS

5.1 Conclusions

The objectives of this study were to develop natural fiber and MWCNT reinforced epoxy composites and investigate the mechanical properties of the developed composites. Another objective of this study was to model the developed composite using FEM and validate it with experimental analysis.

In this investigation, epoxy-natural fiber-MWCNT composites were developed employing the hand layup method. The selection process for the natural fibers was executed using the integrated fuzzy AHP-TOPSIS approach. Two distinctive composite groups were formulated, comprising: (i) 30 wt% fiber with varying MWCNT concentrations (0,1, 2, and 3 wt%), and (ii) 40 wt% fiber integrated with differential MWCNT concentrations (0,1, 2, and 3 wt%). To evaluate these composites, various physical and mechanical tests were carried out. These encompassed assessments of density, void content, and water absorption, alongside mechanical evaluations like tensile and flexural properties. Additionally, the Rockwell hardness and impact energy of the composites were measured. Complementing these tests, an in-depth characterization was performed via FTIR and SEM analyses. Following conclusions can be drawn from this study:

- Through the application of the fuzzy MCDM method, optimal natural fibers were selected. Among the fibers studied, pineapple fiber was found to rank notably high in terms of its mechanical properties. In contrast, sisal fiber did not perform as well, ranking lowest among the three fibers in most of the key mechanical properties examined. This contrast was clearly reflected in the overall ranking of the composites, with pineapple fiber-based composites achieving the highest rank.

- An exhaustive examination of the key mechanical properties such as tensile strength, Young's modulus, flexural strength, flexural modulus, impact energy, and Rockwell hardness number displayed the composite reinforced with 40 wt.% pineapple fiber and 2 wt.% CNT as superior. When compared with other variants of pineapple fiber composites, as well as sisal and coir fiber-reinforced composites, the latter exhibited decreased tensile strength values at the same CNT wt.%.

- Addition of MWCNT resulted in more brittleness in composites as MWCNT itself is a highly brittle material.

- Addition of MWCNT after a certain amount (2wt.%) resulted in the deterioration of mechanical properties as agglomeration took place. Therefore, void contents negatively impacted the mechanical properties.

- The composite properties were largely affected by the internal constituents of the fiber - namely, cellulose, hemicellulose, and lignin.

- The simulated results using MF-FEM aligned well with the experimental data from the mechanical tests, validating the accuracy and reliability of the model. However, a notable discrepancy was observed in the case of composites containing 3wt.% CNT. The FEM model did not account for the agglomeration effect which is a crucial factor influencing the behavior of CNT-reinforced composites.

- The required specific mechanical properties for particular applications in literature could not be incorporated because of the lack of available and reliable sources. Therefore, it remains a limitation of this study. However, through literature presented in this study, composites with similar mechanical properties have been observed to have potential applications in various fields.

Conclusively, the incorporation of MWCNT as a nanofiller enhances both mechanical and physical properties of the composite up to an optimal threshold of 2wt.%. Beyond this concentration, there's a noticeable decline in the composite's characteristics. Leveraging MF-FEM showcases potential in forecasting mechanical attributes accurately. However, discrepancies between experimental and predicted values might arise due to the existence of voids and specific fiber properties. Thus, careful consideration of the optimal MWCNT concentration and addressing the potential sources of deviation can refine the quality and application scope of these composites, promoting them as viable contenders in specialized domains.

5.2 Recommendations for Future Work

In light of the findings and conclusions drawn from this research, it is recommended:

- To explore additional natural fibers and their respective compatibility with the epoxy matrix and CNTs with various proportions of fibers and CNTs.
- To analyze the effect of fiber orientation on the mechanical properties.
- To develop FE model to account for agglomeration effects as well as multiscale modelling approaches to better understand the interaction between the fibers, CNTs, and matrix at the microscopic level.
- To explore other surface modification techniques like silane treatment, acetylation, or permanganate treatment.
- To test additional parameters such as creep, fatigue, and fracture toughness to provide a comprehensive understanding of the composite's performance.

PUBLISHED JOURNAL PAPERS

1. Bhadra, D., & Dhar, N. R. (2022). Selection of the natural fiber for sustainable applications in aerospace cabin interior using fuzzy MCDM model. Materialia, Vol. 21, pp. 101270.
2. Bhadra, D., Dhar, N. R., & Salam, M. A. (2022). Sensitivity analysis of the integrated AHP-TOPSIS and CRITIC-TOPSIS method for selection of the natural fiber. Materials Today: Proceedings, Vol. 56, pp. 2618-2629.

REFERENCES

Abdollah, M. F. Bin, Shuhimi, F. F., Ismail, N., Amiruddin, H., and Umehara, N. (2015). Selection and verification of kenaf fibres as an alternative friction material using Weighted Decision Matrix method. Mater. Des., Vol. 67, pp. 577–582.

Adeniyi, A. G., Ighalo, J. O., and Onifade, D. V. (2019). Banana and plantain fiber-reinforced polymer composites. J. Polym. Eng., Vol. 39(7), pp. 597–611.

Akhil, U. V, Radhika, N., Saleh, B., Aravind Krishna, S., Noble, N., and Rajeshkumar, L. (2023). A comprehensive review on plant-based natural fiber reinforced polymer composites: fabrication, properties, and applications. Polym. Compos.

Alarifi, I. M. (2023). A Review on Factors Affecting Machinability and Properties of Fiber-Reinforced Polymer Composites. J. Nat. Fibers, Vol. 20(1), pp. 2154304.

Alemayehu, Z., Nallamothu, R. B., Liben, M., Nallamothu, S. K., and Nallamothu, A. K. (2020). Experimental investigation on characteristics of sisal fiber as composite material for light vehicle body applications. Mater. Today Proc., Vol. 38, pp. 2439–2444.

Alharbi, A., Alosaimi, W., Alyami, H., Nadeem, M., Faizan, M., Agrawal, A., Kumar, R., and Khan, R. A. (2021). Managing Software Security Risks through an Integrated Computational Method. Intell. Autom. Soft Comput., Vol. 28(1), pp. 179–194.

Aliyu Yaro, N. S., Napiah, M., Sutanto, M. H., Usman, A., Mizwar, I. K., and Umar, A. M. (2022). Engineering Properties of Palm Oil Clinker Fine-Modified Asphaltic Concrete Mixtures. J. Eng. Technol. Sci., Vol. 54(2).

Alkbir, M. F. M., Sapuan, S. M., Nuraini, A. A., and Ishak, M. R. (2016). Fibre properties and crashworthiness parameters of natural fibre-reinforced composite structure: A literature review. Compos. Struct., Vol. 148, pp. 59–73.

Alosaimi, W., Alharbi, A., Alyami, H., Ahmad, M., Pandey, A. K., Kumar, R., and Khan, R. A. (2021). Impact of Tools and Techniques for Securing Consultancy Services. Comput. Syst. Sci. Eng., Vol. 37(3), pp. 347–360.

Alotaibi, M. D., Alshammari, B. A., Saba, N., Alothman, O. Y., Sanjay, M. R., Almutairi, Z., and Jawaid, M. (2019). Characterization of natural fiber obtained from different parts of date palm tree (Phoenix dactylifera L.). Int. J. Biol. Macromol., Vol. 135, pp. 69–76.

Alshammari, B. A., Alsuhybani, M. S., Almushaikeh, A. M., Alotaibi, B. M., Alenad, A. M., Alqahtani, N. B., and Alharbi, A. G. (2021). Comprehensive review of the properties and modifications of carbon fiber-reinforced thermoplastic composites. Polymers (Basel)., Vol. 13(15), pp. 2474.

Alzebdeh, K. I., Nassar, M. M. A., and Arunachalam, R. (2019). Effect of fabrication parameters on strength of natural fiber polypropylene composites: Statistical assessment. Measurement, Vol. 146, pp. 195–207.

Amarnath, K., Babu, K. J., and Kumar, M. V. S. (2021). Selection of optimal Flax Fiber Reinforced Components for Experimental Investigation by using TOPSIS method. IOP Conf. Ser. Mater. Sci. Eng., Vol. 1057(1), pp. 12055.

Amjad, A., Anjang Ab Rahman, A., Awais, H., Zainol Abidin, M. S., and Khan, J. (2022). A review investigating the influence of nanofiller addition on the mechanical, thermal

and water absorption properties of cellulosic fibre reinforced polymer composite. J. Ind. Text., Vol. 51(1_suppl), pp. 65S-100S.

Anbukarasi, K., and Kalaiselvam, S. (2015). Study of effect of fibre volume and dimension on mechanical, thermal, and water absorption behaviour of luffa reinforced epoxy composites. Mater. Des., Vol. 66, pp. 321–330.

Andhare, A. B., and Raju, R. A. (2016). Properties of dispersion of multiwalled carbon nanotubes as cutting fluid. Tribol. Trans., Vol. 59(4), pp. 663–670.

Ansari, M. T. J., Baz, A., Alhakami, H., Alhakami, W., Kumar, R., and Khan, R. A. (2021). P-STORE: Extension of STORE methodology to elicit privacy requirements. Arab. J. Sci. Eng., pp. 1–24.

Aphichartsuphapkhajorn, K., Arao, Y., and Kubouchi, M. (2019). Mechanical properties of unidirectional flax fabric-reinforced furan composites: effect of alkaline treatment and silane coupling treatment. Mater. Sci. Forum, Vol. 951, pp. 33–38.

Arockiam, N. J., Jawaid, M., and Saba, N. (2018). Sustainable bio composites for aircraft components. In *Sustainable composites for aerospace applications* (pp. 109–123). Elsevier.

Ashothaman, A., Sudha, J., and Senthilkumar, N. (2023). A comprehensive review on biodegradable polylactic acid polymer matrix composite material reinforced with synthetic and natural fibers. Mater. Today Proc., Vol. 80, pp. 2829–2839.

Asim, M., Jawaid, M., Abdan, K., and Ishak, M. R. (2016). Effect of alkali and silane treatments on mechanical and fibre-matrix bond strength of kenaf and pineapple leaf fibres. J. Bionic Eng., Vol. 13(3), pp. 426–435.

Asim, M., Jawaid, M., Abdan, K., and Ishak, M. R. (2017). Effect of pineapple leaf fibre and kenaf fibre treatment on mechanical performance of phenolic hybrid composites. Fibers Polym., Vol. 18, pp. 940–947.

Asim, M., Jawaid, M., Abdan, K., and Ishak, M. R. (2018). The effect of silane treated fibre loading on mechanical properties of pineapple leaf/kenaf fibre filler phenolic composites. J. Polym. Environ., Vol. 26, pp. 1520–1527.

Asyraf, M. R. M., Ishak, M. R., Sapuan, S. M., Yidris, N., Ilyas, R. A., Rafidah, M., and Razman, M. R. (2020). Potential application of green composites for cross arm component in transmission tower: A brief review. Int. J. Polym. Sci., Vol. 2020, pp. 1–15.

Athijayamani, A., Thiruchitrambalam, M., Natarajan, U., and Pazhanivel, B. (2009). Effect of moisture absorption on the mechanical properties of randomly oriented natural fibers/polyester hybrid composite. Mater. Sci. Eng. A, Vol. 517(1–2), pp. 344–353.

Avilés, F., Cauich-Rodríguez, J. V, Toro-Estay, P., Yazdani-Pedram, M., and Aguilar-Bolados, H. (2018). 5 - Improving Carbon Nanotube/Polymer Interactions in Nanocomposites. In R. B. T.-C. N.-R. P. Rafiee (Ed.), *Micro and Nano Technologies* (pp. 83–115). Elsevier.

Ayhan, M. B. (2013). A fuzzy AHP approach for supplier selection problem: A case study in a Gear motor company. ArXiv Prepr. ArXiv1311.2886.

Balmat, J.-F., Lafont, F., Maifret, R., and Pessel, N. (2011). A decision-making system to maritime risk assessment. Ocean Eng., Vol. 38(1), pp. 171–176.

Batu, T., Lemu, H. G., and Sirhabizuh, B. (2020). Study of the performance of natural fiber

reinforced composites for wind turbine blade applications. Adv. Sci. Technol. Res. J., Vol. 14(2).

Bellairu, P. K., Bhat, S., Gijo, E. V, and Mangalore, P. (2022). Multi-response modelling and optimization of agave cantala natural fiber and multi-wall carbon nano tube reinforced polymer nanocomposite: application of mixture design. Fibers Polym., Vol. 23(4), pp. 1089–1099.

Bhattacharyya, D., Subasinghe, A., and Kim, N. K. (2015). *Chapter 4 - Natural fibers: Their composites and flammability characterizations* (K. Friedrich & U. B. T.-M. of P. C. Breuer (eds.); pp. 102–143). William Andrew Publishing.

Birniwa, A. H., Abdullahi, S. S., Ali, M., Mohammad, R. E. A., Jagaba, A. H., Amran, M., Avudaiappan, S., Maureira-Carsalade, N., and Flores, E. I. S. (2023). Recent Trends in Treatment and Fabrication of Plant-Based Fiber-Reinforced Epoxy Composite: A Review. J. Compos. Sci., Vol. 7(3), pp. 120.

Buckley, J. J. (1985). Fuzzy hierarchical analysis. Fuzzy Sets Syst., Vol. 17(3), pp. 233–247.

Cakar, T., and Çavuş, B. (2021). Supplier selection process in dairy industry using fuzzy TOPSIS method. Oper. Res. Eng. Sci. Theory Appl., Vol. 4(1), pp. 82–98.

Capricho, J. C., Fox, B., and Hameed, N. (2020). Multifunctionality in epoxy resins. Polym. Rev., Vol. 60(1), pp. 1–41.

Catalanotti, G. (2016). On the generation of RVE-based models of composites reinforced with long fibres or spherical particles. Compos. Struct., Vol. 138, pp. 84–95.

Cha, J., Jun, G. H., Park, J. K., Kim, J. C., Ryu, H. J., and Hong, S. H. (2017). Improvement of modulus, strength and fracture toughness of CNT/Epoxy nanocomposites through the functionalization of carbon nanotubes. Compos. Part b Eng., Vol. 129, pp. 169–179.

Chan, J. X., Wong, J. F., Petrů, M., Hassan, A., Nirmal, U., Othman, N., and Ilyas, R. A. (2021). Effect of nanofillers on tribological properties of polymer nanocomposites: A review on recent development. Polymers (Basel)., Vol. 13(17), pp. 2867.

Chand, N., and Fahim, M. (2021a). 1 - Natural fibers and their composites. In N. Chand & M. B. T.-T. of N. F. P. C. (Second E. Fahim (Eds.), *Woodhead Publishing Series in Composites Science and Engineering* (pp. 1–59). Woodhead Publishing.

Chand, N., and Fahim, M. (2021b). 4 - Jute-reinforced polymer composites. In N. Chand & M. B. T.-T. of N. F. P. C. (Second E. Fahim (Eds.), *Woodhead Publishing Series in Composites Science and Engineering* (pp. 111–130). Woodhead Publishing.

Chandekar, H., Chaudhari, V., and Waigaonkar, S. (2020a). A review of jute fiber reinforced polymer composites. Mater. Today Proc., Vol. 26, pp. 2079–2082.

Chandekar, H., Chaudhari, V., and Waigaonkar, S. (2020b). A review of jute fiber reinforced polymer composites. Mater. Today Proc., Vol. 26, pp. 2079–2082.

Chandramohan, D., and Marimuthu, K. (2011). A review on natural fibers. Int. J. Res. Rev. Appl. Sci., Vol. 8(2), pp. 194–206.

Chatterjee, P., and Stević, Ž. (2019). A two-phase fuzzy AHP-fuzzy TOPSIS model for supplier evaluation in manufacturing environment. Oper. Res. Eng. Sci. Theory Appl., Vol. 2(1), pp. 72–90.

Chen, P.-Y., Lian, H.-Y., Shih, Y.-F., Chen-Wei, S.-M., and Jeng, R.-J. (2017). Preparation, characterization and crystallization kinetics of Kenaf fiber/multi-walled carbon nanotube/polylactic acid (PLA) green composites. Mater. Chem. Phys., Vol. 196, pp. 249–255.

Cheung, H., Ho, M., Lau, K., Cardona, F., and Hui, D. (2009). Natural fibre-reinforced composites for bioengineering and environmental engineering applications. Compos. Part B Eng., Vol. 40(7), pp. 655–663.

CHICHANE, A., BOUJMAL, R., and El BARKANY, A. (2023). Bio-composites and bio-hybrid composites reinforced with natural fibers: Review. Mater. Today Proc., Vol. 72, pp. 3471–3479.

Ciecierska, E., Boczkowska, A., Kurzydlowski, K. J., Rosca, I. D., and Van Hoa, S. (2013). The effect of carbon nanotubes on epoxy matrix nanocomposites. J. Therm. Anal. Calorim., Vol. 111, pp. 1019–1024.

CW Nguong S Debnath, S. N. B. L. (2013). A review on natural fibre reinforced polymer composites. World Acad Sci Eng Technol, Vol. 7(1), pp. 1123–1130.

da Silva, L. B. L., Alencar, M. H., and de Almeida, A. T. (2022). Exploring global sensitivity analysis on a risk-based MCDM/A model to support urban adaptation policies against floods. Int. J. Disaster Risk Reduct., Vol. 73, pp. 102898.

da Silveira, P. H. P. M., Ribeiro, M. P., Silva, T. T., Lima, A. M., Lemos, M. F., Oliveira, A. G., Nascimento, L. F. C., Gomes, A. V, and Monteiro, S. N. (2022). Effect of Alkaline Treatment and Graphene Oxide Coating on Thermal and Chemical Properties of Hemp (Cannabis sativa L.) Fibers. J. Nat. Fibers, Vol. 19(15), pp. 12168–12181.

Das, S., Rahman, M., and Hasan, M. (2018). Physico-mechanical properties of pineapple leaf and banana fiber reinforced hybrid polypropylene composites: effect of fiber ratio and sodium hydroxide treatment. IOP Conf. Ser. Mater. Sci. Eng., Vol. 438(1), pp. 12027.

David Müzel, S., Bonhin, E. P., Guimarães, N. M., and Guidi, E. S. (2020). Application of the finite element method in the analysis of composite materials: A review. Polymers (Basel)., Vol. 12(4), pp. 818.

Deo, C., and Acharya, S. K. (2010). Effect of moisture absorption on mechanical properties of chopped natural fiber reinforced epoxy composite. J. Reinf. Plast. Compos., Vol. 29(16), pp. 2513–2521.

Derrouiche, I., Ben Marzoug, I., Sakli, F., and Roudesli, S. (2015). Study of extraction and characterization of ultimate date palm fibers. Adv. Mater, Vol. 4, pp. 7–14.

Devaraju, S., and Alagar, M. (2021). *Polymer Matrix Composite Materials for Aerospace Applications* (D. B. T.-E. of M. C. Brabazon (ed.); pp. 947–969). Elsevier.

Devnani, G. L., and Sinha, S. (2019). Effect of nanofillers on the properties of natural fiber reinforced polymer composites. Mater. Today Proc., Vol. 18, pp. 647–654.

Dhaliwal, J. S. (2019). Natural fibers: applications. Gener. Dev. Modif. Nat. Fibers, Vol. 2, pp. 1–23.

Dilfi KF, A., Che, Z., and Xian, G. (2019). Grafting ramie fiber with carbon nanotube and its effect on the mechanical and interfacial properties of ramie/epoxy composites. J. Nat. Fibers, Vol. 16(3), pp. 388–403.

Dwivedi, U. K., Trihotri, M., Gupta, S. C., Khan, F. H., Malik, M. M., and Qureshi, M. S.

(2017). Effect of carbon nanotubes implantation on electrical properties of sisal fibre–epoxy composites. Compos. Interfaces, Vol. 24(2), pp. 111–123.

Espert, A., Vilaplana, F., and Karlsson, S. (2004). Comparison of water absorption in natural cellulosic fibres from wood and one-year crops in polypropylene composites and its influence on their mechanical properties. Compos. Part A Appl. Sci. Manuf., Vol. 35(11), pp. 1267–1276.

Fan, Z., and Advani, S. G. (2007). Rheology of multiwall carbon nanotube suspensions. J. Rheol. (N. Y. N. Y)., Vol. 51(4), pp. 585–604.

Faruk, O., Bledzki, A. K., Fink, H.-P., and Sain, M. (2014a). *Progress Report on Natural Fiber Reinforced Composites*. Vol. 299(1), pp. 9–26.

Faruk, O., Bledzki, A. K., Fink, H., and Sain, M. (2014b). Progress report on natural fiber reinforced composites. Macromol. Mater. Eng., Vol. 299(1), pp. 9–26.

Fathi, B., Foruzanmehr, M., Elkoun, S., and Robert, M. (2019). Novel approach for silane treatment of flax fiber to improve the interfacial adhesion in flax/bio epoxy composites. J. Compos. Mater., Vol. 53(16), pp. 2229–2238.

Felisberto, M., Arias-Durán, A., Ramos, J. A., Mondragon, I., Candal, R., Goyanes, S., and Rubiolo, G. H. (2012). Influence of filler alignment in the mechanical and electrical properties of carbon nanotubes/epoxy nanocomposites. Phys. B Condens. Matter, Vol. 407(16), pp. 3181–3183.

Franco, P. J. H., and Valadez-González, A. (2005). Fiber-matrix adhesion in natural fiber composites. In *Natural fibers, biopolymers, and biocomposites* (pp. 196–252). CRC Press.

Fu, S., Sun, Z., Huang, P., Li, Y., and Hu, N. (2019). Some basic aspects of polymer nanocomposites: A critical review. Nano Mater. Sci., Vol. 1(1), pp. 2–30.

Fuqua, M. A., Huo, S., and Ulven, C. A. (2012). Natural fiber reinforced composites. Polym. Rev., Vol. 52(3), pp. 259–320.

George, M., Chae, M., Science, D. B.-P. in materials, and 2016, undefined. (n.d.). Composite materials with bast fibres: Structural, technical, and environmental properties. Elsevier. Retrieved October 25, 2022, from

Gholampour, A., and Ozbakkaloglu, T. (2020). A review of natural fiber composites: properties, modification and processing techniques, characterization, applications. J. Mater. Sci., Vol. 55(3), pp. 829–892.

Goudenhooft, C., Bourmaud, A., and Baley, C. (2019). Flax (Linum usitatissimum L.) fibers for composite reinforcement: exploring the link between plant growth, cell walls development, and fiber properties. Front. Plant Sci., Vol. 10, pp. 411.

Gu, F., Zheng, Y., Zhang, W., Yao, X., Pan, D., Wong, A. S. M., Guo, J., Hall, P., and Sharmin, N. (2018). Can bamboo fibres be an alternative to flax fibres as materials for plastic reinforcement? A comparative life cycle study on polypropylene/flax/bamboo laminates. Ind. Crops Prod., Vol. 121, pp. 372–387.

Gupta, M. K., and Singh, R. (2019). PLA-coated sisal fibre-reinforced polyester composite: Water absorption, static and dynamic mechanical properties. J. Compos. Mater., Vol. 53(1), pp. 65–72.

Hamad, S. F., Stehling, N., Hayes, S. A., Foreman, J. P., and Rodenburg, C. (2019). Exploiting plasma exposed, natural surface nanostructures in ramie fibers for polymer

composite applications. Materials (Basel)., Vol. 12(10), pp. 1631.

Hameed, A. M. (2016). Preparation and studying of some properties of polymer composites reinforced with natural and artificial fibers. Iraqi J. Phys., Vol. 14(31), pp. 138–147.

Hao, B., and Ma, P. C. (2017). Chapter 3 - Carbon Nanotubes for Defect Monitoring in Fiber-Reinforced Polymer Composites. In H. Peng, Q. Li, & T. B. T.-I. A. of C. N. Chen (Eds.), *Micro and Nano Technologies* (pp. 71–99). Elsevier.

Harik, V. (2018). *Chapter 1 - Nanotechnology of Carbon Nanotubes: Sensors, Transistors and Nanocomposites* (V. B. T.-M. of C. N. Harik (ed.); pp. 1–24). Academic Press.

Hasan, R., and Rayyaan, R. (2014). Effect of fibre geometry on the tensile properties of thermoset jute fibre composites. Composites, Vol. 14, pp. 18.

Huang, W.-T., Wu, D.-H., Lin, S.-P., and Liu, W.-S. (2016). A combined minimum quantity lubrication and MWCNT cutting fluid approach for SKD 11 end milling. Int. J. Adv. Manuf. Technol., Vol. 84, pp. 1697–1704.

Ibrahim, I. D., Jamiru, T., Sadiku, R. E., Kupolati, W. K., and Agwuncha, S. C. (2017). Dependency of the Mechanical Properties of Sisal Fiber Reinforced Recycled Polypropylene Composites on Fiber Surface Treatment, Fiber Content and Nanoclay. J. Polym. Environ., Vol. 25(2), pp. 427–434.

Ionescu-Bujor, M., and Cacuci, D. G. (2004). A comparative review of sensitivity and uncertainty analysis of large-scale systems—i: Deterministic methods. Nucl. Sci. Eng., Vol. 147(3), pp. 189–203.

Jabbar, A., and Jabbar, A. (2017). Flexural, creep and dynamic mechanical evaluation of novel surface-treated woven jute/green epoxy composites. Sustain. Jute-Based Compos. Mater. Mech. Thermomechanical Behav., pp. 87–97.

Jafari, S. (2018). 2 - Engineering Applications of Carbon Nanotubes. In R. B. T.-C. N.-R. P. Rafiee (Ed.), *Micro and Nano Technologies* (pp. 25–40). Elsevier.

Jagaba, A. H., Kutty, S. R. M., Baloo, L., Hayder, G., Birniwa, A. H., Taha, A. T. B., Mnzool, M., and Lawal, I. M. (2022). Waste derived biocomposite for simultaneous biosorption of organic matter and nutrients from green straw biorefinery effluent in continuous mode activated sludge systems. Processes, Vol. 10(11), pp. 2262.

Jagadeesh, P., Puttegowda, M., Boonyasopon, P., Rangappa, S. M., Khan, A., and Siengchin, S. (2022). Recent developments and challenges in natural fiber composites: A review. Polym. Compos., Vol. 43(5), pp. 2545–2561.

Jain, A. (2023). 7 - Tribology of carbon nanotubes/polymer nanocomposites. In S. C. George, J. T. Haponiuk, S. Thomas, R. Reghunath, & S. B. T.-T. of P. P. S. Polymer Composites, and Polymer Nanocomposites (Eds.), *Elsevier Series on Tribology and Surface Engineering* (pp. 195–214). Elsevier.

Jian, M. Q., Xie, H. H., Xia, K. L., and Zhang, Y. Y. (2017). Chapter 15 - Challenge and Opportunities of Carbon Nanotubes. In H. Peng, Q. Li, & T. B. T.-I. A. of C. N. Chen (Eds.), *Micro and Nano Technologies* (pp. 433–476). Elsevier.

Jian, W., and Lau, D. (2020). Understanding the effect of functionalization in CNT-epoxy nanocomposite from molecular level. Compos. Sci. Technol., Vol. 191, pp. 108076.

Joseph, K., Tolêdo Filho, R. D., James, B., Thomas, S., and Carvalho, L. H. de. (1999). A review on sisal fiber reinforced polymer composites. Rev. Bras. Eng. Agrícola e Ambient., Vol. 3, pp. 367–379.

Jothibasu, S., Mohanamurugan, S., Vijay, R., Lenin Singaravelu, D., Vinod, A., and Sanjay, M. R. (2020). Investigation on the mechanical behavior of areca sheath fibers/jute fibers/glass fabrics reinforced hybrid composite for light weight applications. J. Ind. Text., Vol. 49(8), pp. 1036–1060.

Karimah, A., Ridho, M. R., Munawar, S. S., Adi, D. S., Damayanti, R., Subiyanto, B., Fatriasari, W., and Fudholi, A. (2021). A review on natural fibers for development of eco-friendly bio-composite: Characteristics, and utilizations. J. Mater. Res. Technol., Vol. 13, pp. 2442–2458.

Karp, S. G., Woiciechowski, A. L., Soccol, V. T., and Soccol, C. R. (2013). Pretreatment strategies for delignification of sugarcane bagasse: a review. Brazilian Arch. Biol. Technol., Vol. 56, pp. 679–689.

Kaufmann, A., and Gupta, M. M. (1988). *Fuzzy mathematical models in engineering and management science*. Elsevier Science Inc.

Kesavan Pillai, S., and Ray, S. S. (2011). *Epoxy-based carbon nanotubes reinforced composites*. IntechOpen.

Khalil, H. P. S. A., Fizree, H. M., Bhat, A. H., Jawaid, M., and Abdullah, C. K. (2013). Development and characterization of epoxy nanocomposites based on nano-structured oil palm ash. Compos. Part B Eng., Vol. 53, pp. 324–333.

Kicińska-Jakubowska, A., Bogacz, E., and Zimniewska, M. (2012). Review of natural fibers. Part I—Vegetable fibers. J. Nat. Fibers, Vol. 9(3), pp. 150–167.

Kim, Y., Hong, J. S., Moon, S. Y., Hong, J.-Y., and Lee, J. U. (2021). Evaluation of carbon nanotubes dispersion in aqueous solution with various dispersing agents. Carbon Lett., Vol. 31, pp. 1327–1337.

Kiran, Nagamadhu, M., Jaiprakash, M., Karthikeyan, K., and shariff, M. (2020). Study the impact of drilling process parameters on natural fiber reinforced chaired epoxy composites. Mater. Today Proc., Vol. 24, pp. 2204–2218.

Komal, U. K., Verma, V., Ashwani, T., Verma, N., and Singh, I. (2018). Effect of chemical treatment on thermal, mechanical and degradation behavior of banana fiber reinforced polymer composites. J. Nat. Fibers.

Koohestani, B., Darban, A. K., Mokhtari, P., Yilmaz, E., and Darezereshki, E. (2019). Comparison of different natural fiber treatments: a literature review. Int. J. Environ. Sci. Technol., Vol. 16, pp. 629–642.

Kou, G., Feng, S., Zhang, W., Chen, J., Xiao, J., Cai, H., and Yang, Z. (2023). Efficient generation of random fiber distributions in fiber reinforced composites. J. Reinf. Plast. Compos., pp. 07316844231162808.

Kumar, B., Agumba, D. O., Pham, D. H., Latif, M., Dinesh, Kim, H. C., Alrobei, H., and Kim, J. (2021). Recent research progress on lignin-derived resins for natural fiber composite applications. Polymers (Basel)., Vol. 13(7), pp. 1162.

Kumar, R., Agrawal, A., and Khan, R. A. (2020). A wake-up call for data integrity invulnerability. Comput. Fraud Secur., Vol. 2020(4), pp. 14–19.

Kumar, S., Manna, A., and Dang, R. (2022). A review on applications of natural Fiber-Reinforced composites (NFRCs). Mater. Today Proc., Vol. 50, pp. 1632–1636.

Kumar, S. S. (2020). Dataset on mechanical properties of natural fiber reinforced polyester composites for engineering applications. Data Br., Vol. 28, pp. 105054.

Kumari, S., Rai, B., and Kumar, G. (2018). A study on effect of ATH on Euphorbia coagulum modified polyester banana fiber composite. AIP Conf. Proc., Vol. 1932(1), pp. 20005.

Kuo, Y., Yang, T., and Huang, G.-W. (2008). The use of grey relational analysis in solving multiple attribute decision-making problems. Comput. Ind. Eng., Vol. 55(1), pp. 80–93.

Kushwaha, D. K., Panchal, D., and Sachdeva, A. (2020). Risk analysis of cutting system under intuitionistic fuzzy environment. Reports Mech. Eng., Vol. 1(1), pp. 162–173.

Kushwaha, P. K., Pandey, C. N., and Kumar, R. (2014). Study on the effect of carbon nanotubes on plastic composite reinforced with natural fiber. J. Indian Acad. Wood Sci., Vol. 11(1), pp. 82–86.

La Mantia, F. P., and Morreale, M. (2011). Green composites: A brief review. In *Composites Part A: Applied Science and Manufacturing* (Vol. 42, Issue 6, pp. 579–588). Elsevier.

Lavagna, L., Nisticò, R., Musso, S., and Pavese, M. (2021). Functionalization as a way to enhance dispersion of carbon nanotubes in matrices: A review. Mater. Today Chem., Vol. 20, pp. 100477.

Li, H., and Qiu, Y. (2019). Dispersion, sedimentation and aggregation of multi-walled carbon nanotubes as affected by single and binary mixed surfactants. R. Soc. Open Sci., Vol. 6(7), pp. 190241.

Li, J., Yang, X., Xiu, H., Dong, H., Song, T., Ma, F., Feng, P., Zhang, X., Kozliak, E., and Ji, Y. (2019). Structure and performance control of plant fiber based foam material by fibrillation via refining treatment. Ind. Crops Prod., Vol. 128, pp. 186–193.

Li, M., Pu, Y., Thomas, V. M., Yoo, C. G., Ozcan, S., Deng, Y., Nelson, K., and Ragauskas, A. J. (2020). Recent advancements of plant-based natural fiber–reinforced composites and their applications. In *Composites Part B: Engineering* (Vol. 200, p. 108254). Elsevier Ltd.

Li, P., Qian, H., Wu, J., and Chen, J. (2013). Sensitivity analysis of TOPSIS method in water quality assessment: I. Sensitivity to the parameter weights. Environ. Monit. Assess., Vol. 185(3), pp. 2453–2461.

Li, W., Du, W., Li, W., Chen, D., Liu, Y., and Ouyang, Y. (2023). Hygrothermal aging behavior and mechanical properties of modified ramie fiber reinforced polyethylene terephthalate glycol composites. Cellulose, Vol. 30(5), pp. 3061–3072.

Liu, J., Wang, S., Peng, Y., Zhu, J., Zhao, W., and Liu, X. (2021a). Advances in sustainable thermosetting resins: From renewable feedstock to high performance and recyclability. Prog. Polym. Sci., Vol. 113, pp. 101353.

Liu, J., Wang, S., Peng, Y., Zhu, J., Zhao, W., and Liu, X. (2021b). Advances in sustainable thermosetting resins: From renewable feedstock to high performance and recyclability. Prog. Polym. Sci., Vol. 113, pp. 101353.

Longkullabutra, H., Thamjaree, W., and Nhuapeng, W. (2010). Improvement in the tensile strength of epoxy resin and hemp/epoxy resin composites using carbon nanotubes. Adv. Mater. Res., Vol. 93, pp. 497–500.

Luo, Y. (2022a). An Accuracy Comparison of Micromechanics Models of Particulate Composites against Microstructure-Free Finite Element Modeling. Materials (Basel).,

Vol. 15(11), pp. 4021.

Luo, Y. (2022b). Microstructure-free finite element modeling for elasticity characterization and design of fine-particulate composites. J. Compos. Sci., Vol. 6(2), pp. 35.

Madhesh, D., and Kalaiselvam, S. (2014). Preparation and characterization of MWCNT-water nanofluids for heat transfer applications. Int. J. Adv. Mech. Eng, Vol. 4, pp. 193–198.

Malekimoghadam, R., and Rafiee, R. (2018). 3 - Carbon Nanotubes Processing. In R. B. T.-C. N.-R. P. Rafiee (Ed.), *Micro and Nano Technologies* (pp. 41–59). Elsevier.

Mansor, M. R., Sapuan, S. M., Hambali, A., Zainudin, E. S., and Nuraini, A. A. (2014). Materials selection of hybrid bio-composites thermoset matrix for automotive bumper beam application using TOPSIS method. Adv. Environ. Biol., pp. 3138–3143.

Maruyama, T. (2021). Chapter 6 - Carbon nanotubes. In S. Thomas, C. Sarathchandran, S. A. Ilangovan, & J. C. B. T.-H. of C.-B. N. Moreno-Piraján (Eds.), *Micro and Nano Technologies* (pp. 299–319). Elsevier.

Maurya, H. O., Gupta, M. K., Srivastava, R. K., and Singh, H. (2015). Study on the Mechanical Properties of Epoxy Composite using Short Sisal Fibre. Mater. Today Proc., Vol. 2(4–5), pp. 1347–1355.

Mavinkere Rangappa, S., Puttegowda, M., Parameswaranpillai, J., Siengchin, S., Ozbakkaloglu, T., and Wang, H. (2022). Chapter 1 - Introduction to plant fibers and their composites. In S. Mavinkere Rangappa, J. Parameswaranpillai, S. Siengchin, T. Ozbakkaloglu, & H. B. T.-P. F. Wang their Composites, and Applications (Eds.), *The Textile Institute Book Series* (pp. 1–24). Woodhead Publishing.

Mayank, Bardenhagen, A., Sethi, V., and Gudwani, H. (2022). Spider-silk composite material for aerospace application. Acta Astronaut., Vol. 193, pp. 704–709.

Mazzanti, V., Pariante, R., Bonanno, A., de Ballesteros, O. R., Mollica, F., and Filippone, G. (2019). Reinforcing mechanisms of natural fibers in green composites: Role of fibers morphology in a PLA/hemp model system. Compos. Sci. Technol., Vol. 180, pp. 51–59.

Mehdikhani, M., Gorbatikh, L., Verpoest, I., and Lomov, S. V. (2019). Voids in fiber-reinforced polymer composites: A review on their formation, characteristics, and effects on mechanical performance. J. Compos. Mater., Vol. 53(12), pp. 1579–1669.

Miliket, T. A., Ageze, M. B., Tigabu, M. T., and Zeleke, M. A. (2022). Experimental characterizations of hybrid natural fiber-reinforced composite for wind turbine blades. Heliyon, Vol. 8(3), pp. e09092.

Mir, S. S., Nafsin, N., Hasan, M., Hasan, N., and Hassan, A. (2013). Improvement of physico-mechanical properties of coir-polypropylene biocomposites by fiber chemical treatment. Mater. Des., Vol. 52, pp. 251–257.

Mishra, V., and Biswas, S. (2013). Physical and Mechanical Properties of Bi-directional Jute Fiber Epoxy Composites. Procedia Eng., Vol. 51, pp. 561–566.

Misnon, M. I., Islam, M. M., Epaarachchi, J. A., and Lau, K. tak. (2014). Potentiality of utilising natural textile materials for engineering composites applications. Mater. Des., Vol. 59, pp. 359–368.

Mittal, M., and Chaudhary, R. (2018). Effect of fiber content on thermal behavior and viscoelastic properties of PALF/Epoxy and COIR/Epoxy composites. Mater. Res.

Express, Vol. 5(12), pp. 125305.

Mohan, K., and Rajmohan, T. (2017). Fabrication and characterization of MWCNT filled hybrid natural fiber composites. J. Nat. Fibers, Vol. 14(6), pp. 864–874.

Mohanavel, V., Ravichandran, M., Sivanraju, R., Velmurugan, P., and Subbiah, R. (2022). Influence of nanofillers on the mechanical characteristics of natural fiber reinforced polymer composites. ECS Trans., Vol. 107(1), pp. 12513.

Monteiro, S. N., Terrones, L. A. H., and D'almeida, J. R. M. (2008). Mechanical performance of coir fiber/polyester composites. Polym. Test., Vol. 27(5), pp. 591–595.

Muñoz, E., and García-Manrique, J. A. (2015). Water absorption behaviour and its effect on the mechanical properties of flax fibre reinforced bioepoxy composites. Int. J. Polym. Sci., Vol. 2015.

Murugan, M. A., Jayaseelan, V., Jayabalakrishnan, D., Maridurai, T., Kumar, S. S., Ramesh, G., and Prakash, V. R. A. (2020). Low velocity impact and mechanical behaviour of shot blasted SiC wire-mesh and silane-treated aloevera/hemp/flax-reinforced SiC whisker modified epoxy resin composites. Silicon, Vol. 12, pp. 1847–1856.

Nabinejad, O., Sujan, D., Rahman, M. E., Liew, W. Y. H., and Davies, I. J. (2018). Hybrid composite using natural filler and multi-walled carbon nanotubes (MWCNTs). Appl. Compos. Mater., Vol. 25, pp. 1323–1337.

Naik, T. P., Singh, I., and Sharma, A. K. (2022). Processing of polymer matrix composites using microwave energy: A review. Compos. Part A Appl. Sci. Manuf., pp. 106870.

Naili, C., Doghri, I., Kanit, T., Sukiman, M. S., Aissa-Berraies, A., and Imad, A. (2020). Short fiber reinforced composites: Unbiased full-field evaluation of various homogenization methods in elasticity. Compos. Sci. Technol., Vol. 187, pp. 107942.

Nayak, S. Y., Shenoy, S., Hameed Sultan, M. T., Kini, C. R., Seth, A., Prabhu, S., and Safri, S. N. A. (2021). Effect of CNT-based resin modification on the mechanical properties of polymer composites. Front. Mater., Vol. 7, pp. 609010.

Neves, A. C. C., Rohen, L. A., Mantovani, D. P., Carvalho, J. P. R. G., Vieira, C. M. F., Lopes, F. P. D., Simonassi, N. T., da Luz, F. S., and Monteiro, S. N. (2020). Comparative mechanical properties between biocomposites of Epoxy and polyester matrices reinforced by hemp fiber. J. Mater. Res. Technol., Vol. 9(2), pp. 1296–1304.

Norizan, M. N., Moklis, M. H., Demon, S. Z. N., Halim, N. A., Samsuri, A., Mohamad, I. S., Knight, V. F., and Abdullah, N. (2020). Carbon nanotubes: Functionalisation and their application in chemical sensors. RSC Adv., Vol. 10(71), pp. 43704–43732.

Nourbakhsh, A., Ashori, A., and Kargarfard, A. (2016). Evaluation of multiwalled carbon nanotubes as reinforcement for natural fiber-based composites. Polym. Compos., Vol. 37(11), pp. 3269–3274.

Nurazzi, N. M., Asyraf, M. R. M., Fatimah Athiyah, S., Shazleen, S. S., Rafiqah, S. A., Harussani, M. M., Kamarudin, S. H., Razman, M. R., Rahmah, M., and Zainudin, E. S. (2021). A review on mechanical performance of hybrid natural fiber polymer composites for structural applications. Polymers (Basel)., Vol. 13(13), pp. 2170.

Oliveira, L. Á., Santos, J. C., Panzera, T. H., Freire, R. T. S., Vieira, L. M. G., and Scarpa, F. (2018). Evaluation of hybrid-short-coir-fibre-reinforced composites via full

factorial design. Compos. Struct., Vol. 202, pp. 313–323.

Orue, A., Jauregi, A., Unsuain, U., Labidi, J., Eceiza, A., and Arbelaiz, A. (2016). The effect of alkaline and silane treatments on mechanical properties and breakage of sisal fibers and poly (lactic acid)/sisal fiber composites. Compos. Part A Appl. Sci. Manuf., Vol. 84, pp. 186–195.

Othman, R. N., and Wilkinson, A. N. (2019). Chapter 2 - Carbon Nanotube Hybrids and Their Polymer Nanocomposites. In S. A. Rashid, R. N. I. Raja Othman, & M. Z. B. T.-S. Hussein Technology and Applications of Carbon Nanomaterials (Eds.), *Micro and Nano Technologies* (pp. 29–60). Elsevier.

Palanikumar, K., Thiagarajan, R., and Latha, B. (2022). *Bio-Fiber Reinforced Composite Materials*. Springer.

Palizvan, M., Tahaye Abadi, M., and Sadr, M. H. (2020). Micromechanical damage behavior of fiber-reinforced composites under transverse loading including fiber-matrix debonding and matrix cracks. Int. J. Fract., Vol. 226, pp. 145–160.

Pantano, A. (2018). 9 - Mechanical Properties of CNT/Polymer. In R. B. T.-C. N.-R. P. Rafiee (Ed.), *Micro and Nano Technologies* (pp. 201–232). Elsevier.

Panyasart, K., Chaiyut, N., Amornsakchai, T., and Santawitee, O. (2014). Effect of surface treatment on the properties of pineapple leaf fibers reinforced polyamide 6 composites. Energy Procedia, Vol. 56, pp. 406–413.

Parameswaranpillai, J., Gopi, J. A., Pathak, C., Rashmi, Dominic C.D., M., Ganguly, S., Radoor, S., and Krishnasamy, S. (2023). 4 - Mechanical properties of epoxy/carbon nanotube composites. In N. M. Nurazzi, R. A. Ilyas, S. M. Sapuan, & A. B. T.-S. and N. N. in P. C. Khalina (Eds.), *Woodhead Publishing Series in Composites Science and Engineering* (pp. 75–87). Woodhead Publishing.

Patnaik, P. K., Swain, P. T. R., Mishra, S. K., Purohit, A., and Biswas, S. (2020). Composite material selection for structural applications based on AHP-MOORA approach. Mater. Today Proc., Vol. 33, pp. 5659–5663.

Petrone, G., and Meruane, V. (2017). Mechanical properties updating of a non-uniform natural fibre composite panel by means of a parallel genetic algorithm. Compos. Part A Appl. Sci. Manuf., Vol. 94, pp. 226–233.

Politowski, I., Regnery, P., Hennig, M. P., Siebers, N., Ottermanns, R., and Schäffer, A. (2021). Fate of weathered multi-walled carbon nanotubes in an aquatic sediment system. Chemosphere, Vol. 277, pp. 130319.

Prasanna Venkatesh, R., Ramanathan, K., and Srinivasa Raman, V. (2016). Tensile, flexual, impact and water absorption properties of natural fibre reinforced polyester hybrid composites. Fibres Text. East. Eur.

Prolongo, S. G., Gude, M. R., and Ureña, A. (2012). Water uptake of epoxy composites reinforced with carbon nanofillers. Compos. Part A Appl. Sci. Manuf., Vol. 43(12), pp. 2169–2175.

Qiu, H., and Yang, J. (2017). Chapter 2 - Structure and Properties of Carbon Nanotubes. In H. Peng, Q. Li, & T. B. T.-I. A. of C. N. Chen (Eds.), *Micro and Nano Technologies* (pp. 47–69). Elsevier.

Quirino, R. L., Monroe, K., Fleischer III, C. H., Biswas, E., and Kessler, M. R. (2021). Thermosetting polymers from renewable sources. Polym. Int., Vol. 70(2), pp. 167–

180.

Radhamani, A. V, Lau, H. C., and Ramakrishna, S. (2020). Nanocomposite coatings on steel for enhancing the corrosion resistance: A review. J. Compos. Mater., Vol. 54(5), pp. 681–701.

Rahman, M. Z., Rahman, M., Mahbub, T., Ashiquzzaman, M., Sagadevan, S., and Hoque, M. E. (2023). Advanced biopolymers for automobile and aviation engineering applications. J. Polym. Res., Vol. 30(3), pp. 106.

Ratna, S., and Misra, S. (2018). An experimental study of mechanical behavior of natural fiber reinforced polymer matrix composites. AIP Conf. Proc., Vol. 1953(1).

Ray, K., Patra, H., Swain, A. K., Parida, B., Mahapatra, S., Sahu, A., and Rana, S. (2020). Glass/jute/sisal fiber reinforced hybrid polypropylene polymer composites: Fabrication and analysis of mechanical and water absorption properties. Mater. Today Proc., Vol. 33, pp. 5273–5278.

Reddy, R. V. S., Mohana Krishnudu, D., Rajendra Prasad, P., and Reddy, P. V. (2022). Alkali treatment influence on characterization of setaria italic (Foxtail Millet) fiber reinforced polymer composites using vacuum bagging. J. Nat. Fibers, Vol. 19(5), pp. 1851–1863.

Reshwanth, K. N. G. ., Muthukumar, C., P, S. K., Jawaid, M., Mallikarjuna Reddy, D., Norrrahim, M. N. F., Rashedi, A., and Naveen, J. (2022). Chapter 8 - Mechanical properties of coir and coir-based hybrid polymeric composites. In M. B. T.-C. F. and its C. Jawaid (Ed.), *Woodhead Publishing Series in Composites Science and Engineering* (pp. 175–191). Woodhead Publishing.

Roy, S., Petrova, R. S., and Mitra, S. (2018). *Effect of carbon nanotube (CNT) functionalization in epoxy-CNT composites*. Vol. 7(6), pp. 475–485.

Rubel, R. I., Ali, M. H., Jafor, M. A., and Alam, M. M. (2019). Carbon nanotubes agglomeration in reinforced composites: A review. AIMS Mater. Sci., Vol. 6(5), pp. 756–780.

Saba, N., Jawaid, M., Alothman, O. Y., Paridah, M. T., and Hassan, A. (2016). Recent advances in epoxy resin, natural fiber-reinforced epoxy composites and their applications. J. Reinf. Plast. Compos., Vol. 35(6), pp. 447–470.

Sahu, K., Alzahrani, F. A., Srivastava, R. K., and Kumar, R. (2021). Evaluating the Impact of Prediction Techniques: Software Reliability Perspective. C. Mater. Contin., Vol. 67(2), pp. 1471–1488.

Saiteja, J., Jayakumar, V., and Bharathiraja, G. (2020). Evaluation of mechanical properties of jute fiber/carbon nano tube filler reinforced hybrid polymer composite. Mater. Today Proc., Vol. 22, pp. 756–758.

Salman, S. D., Sharba, M. J., Leman, Z., Sultan, M. T. H., Ishak, M. R., and Cardona, F. (2015). Physical, mechanical, and morphological properties of woven kenaf/polymer composites produced using a vacuum infusion technique. Int. J. Polym. Sci., Vol. 2015.

Saltelli, A., Ratto, M., Tarantola, S., and Campolongo, F. (2005). Sensitivity analysis for chemical models. Chem. Rev., Vol. 105(7), pp. 2811–2828.

Salwa, H. N., Sapuan, S. M., Mastura, M. T., and Zuhri, M. Y. M. (2019). Analytic Hierarchy Process (AHP)-based materials selection system for natural fiber as

reinforcement in biopolymer composites for food packaging. BioResources, Vol. 14(4), pp. 10014–10046.

Samant, L., Goel, A., Mathew, J., Jose, S., and Thomas, S. (2023). Effect of surface treatment on flax fiber reinforced natural rubber green composite. J. Appl. Polym. Sci., Vol. 140(12), pp. e53651.

Sapiai, N., Jumahat, A., and Mahmud, J. (2018). Mechanical properties of functionalised CNT filled kenaf reinforced epoxy composites. Mater. Res. Express, Vol. 5(4), pp. 45034.

Sapuan, S. M., Leenie, A., Harimi, M., and Beng, Y. K. (2006). Mechanical properties of woven banana fibre reinforced epoxy composites. Mater. Des., Vol. 27(8), pp. 689–693.

Sari, P. S., Thomas, S., Spatenka, P., Ghanam, Z., and Jenikova, Z. (2019). Effect of plasma modification of polyethylene on natural fibre composites prepared via rotational moulding. Compos. Part B Eng., Vol. 177, pp. 107344.

Sarikaya, E., Çallioğlu, H., and Demirel, H. (2019). Production of epoxy composites reinforced by different natural fibers and their mechanical properties. Compos. Part B Eng., Vol. 167, pp. 461–466.

Sayuti, M., Sarhan, A. A. D., Tanaka, T., Hamdi, M., and Saito, Y. (2013). Cutting force reduction and surface quality improvement in machining of aerospace duralumin AL-2017-T4 using carbon onion nanolubrication system. Int. J. Adv. Manuf. Technol., Vol. 65, pp. 1493–1500.

Shahzad, A., Teacă, C.-A., and Tanasă, F. (2022). 1 - Natural fibers and surface treatment methods. In A. Shahzad, F. Tanasa, & C.-A. B. T.-S. T. M. of N. F. and their E. on B. Teaca (Eds.), *Woodhead Publishing Series in Composites Science and Engineering* (pp. 1–18). Woodhead Publishing.

Sharma, A. K., Bhandari, R., Aherwar, A., and Rimašauskienė, R. (2020). Matrix materials used in composites: A comprehensive study. Mater. Today Proc., Vol. 21, pp. 1559–1562.

Shen, X., Jia, J., Chen, C., Li, Y., and Kim, J.-K. (2014). Enhancement of mechanical properties of natural fiber composites via carbon nanotube addition. J. Mater. Sci., Vol. 49(8), pp. 3225–3233.

Siakeng, R., Jawaid, M., Ariffin, H., and Salit, M. S. (2018). Effects of surface treatments on tensile, thermal and fibre-matrix bond strength of coir and pineapple leaf fibres with poly lactic acid. J. Bionic Eng., Vol. 15, pp. 1035–1046.

Singh, M. K., and Singh, A. (2022a). Chapter 1 - Fibers and fiber-forming polymers. In M. K. Singh & A. B. T.-C. of P. and F. Singh (Eds.), *The Textile Institute Book Series* (pp. 1–27). Woodhead Publishing.

Singh, M. K., and Singh, A. (2022b). Chapter 6 - Fiber characterization. In M. K. Singh & A. Singh (Eds.), *Characterization of Polymers and Fibres* (pp. 133–152). Woodhead Publishing.

Singh, N. P., Gupta, V. K., and Singh, A. P. (2019). Graphene and carbon nanotube reinforced epoxy nanocomposites: A review. Polymer (Guildf)., Vol. 180, pp. 121724.

Sinha, A. K., Narang, H. K., and Bhattacharya, S. (2018). Tensile strength of abaca epoxy laminated composites. Mater. Today Proc., Vol. 5(14), pp. 27861–27864.

Soares, B. G., and Alves, F. F. (2018). Nanostructured epoxy—rubber network modified with mwcnt and ionic liquid: Electrical, dynamic-mechanical, and adhesion properties. Polym. Compos., Vol. 39(S4), pp. E2584–E2594.

Soni, S. K., Thomas, B., and Kar, V. R. (2020). A comprehensive review on CNTs and CNT-reinforced composites: syntheses, characteristics and applications. Mater. Today Commun., Vol. 25, pp. 101546.

Soni, S. K., Tody, V., and Thomas, B. (2021). Influence of dispersion technique/time on dispersion stability, aspect ratio and morphology of multi-walled carbon nanotubes. Int. J. Nanotechnol., Vol. 18(5–8), pp. 590–609.

Souza, A. T., Pereira Junio, R. F., Neuba, L. de M., Candido, V. S., da Silva, A. C. R., de Azevedo, A. R. G., Monteiro, S. N., and Nascimento, L. F. C. (2020). Caranan Fiber from Mauritiella armata palm tree as novel reinforcement for epoxy composites. Polymers (Basel)., Vol. 12(9), pp. 2037.

Stanciu, M. D., Teodorescu Draghicescu, H., Tamas, F., and Terciu, O. M. (2020). Mechanical and Rheological Behaviour of Composites Reinforced with Natural Fibres. In *Polymers* (Vol. 12, Issue 6).

Sudha, S., and Thilagavathi, G. (2018). Analysis of electrical, thermal and compressive properties of alkali-treated jute fabric reinforced composites. J. Ind. Text., Vol. 47(6), pp. 1407–1423.

Tanabi, H., and Erdal, M. (2019). Effect of CNTs dispersion on electrical, mechanical and strain sensing properties of CNT/epoxy nanocomposites. Results Phys., Vol. 12, pp. 486–503.

Tanasă, F., Teacă, C.-A., Nechifor, M., and Stanciu, M.-C. (2022). 6 - Physical methods for the modification of the natural fibers surfaces. In A. Shahzad, F. Tanasa, & C.-A. B. T.-S. T. M. of N. F. and their E. on B. Teaca (Eds.), *Woodhead Publishing Series in Composites Science and Engineering* (pp. 125–146). Woodhead Publishing.

Thakur, A., Purohit, R., Rana, R. S., and Bandhu, D. (2018). Characterization and evaluation of mechanical behavior of epoxy-CNT-bamboo matrix hybrid composites. Mater. Today Proc., Vol. 5(2), pp. 3971–3980.

Torres-Arellano, M., Renteria-Rodríguez, V., and Franco-Urquiza, E. (2020). Mechanical properties of natural-fiber-reinforced biobased epoxy resins manufactured by resin infusion process. Polymers (Basel)., Vol. 12(12), pp. 2841.

Valadez-Gonzalez, A., Cervantes-Uc, J. M., Olayo, R., and Herrera-Franco, P. J. (1999). Chemical modification of henequén fibers with an organosilane coupling agent. Compos. Part B Eng., Vol. 30(3), pp. 321–331.

Veit, D. (2023a). Internal Structure of Fibers. In *Fibers: History, Production, Properties, Market* (pp. 63–90). Springer.

Veit, D. (2023b). Other Natural Fibers. In *Fibers: History, Production, Properties, Market* (pp. 403–409). Springer.

Velzeboer, I., Kupryianchyk, D., Peeters, E., and Koelmans, A. A. (2011). Community effects of carbon nanotubes in aquatic sediments. Environ. Int., Vol. 37(6), pp. 1126–1130.

Venkatachalam, G., Hemanth, V., Logesh, M., Piyush, A., Siva kumar, M., Pragasam, V., and Loganathan, T. G. (2023). Investigation of Tensile Behavior of Carbon

Nanotube/Coir Fiber/Fly Ash Reinforced Epoxy Polymer Matrix Composite. J. Nat. Fibers, Vol. 20(1), pp. 2148151.

Verma, A., Jain, N., and Mishra, R. R. (2022). Applications and drawbacks of epoxy/natural fiber composites. In *Handbook of Epoxy/Fiber Composites* (pp. 1–15). Springer.

Verma, D., Gope, P. C., Maheshwari, M. K., and Sharma, R. K. (2012). Bagasse fiber composites-A review. J. Mater. Environ. Sci, Vol. 3(6), pp. 1079–1092.

Verma, D., and Senal, I. (2019). Natural fiber-reinforced polymer composites: Feasibiliy study for sustainable automotive industries. In *Biomass, biopolymer-based materials, and bioenergy* (pp. 103–122). Elsevier.

Vigneshwaran, S., Sundarakannan, R., John, K. M., Johnson, R. D. J., Prasath, K. A., Ajith, S., Arumugaprabu, V., and Uthayakumar, M. (2020). Recent advancement in the natural fiber polymer composites: A comprehensive review. J. Clean. Prod., Vol. 277, pp. 124109.

Vinay, S. S., Sanjay, M. R., Siengchin, S., and Venkatesh, C. V. (2022). Basalt fiber reinforced polymer composites filled with nano fillers: A short review. Mater. Today Proc., Vol. 52, pp. 2460–2466.

Wang, B., Panigrahi, S., Tabil, L., and Crerar, W. (2007). Pre-treatment of Flax Fibers for use in Rotationally Molded Biocomposites. J. Reinf. Plast. Compos., Vol. 26(5), pp. 447–463.

Wang, F., Ma, Y., Zhang, H., Gu, J., Yin, J., Jia, X., Zhang, H., Wang, Y., Fu, X., and Yu, R. (2021). Rheological properties and sedimentation stability of magnetorheological fluid based on multi-walled carbon nanotubes/cobalt ferrite nanocomposites. J. Mol. Liq., Vol. 324, pp. 115103.

Wang, H., Yang, L., Guo, H., Zhao, Y., and Zhao, J. (2019). Mechanical and thermodynamic properties of unidirectional flax fiber reinforced CNT modified epoxy composites. Fibers Polym., Vol. 20, pp. 1266–1276.

Wu, G., Gu, Y., Hou, X., Li, R., Ke, H., and Xiao, X. (2019). Hybrid nanocomposites of cellulose/carbon-nanotubes/polyurethane with rapidly water sensitive shape memory effect and strain sensing performance. Polymers (Basel)., Vol. 11(10), pp. 1586.

Xue, Y. (2017). Chapter 11 - Carbon Nanotubes for Biomedical Applications. In H. Peng, Q. Li, & T. B. T.-I. A. of C. N. Chen (Eds.), *Micro and Nano Technologies* (pp. 323–346). Elsevier.

Yadav, P., Gupta, S. M., and Sharma, S. K. (2021). A review on stabilization of carbon nanotube nanofluid. J. Therm. Anal. Calorim., pp. 1–25.

Yadav, P., Gupta, S. M., and Sharma, S. K. (2022). A review on stabilization of carbon nanotube nanofluid. J. Therm. Anal. Calorim., Vol. 147(12), pp. 6537–6561.

Yallew, T. B., Kassegn, E., Aregawi, S., and Gebresias, A. (2020). Study on effect of process parameters on tensile properties of compression molded natural fiber reinforced polymer composites. SN Appl. Sci., Vol. 2, pp. 1–8.

Yan, L., Chouw, N., Huang, L., and Kasal, B. (2016). Effect of alkali treatment on microstructure and mechanical properties of coir fibres, coir fibre reinforced-polymer composites and reinforced-cementitious composites. Constr. Build. Mater., Vol. 112, pp. 168–182.

Yang, W., Jia, Z., Chen, Y., Zhang, Y., Si, J., Lu, H., and Yang, B. (2015). Carbon nanotube reinforced polylactide/basalt fiber composites containing aluminium hypophosphite: thermal degradation, flame retardancy and mechanical properties. RSc Adv., Vol. 5(128), pp. 105869–105879.

Yeh, C.-H., and Yang, T.-C. (2020). Utilization of waste bamboo fibers in thermoplastic composites: Influence of the chemical composition and thermal decomposition behavior. Polymers (Basel)., Vol. 12(3), pp. 636.

Yong, C. K., Ching, Y. C., Chuah, C. H., and Liou, N.-S. (2015). Effect of fiber orientation on mechanical properties of kenaf-reinforced polymer composite. BioResources, Vol. 10(2), pp. 2597–2608.

Yusup, E. M., Mahzan, S., and Kamaruddin, M. A. H. (2019). Natural fiber reinforced polymer for the application of sports equipment using mold casting method. IOP Conf. Ser. Mater. Sci. Eng., Vol. 494(1), pp. 12040.

Zafar, M. T., Maiti, S. N., and Ghosh, A. K. (2016). Effect of surface treatment of jute fibers on the interfacial adhesion in poly (lactic acid)/jute fiber biocomposites. Fibers Polym., Vol. 17, pp. 266–274.

Zaman, A. C., Kaya, F., and Kaya, C. (2020). A study on optimum surfactant to multiwalled carbon nanotube ratio in alcoholic stable suspensions via UV–Vis absorption spectroscopy and zeta potential analysis. Ceram. Int., Vol. 46(18), pp. 29120–29129.

Zarour, M., Alenezi, M., Ansari, M. T. J., Pandey, A. K., Ahmad, M., Agrawal, A., Kumar, R., and Khan, R. A. (2021). Ensuring data integrity of healthcare information in the era of digital health. Healthc. Technol. Lett., Vol. 8(3), pp. 66.

Zeleny, M. (2012). *Multiple criteria decision making Kyoto 1975* (Vol. 123). Springer Science & Business Media.

Zhao, H., and Li, R. K. Y. (2008). Effect of water absorption on the mechanical and dielectric properties of nano-alumina filled epoxy nanocomposites. Compos. Part A Appl. Sci. Manuf., Vol. 39(4), pp. 602–611.

Zhu, K.-J., Jing, Y., and Chang, D.-Y. (1999). A discussion on extent analysis method and applications of fuzzy AHP. Eur. J. Oper. Res., Vol. 116(2), pp. 450–456.

Zwawi, M. (2021). A review on natural fiber bio-composites, surface modifications and applications. Molecules, Vol. 26(2), pp. 404.